Alexey N. Hopersky
Victor A. Yavna

Scattering of Photons by Many-Electron Systems

Springer

Springer Series on
ATOMIC, OPTICAL, AND PLASMA PHYSICS   58

Springer Series on
ATOMIC, OPTICAL, AND PLASMA PHYSICS

The Springer Series on Atomic, Optical, and Plasma Physics covers in a comprehensive manner theory and experiment in the entire field of atoms and molecules and their interaction with electromagnetic radiation. Books in the series provide a rich source of new ideas and techniques with wide applications in fields such as chemistry, materials science, astrophysics, surface science, plasma technology, advanced optics, aeronomy, and engineering. Laser physics is a particular connecting theme that has provided much of the continuing impetus for new developments in the field. The purpose of the series is to cover the gap between standard undergraduate textbooks and the research literature with emphasis on the fundamental ideas, methods, techniques, and results in the field.

Please view available titles in *Springer Series on Atomic, Optical, and Plasma Physics* on series homepage http://www.springer.com/series/411

Alexey N. Hopersky
Victor A. Yavna

Scattering of Photons by Many-Electron Systems

With 29 Figures

Authors
Professor Alexey N. Hopersky
Professor Victor A. Yavna
Rostov State University of Transport Communication
Department of Mathematics
Rostov-on-Don, Russia
E-mail: hopersky_vm_1@rgups.ru, pr1@rgups.ru

Preface

The subject of this monograph is the results of the recent theoretical studies of the nature and the role of many-particle and orientation effects in the process of anomalous elastic scattering of X-ray photon by *free* atom, atomic ion, and linear molecule.

Theoretical and experimental investigations of anomalous elastic scattering of X-ray photon having energy in the range of 0.35 keV$\leq \eta\omega \leq$1.4 MeV by a many-electron system are immediate requirements in modern fundamental and applied physics from the point of view of the conditions of the anomalous dispersion when an incident photon energy is close to that of an *inner-shell ionization thresholds.* They are important, firstly, because of the construction and subsequent application of the X-ray free electron laser and because of laboratory-plasma X-ray laser generation. Also, it is urgent to solve important problems, such as maintaining a laser thermonuclear fusion, as well as majority of problems in plasma physics, ionizing radiation physics, surface physics, metal and semiconductor physics, and astrophysics.

However, in spite of the existence of a general quantum-mechanical theory for the process of anomalous scattering of the electromagnetic radiation by matter, following from the works by Kramers and Heisenberg (1925) [1] and Waller (1928,1929) [2,3], both the calculation methods and the assignments of the anomalously dispersive regions of the elastic scattering spectra in the immediate vicinity ($\sim$1 $\div$ 100 eV) of the inner-shell ionization thresholds of free atom, atomic ion, and molecule are absent in the world scientific practice, including the many-particle effects. Indeed, the existing methods within the anomalously dispersive regions of elastic scattering lead to infinite (nonphysical) intensities of the differential cross-section resonances. Thus, more than 50% discrepancy follows between theoretical and experimental results near the inner-shell ionization thresholds. The principal reason for that is the neglection of *wide hierarchy of the many-electron effects* that take place in this case on the virtual level and influence significantly the structure and shape of the observed anomalous elastic scattering spectrum. Moreover, together with the

problem of the accounting for the many-particle effects, some other *analytical* aspects of the process' quantum theory should be resolved.

Then, the problem of creation of the quantum theory and the methods of calculation of the spectral characteristics in the process of X-ray photon resonant elastic scattering by free atom, atomic ion, and molecule near their inner-shell thresholds accounting for the many-particle effects arises.

In the theoretical description of the anomalous elastic scattering of X-ray photon by an atom placed within a *chemical compound*, the anomalously dispersive real and imaginary parts of the scattering probability amplitude can be represented with a good accuracy as a product in terms of atomic and solid bodies [4]. Numerous experimental and theoretical results of the investigations on the near-inner-shell-edge *fine structure* of the X-ray absorption spectra in crystals allow one to suggest the following. Satisfactory results are expected for the solid-body part even in one-electron approximation (i.e., one-configuration Hartree–Fock approximation), whereas in the calculation of the atomic part, one has to go beyond the frames of this approximation. So, it includes the many-particle effects following from the effect of radial rearrangement of the atomic residue electron shells in the electrostatic field of a deep vacancy. Therefore, in the study of complete many-particle structure of the atomic part, the preliminary stage is necessary for obtaining the information on the nature of the anomalies in the differential cross-section of elastic scattering of an X-ray photon by *solids*, and in reliable identification of the solid-body effects.

It should be noted that the many-particle theory and the methods developed in this monograph *can be generalized*, particularly onto the case of solids. Therefore, they can be used for further development in the process of the anomalous elastic scattering of an X-ray photon by matter in a *condensed state* theory.

Once a photon is scattered elastically, the system comes back to its initial state. Nevertheless, during its *virtual* existence in an excited state, it has time to demonstrate its real many-electron nature. As our studies have shown, this demonstration becomes most bright and individual near the ionization thresholds, and it manifests itself in the strong disturbances of the smoothness of the differential elastic scattering cross-section. The studies of those spectral regions may produce the unique information on the structure and properties of the scattering objects, specifically on the many-particle effects and their quantum interference. Then, the study of the anomalous elastic scattering of X-ray photon by matter becomes an independent instrument to study the many-electron nature of the scattering objects.

In this monograph, we also present the *analytical* solution of the stationary many-electron Schrödinger equation for nonrelativistic wave functions for the set of electrostatically interacting states of photoionization of the atomic inner shell and the state of the Auger decay of the virtual deep vacancy with Auger- and photoelectron states in the *continuum*. This solution was obtained *outside the frames* of the quantum perturbation theory for the first time in scientific

practice. This result, having a specific importance for the quantum theory of the absorption of an X-ray photon by free atom, atomic ion, and molecule, has also an important methodical value for the further development of the many-particle quantum theory of anomalous elastic scattering of an X-ray photon by a many-electron system.

The results of the calculation of the absolute values and shapes of the differential cross-sections of anomalous elastic scattering of X-ray photon by a free atom and a multipe-charged positive atomic ion can be used in the development of the methods of production and diagnostics of the high-temperature laboratory plasma, the plasma "string" as an active medium, and in the construction of the multiple-layer interference mirrors used as resonators in an X-ray laser [5]. The results of the studies of anomalous elastic scattering of polarized X-ray photon by a molecule fixed in space may be considered as a base for the construction of experimental methods to form and control the fixed-in-space many-electron systems.

The monograph is organized as follows.

In the first chapter, a review of the modern state of experimental and theoretical studies of the anomalous elastic scattering of an X-ray photon by a many-electron system is given. The principal attention is paid to the theoretical models for the differential cross-section of the process, on the basis of which the method of this monograph is developed. The modern situation is characterized, and the aims of the studies are specified.

In the second chapter, within the second-order quantum-mechanical perturbation theory, the many-particle quantum theory and the methods of calculation of the differential cross-section of the anomalous elastic scattering of an X-ray photon by an atom and an atomic ion in near inner-shell ionization thresholds are formulated. A general *analytical* structure of the form-factor of an atom with *any* ground-state term is stated. The effect of the many-electron correlations and nonsphericity of the absolute values and shapes of the form-factor of the spherical-symmetry approximation are studied. The absolute values and the shapes of the differential cross-sections of the anomalous elastic scattering cross-sections are calculated for a set of particular atoms and ions.

In the third chapter, the results of the theoretical studies of the role of the many-particle phenomenon of *postcollision interaction* in the absorption and anomalous elastic scattering of X-ray photon near the inner-shell ionization threshold are presented. Outside the frame of the quantum-mechanical perturbation theory, the analytical solution of the Schrödinger equation is obtained for the nonrelativistic wave function of the system of the atomic *continua* interacting electrostatically.

In the fourth chapter, the many-particle theory and the methods of calculation of the differential cross-section of the anomalous elastic scattering of X-ray photon by a fixed-in-space hydrogen-ligand and nonhydrogen-ligand diatomic molecules are presented. The general *analytical* structure of the form-factor of a linear molecule is stated. The absolute values and shapes

of the differential cross-sections of the anomalous elastic scattering for specific molecules near the ionization thresholds of deep molecular orbitals are stated.

The methods developed in this monograph are not limited by the X-ray energy range. They *can be generalized* up to the vacuum ultraviolet (optical: $6.0\ \text{eV} \le \eta\omega \le 12.4\ \text{eV}$) range of energies for the elastically scattered photon.

To be able to understand this monograph, the readers should know quantum mechanics and mathematical analysis at the university-level.

The authors are indebted to Prof. V. Demekhin, Prof. A. Kochur, Prof. I. Petrov, and Prof. V. Sukhorukov of Rostov State University of Transport Communication (Russia) for their critical remarks during the discussion of the results of this monograph. We also apologize to those numerous authors whose valuable works have not been mentioned in this monograph.

Rostov-on-Don, Russia   *Alexey Hopersky*
September 2009   *Victor Yavna*

Contents

1

Research Results of the Process of the Anomalous Elastic X-Ray Photon Scattering by a Many-Electron System

Technological advancements of experimental investigations in the field of atomic, molecular spectroscopy and spectroscopy of the solid state, the use of synchrotron polarized X-ray radiation, and the high level of energy resolution of the incident photon in the first place led to an intensive development of experimental and theoretical analysis of the electronic structure of matter, which use the information being received from the spectra of the anomalous elastic X-ray photon scattering by an atom, a molecule, and a solid state.

Before we make a brief review of the main experimental and theoretical results obtained in the spectroscopy of the anomalous elastic X-ray photon scattering by a many-electron system and concretize our research tasks, we shall give a description of the main modern theoretical analysis methods.

1.1 Theoretical Process Description

Describing in theory the differential cross-section of the X-ray anomalous elastic scattering process by an atom:

$$\frac{\mathrm{d}\sigma}{\mathrm{d}\Omega} = r_0^2 \, |Q|^2 \,, \tag{1.1}$$

(Ω is the solid angle, $r_0 = 2,818 \cdot 10^{-13}$ cm is the classical electron radius, Q is the process probability amplitude), there are *two schemes* mainly used in modern scientific literature.

The *first scheme* is the second order of the nonrelativistic quantum-mechanical perturbation theory developed in the fundamental works by Dirac [6] and first realized while describing the anomalous scattering process of the electromagnetic radiation by a matter in the works by Kramers and Heisenberg [1] and Waller [2, 3].

In our study, the nonrelativistic variant of the first scheme of the differential cross-section description (1.1) with allowance for the non-zero widths of

the atomic vacancy decay in its structure will be identified as an approximation of the Kramers–Heisenberg–Waller formula. The relativistic variant of this scheme for an atom (the relativistic Hamiltonian and the description of one-electron wave functions by Dirac spinors) reproduces formally and mathematically the second order $\hat{S}$ of the quantum electrodynamics matrix formalism [7] and its present form for the calculation of the differential cross-section (1.1) is presented by *Kissel–Pratt algorithm* [8]. In the context of the relativistic variant of the description of the gamma radiation elastic scattering (photon energy $\hbar\omega \sim 500\,\text{keV}$–$10\,\text{MeV}$ and more) and in computing the differential cross-section (1.1) for heavy atoms, we can register the photon elastic scattering at the virtual electron-positron pairs created by the Coulomb nuclear field, in addition to the Rayleigh atomic electron scattering, the Thomson nuclear scattering, Rayleigh nucleon scattering, and the Delbrück scattering.

Here we shall remind the reader that in the scientific literature the "Rayleigh scattering" is understood as the photon contact and non-localized (through absorption and following radiation) elastic scattering by atomic electrons (nucleons), whereas the "Thompson nuclear scattering" means just the photon contact elastic scattering by a nucleus, if we imagine it as a point object.

In the wavelength mode from the long wave $\lambda \sim 2 - 20$ Å until the ultra short $\lambda \sim 0,3 - 0,01$ Å ranges of the incident X-ray photon that exceed distinctly the average atomic nucleus diameter the mentioned additional elastic scattering process types are insignificant, and the studied process can be theoretically examined with allowance for the Rayleigh photon scattering by the electrons of a free atom only.

The *second scheme* is a form factor approximation and its modifications. From the mathematical standpoint, it is just a particular case of the first scheme. The form factor approximation describes satisfactorily the differential cross-section (1.1) in the energy range of a scattering X-ray photon that is far from the energy of the ionization thresholds of the atomic shells. To describe the anomalously dispersing scattering range its modifications are necessary for the purpose of registration of the dispersing contributions.

Let us describe these calculation schemes.

1.1.1 Quantum-Mechanical Perturbation Theory

In the second order of the quantum-mechanical perturbation theory, the probability amplitude of the process of the photon anomalous elastic scattering by an atom in (1.1) for the atomic state wave functions takes nonrelativistically the form [10]:

$$Q = (\boldsymbol{e}_1 \cdot \boldsymbol{e}_2)F(\theta;\omega) + A; \tag{1.2}$$

where $\boldsymbol{e}_1$ and $\boldsymbol{e}_2$ are the unit polarization vectors of the incident (generated) and the scattered (registered) energy photon $\hbar\omega$. In (1.2) atomic system of units ($e = m_e = \hbar = 1$) the following values are defined:

(a) Atomic form factor (structure function)

$$F(\theta; \omega) = \langle 0| \sum_{j=1}^{N} \exp\left[i\left(\boldsymbol{k} \cdot \boldsymbol{r}_j\right)\right] |0\rangle, \tag{1.3}$$

if an atom has filled shells in the ground state (term $^1S_0$), it is equal to

$$F(\theta; \omega) = \sum_{nl} N_{nl} \int_0^\infty P_{nl}^2(r) \frac{\sin(kr)}{kr} dr, \tag{1.4}$$

$$k = |\boldsymbol{k}| = |\boldsymbol{k}_1 - \boldsymbol{k}_2| = (2\omega/c)\sin(\theta/2),$$

(b) Anomalously dispersing Kramers–Heisenberg–Waller terms in the *dipole* approximation ($\boldsymbol{k} \cdot \boldsymbol{r}_j \ll 1$) for Fourier components of the electromagnetic field operator

$$A = \underset{m>f}{S}\, a_1^m a_2^m \left(\frac{1}{E_{0m} + \omega} + \frac{1}{E_{0m} - \omega}\right), \tag{1.5}$$

$$a_{1,2}^m = \langle 0| \sum_{j=1}^{N} \left(\boldsymbol{e}_{1,2} \cdot \boldsymbol{p}_j\right) |m\rangle,$$

$$E_{0m} = E_0 - E_m + i\Gamma_{nl}/2.$$

In the formulas (1.3)–(1.5) are defined: N– the number of electrons in the atom, $\boldsymbol{r}_j$ – the radius vector of the j – electron in the atom, N_{nl} – the number of electrons in the atomic nl – shell, $P_{nl}(r)$ – the radial part of the wave function of the nl – shell electron, $\boldsymbol{k}_1$– and $\boldsymbol{k}_2$ – the wave vectors of the incident and the scattered photons, $\boldsymbol{k}$ – the scattering vector, θ – the scattering angle (the angle between the vectors $\boldsymbol{k}_1$ and $\boldsymbol{k}_2$), c – the light speed, E_0 – the energy of the atom ground $|0\rangle$ – state, E_m – the energy of the atom in the $|m\rangle$ – intermediate (virtual) scattering state, $\boldsymbol{p}_j$ – the impulse operator of the j – electron in the atom, Γ_{nl} – the total width of the nl – vacancy decay at the radiation and autoionization channels, f – the *Fermi level* (the set of quantum numbers of the atom valence shell), and the symbol S means the summation (integration) according to the virtual states of the discrete (continuous) excitation/ionization spectrum of all atom nl – shells, including the states of its multiple excitation/ionization.

The summation (integration) in (1.5) follows the countable (discrete spectrum) and the noncountable (continuous spectrum) infinite sets of the virtual (unobserved) states. The sign choice before the imaginary part in the energy denominators (1.5) corresponds to the well known in the quantum scattering theory *Gamov procedure* [11] $E_m \rightarrow E_m - i\Gamma_{nl}/2$, obeying the formation of the scattered diverging wave $P(r) \propto \exp(ikr)$ at the asymptotic form ($r \rightarrow \infty$).

In Chap. 2, we shall show that the form factor of an *open*-shell atom in the ground state has in general a more complex analytic structure than (1.4).

The expression for the differential cross-section of the elastic scattering (1.1) results from the *Fermi golden rule* for the expectancy differential of changing the system "atom + radiation" in unit time from the initial state with the energy E_i to the final states' interval $(f, f + \mathrm{d}f)$ of the continuous spectrum

$$\mathrm{d}W_{if} = 2\pi \left|Q_{if}\right|^2 \delta\left(E_i - E_f\right) \mathrm{d}f,$$
$$\mathrm{d}f = (2\pi c)^{-3} V\omega^2 \mathrm{d}\omega \, \mathrm{d}\Omega,$$

determining for its part the differential cross-section of the process

$$\mathrm{d}s_{if} = (1/\rho)\mathrm{d}W_{if}$$
$$\rho = cn/V,$$

where ρ is the flux density, n is the number of the incident photons, V is the volume, where the photons spread out. In this connection, the expression for Q_{if} – the probability amplitude of the process is based on the operator of the electromagnetic interaction

$$\hat{H}_{\mathrm{int}} = \sum_{j=1}^{N} \left[\frac{1}{2c^2} \left(\boldsymbol{A}_j\right)^2 - \frac{1}{c} \left(\boldsymbol{p}_j \cdot \boldsymbol{A}_j\right) \right], \qquad (1.6)$$
$$\boldsymbol{A}_j \equiv \boldsymbol{A}(\boldsymbol{r}_j; 0).$$

Here, the operator of the vector potential of the free electromagnetic field in the form of the secondary quantization

$$\boldsymbol{A} = \sum_{\boldsymbol{k}, \eta} \sqrt{\frac{2\pi}{|\boldsymbol{k}|}} \boldsymbol{e}_{\boldsymbol{k}\eta} \left(\hat{a}_{\boldsymbol{k}\eta}^- e^{i\boldsymbol{k}\boldsymbol{r}} + \hat{a}_{\boldsymbol{k}\eta}^+ e^{-i\boldsymbol{k}\boldsymbol{r}} \right), \qquad (1.7)$$

is presented as the solution [7] of the wave equation at time point $t = 0$:

$$\Omega \boldsymbol{A}(\boldsymbol{r}; t) = 0, \qquad (1.8)$$

and is defined: $\hat{a}_{\boldsymbol{k}\eta}^+ \left(\hat{a}_{\boldsymbol{k}\eta}^-\right)$ – the creation (annihilation) operator of the photon with the wave vector $\boldsymbol{k}$ and the polarization $\eta(=1, 2)$, $\boldsymbol{e}_{\boldsymbol{k}\eta}$ – the photon's polarization vector $\boldsymbol{e}_1 \perp \boldsymbol{e}_2 \perp \boldsymbol{k}$.

Let us state here that the structures of the (1.8) and the linear in the electromagnetic field items in the interaction operator (1.6) are determined by the choice of the *Coulomb field calibration* that makes the commutator vanish

$$div\,\boldsymbol{A}(\boldsymbol{r}; t) = 0; \quad \varphi(\boldsymbol{r}) = 0,$$

where $\varphi(\boldsymbol{r})$ is the scalar part of the field 4-potential $A^\mu = (\varphi, \boldsymbol{A})$, $\mu = 0, 1, 2, 3$.

The quadratic in the electromagnetic field terms of the operator (1.6) describes the so-called *contact interaction* of a photon with atomic electrons and determines the analytic structure of the atomic form factor (1.3). The linear in the electromagnetic field terms of the operator (1.6) describes the absorption process and the photon radiation by an atom by means of its virtual excitation/ionization of different multiplicity and determines the analytic structure of the anomalously dispersing Kramers–Heisenberg–Waller terms (1.5) of the total probability amplitude of the elastic scattering process.

The formulas (1.1)–(1.7) form the basis of the nonrelativistic variant of the first theoretical scheme for describing the anomalous elastic X-ray photon scattering by free atomic electrons. We shall use them in Chap. 2 of our study for the development of the many-body quantum theory of the process.

1.1.2 Form Factor Approximation and its Modifications

The form factor modification follows from the expression for the probability scattering amplitude (1.2), if we set aside the anomalously dispersing Kramers–Heisenberg–Waller terms. Then the differential cross-section of the process takes the form:

$$\frac{d\sigma}{d\Omega} = r_0^2 \left(\boldsymbol{e}_1 \cdot \boldsymbol{e}_2\right)^2 \left|F(\theta, \omega)\right|^2. \tag{1.9}$$

In the case of the elastic scattering of nonpolarized electromagnetic radiation by a many-electron system the polarization factor $\left(\boldsymbol{e}_1 \cdot \boldsymbol{e}_2\right)^2$ in (1.9) is equal to $\left(1 + \cos^2\theta\right)/2$.

In the context of this approximation the relativistic corrections to the atomic form factor in (1.9) are considered by building the modified atomic form factor, where the contribution from each nl-electron of the atomic core has the form [10]:

$$g_{nl}(\theta; \omega) = 4\pi \int_0^\infty \rho_{nl}(r) \left(1 - \alpha_{nl}(r)\right)^{-1} \frac{\sin(kr)}{kr} r^2 dr, \tag{1.10}$$

$$\alpha_{nl}(r) = \frac{1}{mc^2} \left(E_{nl} + V_{nl}(r)\right).$$

In (1.10) the following values are determined: E_{nl} is the binding energy and $V_{nl}(r)$ is the potential energy of the nl-electron as well as the relativistic probability density of the electron location in the nucleus:

$$\rho_{nl}(r) = \frac{1}{4\pi r^2} \left[R_{nl}^2(r) + Q_{nl}^2(r)\right],$$

where $R_{nl}(r)$ and $Q_{nl}(r)$ are the radial spinor components of the one-electron wave function. In the nonrelativistic limit $(v/c << 1)$ we derive

$Q_{nl}(r) \to 0$, $R_{nl}(r) \to P_{nl}(r)$ – the nonrelativistic radial part of the electron wave function, $\alpha_{nl}(r) \to 0$ and return to the expression (1.4).

The energy of the scattered X-ray photon approaching the energy of the ionization threshold of the *deep* atom shell and the anomalously dispersing terms of the probability amplitude of the elastic scattering (1.2) begin to play a decisive role in determining the process probability and the form factor approximation becomes inapplicable.

In this situation, we can make the following first move towards the modification of the form factor approximation. Passing in (1.5) to the limit of zero widths of the vacancy decay $\Gamma_{nl} \to 0$ for each atomic nl-shell, deleting the sum in the intermediate states of the discrete spectrum scattering, and considering the operator equation:

$$\lim_{\eta \to 0} \left(\frac{\eta}{\pi} \right) \left[(x - y)^2 + \eta^2 \right]^{-1} = \delta(x - y),$$

for the probability amplitude of the elastic scattering we obtain the expression:

$$Q = (\boldsymbol{e}_1 \cdot \boldsymbol{e}_2) \left[F(\theta; \omega) + \sum_{nl} (\operatorname{Re} A_{nl} - i \operatorname{Im} A_{nl}) \right], \qquad (1.11)$$

$$\operatorname{Re} A_{nl} = \left(2\pi^2 cr_o \right)^{-1} P \int\limits_o^\infty \frac{x^2 \sigma_{nl}(x)}{\omega^2 - x^2} dx, \qquad (1.12)$$

$$\operatorname{Im} A_{nl} = \omega \left(4\pi cr_o \right)^{-1} \sigma_{nl}(\omega), \qquad (1.13)$$

$$\sigma_{nl}(\omega) = (4/3)\pi^2 \alpha \, a_o^2 \omega \, |D_{nl}|^2 . \qquad (1.14)$$

In (1.11)–(1.14) the following values are determined: D_{nl} is the probability amplitude and $\sigma_{nl}(\omega)$ is the cross-section of the atomic nl-shell photoionization, α is the fine structure constant, a_0 is the Bohr radius, and P is the symbol of the *Cauchy principal value*. The connection (1.13) shows the **optical theorem** [11], well known in the quantum absorption and scattering theory.

In the case of the zero scattering angle (forward scattering), the expression (1.12) can be derived on the basis of the optical theorem (1.13) and from the causality principle of the light-signal propagation, the mathematical representation of which leads to the amplitude analyticity of the forward elastic scattering [12].

Actually, from the Cauchy integral formula,

$$\psi(\omega) = (2\pi i)^{-1} \oint\limits_L \psi(x)(x - \omega)^{-1} dx,$$

for the arbitrary analytical function $\psi(x) = \operatorname{Re} \psi(x) + i \operatorname{Im} \psi(x)$, $\psi(x) \to 0$ at $x \to \infty$, the *Kramers-Kronig dispersion relations* [13] follow:

$$\operatorname{Re}\psi(\omega) = \left(\frac{1}{\pi}\right) P \int\limits_{-\infty}^{+\infty} \operatorname{Im}\psi(x) \, (x - \omega)^{-1} \, dx,$$

$$\operatorname{Im}\psi(\omega) = -\left(\frac{1}{\pi}\right) P \int\limits_{-\infty}^{+\infty} \operatorname{Re}\psi(x)(x - \omega)^{-1} dx.$$

Now, the expression for the real part of the function $\psi(x)$ can be transformed to the integral on the physically meaningful energy interval $x \in [0; \infty)$:

$$\operatorname{Re}\psi(\omega) = \left(\frac{2}{\pi}\right) P \int\limits_{0}^{\infty} x \operatorname{Im}\psi(x) \, \left(x^2 - \omega^2\right)^{-1} dx. \qquad (1.15)$$

Finally, the substitution of (1.13) in (1.15) leads to (1.12) accounting for a sign in (1.11).

Then, keeping in mind that $F(0; \omega) = N$ follows from the formula (1.4) for the atomic form factor at the zero scattering angle, on the basis of the expressions (1.12)–(1.14) we arrive at the formulas of the form factor approximation, modified in terms of the Kramers-Kronig dispersion relations for the forward scattering amplitude:

$$Q = (\boldsymbol{e}_1 \cdot \boldsymbol{e}_2) \, (N + f' - if''), \qquad (1.16)$$

$$f' = \sum_{nl} \operatorname{Re} A_{nl}; \quad f'' = \sum_{nl} \operatorname{Im} A_{nl}.$$

For the interpretation of the experimental results, the expression (1.16) has been used in many scientific works of reference dealing with the analysis of the *anomalous* elastic X-ray photon scattering by a many-electron system.

The further attempt to fall outside the limits of the approximation (1.16) in order to consider the probability amplitude of the elastic scattering in the theoretical description, the radiation transitions to virtual states of the continuous spectrum scattering along with the transitions to states of the discrete spectrum scattering, the non-zero values of widths of atomic vacancy decays and the scattering angles, the many-body effects as well make the second step in the modification of the form factor approximation unavoidable – the return to the structures of the probability scattering amplitudes in the quantum mechanical perturbation theory at least (1.1)–(1.7).

In closing this section, the following can be noted. The building of the anomalous dispersion part (1.5) of the probability amplitude of the elastic scattering is realized by us in the *dipole approximation* for the Fourier components of the electromagnetic field operator (1.7): $\exp\left[i\left(\boldsymbol{k} \cdot \vec{r}\right)\right] \cong 1$. As a result, the expression (1.5) turns out to be independent of the scattering angle, the polarization factor $(\boldsymbol{e}_1 \cdot \boldsymbol{e}_2)$ being extracted from it. Exceeding the limits of the dipole approximation makes the anomalously dispersing Kramers-Heisenberg-Waller terms theoretically depend on the scattering angle even

after extracting the polarization factor [14]. Such investigation is outside the scope of our work. It will be required in the *hard* X-ray mode, because in the short-wave range of the wave-lengths $\lambda \propto 0,30 \div 2,00$ $\mathring{A}$ the limitation through the dipole approximation, if the average value of the atomic diameter is $d \sim 1 \div 2$ $\mathring{A}$, can distinctly degrade the quality of the theoretical description of the differential cross-section of the process.

1.2 Measurement and Calculation Results of Spectral Characteristics of the Process

Performed at present, the scientific works dealing with the study of the anomalous elastic X-ray photon scattering by a many-electron system generally can be divided into three groups: (a) the works, where the imaginary and real parts of the probability amplitude of the anomalous elastic scattering in (1.2) and (1.16) were studied; (b) the works, where the differential cross-section of the process was investigated; (b) the works, where the atomic form factor was analyzed.

Let us review the main research results following this classification. We shall however confine our review to the works, where the energy region $\omega = \omega_I \pm 200$ (eV) (ω_I is the energy of the ionization threshold of the deep atomic *I*-shell) was studied – the main area of "action" of the *many-body effects* investigated in the present book.

1.2.1 Study of the Real and Imaginary Parts of the Probability Amplitude of the Process.

In the work by Fukamashi and Hosoya (1975) [15] the near structure of the functions f' and f'' in the area of the K-ionization threshold of Ga ($\omega_K = 10{,}368$ eV) in the GaP crystal was detected using the characteristic monochromatic X-ray radiation and measured with a high resolution (~ 2 eV). In the photon energy area $\omega \sim \omega_K \pm 6$ (eV) the $\sim 20\%$ divergence of the theory (one-electron hydrogen-like approximation without considering the relaxation of the atomic core in the $1s$-vacancy field, the near fine structure of the absorption section, the transitions to the intermediate states of the discrete spectrum, and the finite values of the decay widths of the core vacancies) and experiment was detected. The authors do not state the divergence causes.

The synchrotron X-ray radiation (DESY; Hamburg, Germany) for studying the spectral characteristics of the anomalous elastic scattering process was used for the first time in the work by Bonse and Materlik (1976) [16]. In this work the near fine structure of the function f' in the energy area of the K-ionization threshold of the metallic Ni ($\omega_K = 8{,}332$ eV) was detected and measured with high resolution of the scattered photon wavelength $\left(\Delta\lambda/\lambda \leq 2 \cdot 10^{-4} \right)$. The authors point to the fact that their measurement results differ from the results of the one-electron hydrogen-like

approximation, and connect it with ignoring the finite decay width of the $1s$-vacancy of Ni incalculation.

In the work by Fukamashi *et al* (1978) [17] the synchrotron X-ray radiation (Stanford Synchrotron Radiation Laboratory; SSRL, USA) is used for studying the functions f' and f'' in the energy region of the K-ionization threshold of the metallic copper (Cu: $\omega_K = 8,980$ eV). The absolute values and shapes of these functions are derived with a high scattered photon energy resolution (~ 2 eV), their nonlinear near-threshold structure is ascertained and it is demonstrated that the one-electron hydrogen-like approximation in the context of the second-order quantum mechanical perturbation theory and the modified form factor approximation (1.16) lead to more than 20% divergence with the experiment in the threshold area. The authors do not determine the divergence causes.

The structure of the function f' in the energy region of the $K-$ionization threshold of the metallic Se ($\omega_K = 12,658$ eV) is measured with a high scattered photon energy resolution ($\omega / \Delta\omega \propto 1,5\cdot10^4$) in the work by Bonse *et al* (1980) [18]. The synchrotron X-ray radiation (DESY; Hamburg, Germany) was used. The authors did not explain in theory the results of the experiment.

In the works of Templeton's team (1980–1982) [19–21] the synchrotron X-ray radiation (Stanford Synchrotron Radiation Laboratory; SSRL, USA) is used for the first time for studying the functions f' and f'' in the energy region of the atomic ionization $L_{1,23}$ – thresholds. The measurements are performed with a high-scattered photon wavelength resolution $(\Delta\lambda / \lambda \cong 10^{-3})$. The resonance structure of these functions is detected for atoms of Cs (crystal of **Cs**HC$_4$H$_4$O$_6$) [20] ($L_{1,23}$-thresholds), Pr (crystal of Na**Pr**C$_{10}$H$_{12}$N$_2$O$_8$ [8H$_2$O]), Sm (isomorphic Sm) [19] (L_3-threshold), and Gd (isomorphic Gd) [21] (L_3-threshold). The results of the experiment for the atom of Cs in the L_3-threshold area are compared with the results of the relativistic Cromer-Liberman algorithm [22]. The divergence between theory and experiment in the photon energy region $\omega = \omega_{L_3} \pm 15$ (eV) amounts to 30%. The results of the experiment for the f'-function of atoms of Pr and Sm are compared with the results of the modified form factor approximation (1.16). The divergence between theory and experiment in the photon energy region $\omega = \omega_{L_3} \pm 10$ (eV) amounts to 30%. The authors do not determine the causes of the mentioned divergences.

In the works by Hart (1980) [23] and Hart and Siddons (1981) [24] the functions f' and f'' are measured in the K-ionization threshold area of the metallic Zr ($\omega_K = 17,998$ eV), Nb ($\omega_K = 18,986$ eV), and Mo ($\omega_K = 20,008$ eV) by using the synchrotron X-ray radiation (Wheatstone Laboratory; London, England) with a scattered photon energy resolution ~ 25 eV. The divergence of results between the relativistic Cromer-Liberman algorithm and the experiment in the photon energy region $\omega = \omega_K \pm 100$ (eV) amounts to 40%. According to these authors, their modification of the mentioned model decreases the divergences to 10%. However, there are no physical and mathematical arguments for the realized modification.

In the work by Henke *et al* (1982) [25] the first attempt is made in scientific practice to generate the theoretical data bank for the functions f' and f'' and the photoabsorption coefficients in the incident photon energy region $\omega \in [100; 2000]$ eV, including the energy regions of the deep shells ionization thresholds on the basis of the modified form factor approximation (1.16) for elements of the Mendeleev's table with the nuclear charge $Z = 1 \div 94$. In the work by Henke *et al* (1993) [26] the region $\omega \in [2; 30]$ keV is added to the research results of [25], as well as the results by Windt (1991) [27] coming out from the experimental studies of the function f' for the elements C, Si, Mo, and W in the region $\omega \in [50; 1000]$ eV ,the results of the relativistic Kissel-Pratt algorithm [28] for the function f' of the elements Al, Zn, and Pb in the energy region $\omega \in [50; 20000]$ eV, and the scattering angles $\theta = 0°$, $30°$, $90°$. The results of the mentioned works demonstrate the nonlinear near-threshold structure of the functions f' and f''. The calculations are made without considering the many-particle effects and it seems to be methodically necessary to compare them (and their confidence estimation) with the results of the quantum many-particle theory.

In the context of the relativistic Kissel-Pratt algorithm Basavaraju *et al* (1986) [29] researched theoretically for the first time the functions f', f'' and the differential cross-sections of the anomalous elastic X-ray scattering for the neutral atoms C, O, Ne, and their ions C^{1+}, C^{2+}, C^{4+}, C^{5+}, O^{1+}, O^{6+}, O^{7+}, Ne^{1+}, Ne^{2+}, Ne^{4+}, Ne^{6+}, Ne^{8+}, Ne^{9+} in the energy region of the $1s$- and $2s$-shells ionization thresholds. The nonlinear structure of the calculated values is determined as well as the fact, that the giant resonances of the differential scattering cross-section appear, if there are multicharged positive ions in immediate proximity to the energies of the ionization thresholds. The transitions to the intermediate states of the discrete spectrum scattering, the finite values of the decay widths of the virtual core vacancies, and the many-particle effects are not taken into consideration.

In the work by Zhou *et al* (1990) [30] in the context of the relativistic Cromer-Liberman algorithm modified by the authors (additional calculation of transitions to the intermediate states of the discrete spectrum scattering), the functions f', f'' and the differential cross-sections of the anomalous elastic X-ray forescattering are studied theoretically in the photon energy region $\omega \in [1; 70]$ keV for the neutral atom Ne and its ions Ne^{2+}, Ne^{4+}, Ne^{6+}, Ne^{7+}. The giant resonances of the differential scattering cross-section (transition $1s$–$2p$) in the energy region of the ion $1s$-shells ionization thresholds, where the oscillator strengths are vastly superior to the same for the $1s$–$3p$ resonance in the neutral Ne are investigated. The results of this work for the atom Ne and its ion Ne^{6+} are supplemented in the work by Zhou *et al* (1992) [31]. In both the works the finite values of the decay widths of the virtual core vacancies and the many-particle effects are not taken into consideration.

In the work by Barkyoumb *et al* (1990) [32] the extended far fine structure (EXAFS: Edge extended X-ray-Absorption Fine Structure) of the K-spectrum of the metallic copper absorption (Cu : $\omega_K = 8,980$ eV) was measured

using the synchrotron X-ray radiation (Synchrotron Radiation Laboratory; Brookhaven, USA) in the scattered photon energy region $8,600\,eV \leq \omega \leq 9,600\,eV$ with a high resolution ($\sim 2\,eV$). In the context of the modified form factor approximation (1.16), the authors show for the first time in scientific practice, that the EXAFS-oscillations of the photoabsorption spectrum lead to the corresponding oscillations of the f'-function, determining in this way its extended fine structure in the photon energy region $\omega_K \leq \omega \leq \omega_K + 200$ (eV). Similar result is achieved in the work by Barkyoumb and Smith (1990) [33] for the f'-function of the metallic aluminum (Al : $\omega_K = 1,560\,eV$) in the photon energy region $1,450\,eV \leq \omega \leq 1,800\,eV$.

Using the synchrotron radiation (HASYLAB; Hamburg, Germany) in the work by Stanglmeier *et al* (1992) [34] the f'-function is measured in the ionization K-threshold area of Ni and Cu, the ionization $L_{1,23}$-thresholds area of Ta and Au, and the ionization L_3-threshold area of Pt. The experimental data are compared with the calculation results in the Cromer-Liebermann model, and wide disagreements are discovered between theory and experiment in the neighborhood of the ionization threshold energies ($\pm 300\,eV$). The authors associated this first, with the defects of the theoretical scheme they used. In the work by Kissel *et al* (1995) [9] a good fit of the independent particle relativistic approximation (dropping of the relaxation processes of the atomic core electron shell in the field of virtual deep vacancies) to the results of the experiment [34] is achieved. However, both experimental and theoretical data in immediate proximity ($\pm 50\,eV$) to the ionization thresholds of the researched elements are lacking.

The intensive development of methods of synchrotron X-ray radiation production and use has been accompanied in the past 15 years by publication of a great number of both experimental and theoretical studies of scattering amplitude Q from (1.2) first of all for the solid-state bodies. In order to finish the brief review of this section we shall restrict ourselves to the examination of the works [35, 36]. In the work [35] a radically new step is taken in the development of the theory of the anomalous elastic X-ray radiation scattering by a solid body after the works by Barkyoumb *et al* (1990) [32, 33]. The work [36] gives an example of a typical experimental study, where the DAFS-spectroscopy (DAFS: Diffraction Anomalous Fine Structure) method that is widely developed in recent years is realized.

Using the Green function method in the work by Vedrinskii *et al* (1992) [35] the theoretical model of the real and imaginary parts of the probability amplitude of the anomalous elastic X-ray radiation scattering by a crystal in the energy region of the central atom deep shell ionization threshold, accounting for the near fine structure of its photoabsorption spectrum (XANES: X-ray Absorption Near Edge Structure) is developed in the context of the second-order quantum mechanical perturbation theory for the first time in the scientific practice. The theory is reduced to calculating the functions ReA and ImA of the anomalous dispersive part (1.5) of elastic scattering probability amplitude for the monocrystal BN in the scattered photon energy region

$170 \, \text{eV} \leq \omega \leq 230 \, \text{eV}$, including the ionization threshold energy of atom B $1s$-shell ($\omega_K = 188 \, \text{eV}$). The nonzero values of the atomic vacancies decay widths and the potential of the virtual appearing deep $1s$-shell vacancy is taken into consideration.

Using the synchrotron X-ray radiation (Synchrotron Radiation Laboratory; Brookhaven, USA) in the work by Frenkel *et al* (1999) [36] the XANES- and EXAFS-structures of the functions f' и f'' of the crystal Fe_3O_4 are measured in the scattered photon energy region $\omega_K \leq \omega \leq \omega_K + 600 \, \text{(eV)}$, in the ionization threshold energy region of the atom Fe $1s$-shell ($\omega_K = 7{,}112 \, \text{eV}$). The structural information is extracted from the experimental results using the DAFS-spectroscopy methods.

1.2.2 Differential Cross-Section Study of the Process

In the work by Kissel *et al* (1980) [37] the relativistic *Kissel-Pratt algorithm* is represented. It is developed by the authors and extensively used presently for describing the differential cross-section of the elastic photon scattering process by an atom in theory. This algorithm is based on the following main principles: the probability amplitude of the elastic scattering is examined accurate to the second order of the $\widehat{S}$-matrix formalism of the quantum electrodynamics; the electron wave functions in the atom (Dirac spinors) are taken as solutions of the Dirac equation with the central self-consistent Dirac-Hartree-Fock-Slater potential (the exchangeable part of the potential is localized according to Slater [39]). The authors underscore that such a model does not account for the vacuum polarization effect of the quantum electrodynamics [7] at high photon energies (gamma range) and the many-particle effects at low photon energies (X-ray range). The calculation results of absolute values and differential cross-section forms of the elastic photon scattering by the atoms Al, Zn, Ag, Sn, Sm, Ta, Au, Hg, and Pb are represented. The conclusion is made that in the photon energy range from $100 \, \text{eV}$ till $100 \, \text{keV}$, including the X-ray range, the effects of the Thomson nuclear scattering, the Rayleigh nucleon scattering, and the Delbrück scattering [40] on virtual electron-positron pairs created by Coulomb nuclear field are unessential and the dominating type of elastic scattering process is the Rayleigh photon scattering by atom electrons. Outside the anomalous dispersing areas of the elastic scattering, the calculation results fit well with the results of the experiment by Schumacher and Stoffregen (1977) [41] for the atoms Zn, Sn, Ta, Au, and Pb. The authors show by the example of the Pb atom, that as the scattered photon energy approaches the $1s$-shell ionization threshold energy ($\omega_K = 88{,}006 \, \text{eV}$), the differential cross-section of the elastic scattering becomes singular and their model turns out to be inapplicable.

The first and still only one published experiment dealing with measuring the absolute values and forms of the anomalous elastic X-ray radiation scattering process as a function of the photon energy and scattering angle in the immediate energy region of the $1s$-shell ionization threshold with a high

scattered photon energy resolution ($\propto 25\,\mathrm{eV}$) is realized using the metallic molybdenum (Mo: $\omega_K = 20,008\,\mathrm{eV}$) in the work by Hribar *et al* (1984) [42]. The differential cross-section for scattering is measured in the photon energy region $\omega_K - 200(\mathrm{eV}) \leq \omega \leq \omega_K + 300\,(\mathrm{eV})$. The characteristic monochromatic X-ray radiation is used. The nonlinear structure of the differential cross-section is determined in the energy region of the ionization $K-$threshold. The authors do not interpret the results of the experiment.

Using the synchrotron linearly polarized X-ray radiation (DESY; Hamburg, Germany) in the photon energy region $21,2\,\mathrm{keV} \leq \omega \leq 43,7\,\mathrm{keV}$ in the work by Smend *et al* (1987) [43] the absolute values and forms of the differential cross-section for the elastic angle scattering $\theta = 60°$, $90°$, $120°$, $180°$ of the X-ray photon by atoms Kr ($\omega_K = 14,327\,\mathrm{eV}$) and Xe ($\omega_K = 34,561\,\mathrm{eV}$) in the gas phase are measured for the first time in scientific practice. Outside the anomalous dispersing areas of the scattering the calculation results of the authors (the relativistic Kissel-Pratt algorithm) fit well (the difference does not exceed $5 \div 10\,\%$) overall with the experimental ones. The measurement and calculation in the immediate energy region of the ionization $K-$thresholds of the atoms Kr and Xe are not performed.

In the work by Kane *et al* (1987) [44] the differential cross-sections are measured for elastic $125°$ angle scattering of the X-ray photon with a fixed energy $88,03\,\mathrm{keV}$ by the metallic Al ($\omega_K = 1,560\,\mathrm{eV}$), Au ($\omega_K = 80,729\,\mathrm{eV}$), Pb ($\omega_K = 88,006\,\mathrm{eV}$), and Bi ($\omega_K = 90,527\,\mathrm{eV}$). In the context of the relativistic Kissel-Pratt algorithm, we can find that the difference between theory and experiment amounts to 40% in the anomalous dispersing elastic scattering region in case of Pb ($\omega - \omega_K \approx 24\,\mathrm{eV}$). In case of Bi ($\omega - \omega_K \approx 2,5\,\mathrm{keV}$) it amounts to 50%. It is the authors' opinion that the mentioned divergences can be concerned with the fact that the relativistic Kissel-Pratt algorithm uses the one-electron basis of the wave functions taking no account of atom self-consistent field distortion, when the deep virtual vacancy appears, and ignores the finite values of the $1s$-vacancy decay width. In the more recent work by Basavaraju *et al* (1995) [45] the authors performed measurements and calculations and came to the conclusion that the divergence between theory and experiment decreases to 20% in the case of Pb and to 24% in the case of Bi.

In the work by Bhattacharyya *et al* (1988) [46] the differential cross-sections are measured for elastic angle scattering ($\theta = 8,9°$; $12,6°$; $14,2°$; $17,7°$) of the X-ray photon with a fixed energy $59,54\,\mathrm{keV}$ by the metallic Cu ($\omega_K = 8,980\,\mathrm{eV}$), Ag ($\omega_K = 25,520\,\mathrm{eV}$), Sn ($\omega_K = 29,204\,\mathrm{eV}$), Ta ($\omega_K = 67,419\,\mathrm{eV}$), Au ($\omega_K = 80,729\,\mathrm{eV}$), and Pb ($\omega_K = 88,006\,\mathrm{eV}$). Wide disagreements are detected between experimental results and theory (relativistic Kissel-Pratt algorithm) at the narrow scattering angles ($\leq 12,6°$). These disagreements amount to 45% in case of Ta atom. The authors do not determine the causes of the mentioned disagreements.

Casnati *et al* (1990) [47] measured the differential cross-sections for elastic angle scattering ($\theta = 60°$; $90°$; $120°$) of the X-ray photon with a fixed energy

59,54 keV by the metallic Al, V ($\omega_K = 5,463\,\text{eV}$), Mo, Cd ($\omega_K = 26,711\,\text{eV}$), Sn, and Pb. They did not detect any noticeable discrepancy with the results of the relativistic Kissel-Pratt algorithm at such marked distance of the scattered photon energy from the energies of the deep 1s-shell ionization thresholds of the researched elements.

In the work by Shahi *et al* (1998) [48] the differential cross-sections are measured for elastic angle scattering ($\theta = 121°$) of the X-ray photon with a fixed energy 59,54 keV by the elements with nuclear charge $12 \leq Z \leq 92$: 42 elements from Mg ($\omega_K = 1,305\,\text{eV}$) till U ($\omega_K = 115,606\,eV$). The difference between experimental findings and the results of the relativistic Kissel-Pratt algorithm amounted to 12% for the element Er ($\omega_K = 57,486\,\text{eV}$) with the K-ionization threshold energy being nearest to the incident photon energy. The authors establish a fact of divergences with the modified form factor approximation and the relativistic Kissel-Pratt algorithm for all analyzed elements, but they do not determine the causes of the mentioned divergences.

Elyaseery *et al* (1998) [49] measured the differential cross-sections for elastic angle scattering ($\theta = 145°$; $154°$; $165°$) of the X-ray photon with fixed energies 13,95; 17,75; 26,36 and 59,54 keV for the elements Cu, Zn, Zr, Nb, Mo, Ag, Cd, In, Sn, Ta, and W. The authors did not manage to measure the scattering cross-sections at the photon energy 17,75 keV for Zr ($\omega_K = 17,998\,\text{eV}$) and 26,36 keV for Cd ($\omega_K = 26,711\,\text{eV}$). The results of the experiments are compared with the modified relativistic form factor approximation algorithm, the description of the anomalous dispersing scores. The divergence between theory and experiment amounted to 10%. The authors did not determine the causes of the mentioned divergences.

In the work by Rao *et al* (1999) [50] the differential cross-section are measured for elastic angle scattering $\theta = 90°$ of the X-ray photon with fixed energies 5,41; 6,40; 6,93; 7,47 and 8,04 keV for heavy elements with nuclear charge $46 \leq Z \leq 82$: Pd, Ag, Cd, In, Sn, Sb, Pt, Au, and Pb. The divergence between the experimental findings and the results of the relativistic Kissel-Pratt algorithm amounted in particular to 12% in the ionization $L-, M-$thresholds area of the elements Pt ($\omega(L_1) = 13,880\,\text{eV}$; $\omega(M_1) = 3,296\,\text{eV}$), Au ($\omega(L_1) = 14,353\,\text{eV}$; $\omega(M_1) = 3,425\,\text{eV}$), and Pb ($\omega(L_1) = 15,861\,\text{eV}$; $\omega(M_1) = 3,851\,\text{eV}$). The authors did not analyze the divergence causes.

Kumar *et al* (2001) [51] performed precision measurements of the differential cross-sections for elastic angle scattering $\theta = 125°$ of the photon with energy 88,03 keV for 17 elements with nuclear charge $30 \leq Z \leq 92$. The divergence between the experimental findings and the results of the relativistic Kissel-Pratt algorithm amounts to 10%. The experimental findings are 28 times smaller for Pb ($\omega_K = 88,006\,\text{eV}$) and 31% greater for Bi ($\omega_K = 90,527\,\text{eV}$) in comparison with the form factor approximation modified for accounting of anomalous dispersing scores. The authors did not determine the divergence causes.

Mandal *et al* (2002) [52] measured the differential cross-sections for elastic angle scattering $\theta = 90°$ of the X-ray photon with a fixed energy 22,1 keV for 20 elements with nuclear charge $22 \leq Z \leq 82$. The experimental findings are compared with the calculation results in the modified form factor approximation and in the relativistic Kissel-Pratt algorithm. The divergences are determined in particular with the last-mentioned: the experimental findings are 16% greater for Nb ($\omega_K = 18,986$ eV), 29% greater for Mo ($\omega_K = 20,008$ eV), and 8% greater for Pb ($\omega_K = 88,006$ eV). Following the conclusions of the work [53] (the measurements are performed and the results are analyzed in theory for the differential cross-section of the elastic and Compton X-ray photon scattering with the energy $11 \div 22$ keV by light atoms ^{2}He and ^{10}Ne), the authors connected the divergences with the fact that the mentioned theoretical models do not consider first of all the nonlocality effects of the exchange self-consistent atomic potential and the electron correlation, and in that way they require a more precise definition.

1.2.3 Study of the Atomic form Factor Structure

When describing the differential cross-section of the elastic photon scattering by an atom, its form factor (the structure function) plays a large role. It is a value (1.3) that determines the probability amplitude of the contact (without virtual reorganisation of the many-electron system) photon-atom interaction.

For the development of the many-particle quantum theory of the process in relation to form factor it is necessary to solve two main problems. The first problem lies in the necessity to study the influence of the many-particle effects in the ground state of the atom on the analytic structure, value, and configuration of its form factor. As the ground state of most of the elements in the Mendeleev's table is not spherically symmetric, the second problem is the need to study the influence of the nonsphericity effects of the open-shell atoms on the analytic structure, value, and configuration of their form factors. However , the degree to which the traditionally used procedure is validated to substitute the form factor of the examined atom [26, 37] or its ion [29, 31] for their analogs of the spherically symmetric (term $^1S_0$) approximation (1.4) or its relativistic variant (1.10) needs to be ascertained.

The influence of electron correlations in the ground state of the atom on the analytic structure, value, and configuration of its form factor is studied for light elements for the first time theoretically in the work by Kim and Inokuti (1968) [54] (atom He) and in the works by Brown (1970) [55] (atom He), (1970) [56] (atoms Li and Be), (1972) [57] (atom C), (1974) [58] (atom B and ion C^{1+}). The results of these works led to the conclusion that at least for the examined elements the accounting for correlation effects changes the absolute values of the one-electron approximation form factors not more than $1 \div 2\%$, when describing the wave function of the atomic ground state. The role of correlation effects in the X-ray energy region of the atomic deep shell ionization thresholds is not investigated.

The theoretical studies of the generic analytic structure of the *open*-shell ground-state atom form factor are absent in published works. In Chapter 2 of our treatise, we pursue the pioneering studies in this field.

There is no experimental study of the spectral characteristics of the anomalous elastic X-ray photon scattering by a molecule in the gas-phase. However, the results of numerous investigations of the X-ray photon-molecule absorption resonance and near-edge structure spectra let us suppose the inevitable existence of complex resonance structure of its differential cross-section for anomalous elastic scattering. This structure is determined first through formation of the virtual resonance photoabsorption states in the energy regions of the ionization thresholds of deep molecular orbitals.

This supposition is confirmed in the work by Gel'mukhanov and Ǎgren (1997) [59]. The nonrelativistic quantum theory of the resonance elastic X-ray photon scattering by a free molecule, first published in scientific literature, is presented by the authors in this work. The theory is developed in the context of the quantum mechanical perturbation theory (Kramers-Heisenberg-Waller formula) for the anomalous dispersing items of the process probability amplitude. The form factor part of the scattering amplitude is taken, when $\kappa = 0$, as the nonrelativistic limit of the expression (1.10), where $\rho(\boldsymbol{r})-$ is now the function of the electron density distribution in the molecule. The calculation of the $f'-, f''-$functions and the differential cross-sections for the anomalous elastic scattering is performed for the linear-polarized X-ray photon taking into consideration the finite values of the deep vacancies decay widths in the energy region of the $1s$-shell ionization threshold of carbon ($\omega_K = 284, 20\,\text{eV}$) and oxygen ($\omega_K = 543, 10\,\text{eV}$) atoms in the CO molecule. The many-particle and orientation effect are not examined.

1.3 Statement of the Study Problems

Thus, the following situation has been formed in the problem solving of the development of the many-particle quantum theory of the anomalous elastic X-ray photon scattering by free atoms, an ion, and a molecule, before the present work of the authors appears:

1. The measurements of the real and imaginary part of the process probability amplitude in the energy region of the deep $1s$-, $2s$-, $2p$-shell ionization thresholds for a number of atoms of the crystalline solid lattice show a complicated near and extended structure of the functions f' and f''. The attempts to describe in theory the results of the experiments within the bounds of the existing and above mentioned atomic models lead to $20 \div 40\%$ disagreement among the absolute values of the functions f' and f'' in theory and experiment. The causes of the disagreement are not determined. Nevertheless, exceeding the limits of the atomic models for extracting information about structure in the solid body experiments, as

well as the information reliability are inevitably determined by knowledge of the atomic constituent of the spectral characteristics measured in the process.

The atomic models represented in the review surely cannot separate in theory the contribution of the solid-state effects to the order of the mentioned disagreements between theory and practice. Finally, as the energy of the incident upon the crystal X-ray photon approaches the energy region of the deep shell ionization thresholds of the lattice atoms, it is necessary to exceed the limits of the one-electron approximation (one-configuration Hartree-Fock approximation) in order to take into consideration the wide hierarchy of the many-particle effects when describing the atomic constituent in theory.

2. The measurement results of the absolute values and forms of the differential process cross-sections for a number of atoms in the normal scattering regions agree well with the theoretical ones. In the energy region of the deep $1s$-shell ionization thresholds, we can discover the wide disagreement (up to $\sim 50\%$) between theory and experiment. The causes of the disagreement are not determined.

3. The differential process cross-section for an atom in immediate proximity to the energy of its deep $1s$-shell ionization threshold as the energy function of the elastic scattered X-ray photon is measured for the metallic molybdenum [42]. The results of the experiment are not construed. Similar experiment needs to be used as a test for the many-particle quantum theory of the differential elastic scattering cross-section developing in this treatise.

4. The calculations of the absolute values and forms are performed, and the nonlinearity of the probability amplitude and differential process cross-sections is determined for a number of free atoms and atomic ions in the regions adjacent to the anomalous dispersing region. There is no theoretical study of the immediate anomalous dispersing regions of the elastic scattering for atoms. For atomic ions, the fact is established that the giant resonance of the elastic scattering differential cross-section appears in the energy region of the deep $1s-$shell ionization threshold. However the absolute intensity values of the scattering resonance and the many-particle effects are not examined.

5. The many-particle effect of the nonzero decay width of the virtual deep atom vacancy and atomic ion is very important for the resonance structure formation of the anomalous elastic scattering differential cross-section;but its role is not studied in theory. Moreover, for both the quantum theory of the photoabsorption process and the quantum theory of the anomalous elastic X-ray photon scattering by an atom we cannot accept the problem, that deals with describing and accounting of the many-particle effect of the post-collision interaction as a quantum interference of the radial and angle restructuring effects of the photoelectron wave function and its electrostatic interaction with Auger-electron in Auger-decay state of the virtual deep vacancy as being solved. This problem requires a precision theoretical

investigation. There is a need to make such investigation mainly for light atoms with the nuclear charge $Z \leq 20$, where life span of the deep virtual vacancies is generally [60,61] determined through the auto ionization decay channels of Auger type.

6. The generic analytical form factor structure of the *open*-shell atom is not determined in the ground state. The results are: (a) how the nonsphericity effect of the atom influences the theoretical absolute values and forms of its form factor and the differential cross-sections of the anomalous elastic X-ray photon scattering by it is not examined; (b) there is no theoretical study, to find whether if substitution of the form factor of any given atom for its spherically symmetrical analog, as is traditionally used in scientific literature is justified.

7. The influence of the electron correlation in the atom ground state on the value of the spherically symmetrical form factor of the one-electron approximation for the light atoms (He, Li, Be, B and C) is analyzed in theory. The energies of the deep shell ionization thresholds for these atoms are much lower than the X-ray lower range limit ($\sim$350 eV). There is no theoretical study for the atoms having at least one of the deep shell ionization thresholds in the X-ray energy range of the scattered photon.

8. The nonrelativistic variant of the quantum theory of elastic X-ray photon scattering by a free nonoriented in space molecule [59] is developed. The theory is not summarized in order to account for (a) orientation and many-particle effects and (b) analytical structure of the free molecule form factor *beyond* the scope of its presentation through the electron inventory in a molecule.

The study of the problems mentioned above and, as a result, the development of the *many-particle* quantum theory and analysis methods for the absolute values and forms of the differential cross-section of the anomalous elastic X-ray photon scattering by a free atom, atomic ion, and molecule in the *gas*-phase form the contents of the present treatise.

2

Many-Particle Effects at Anomalous Elastic X-Ray Photon Scattering by an Atom and an Atomic Ion

As noted in Chap. 1, the modern theoretical models for describing the elastic X-ray photon scattering by an atom led to wide disagreements with the experiment in the energy region of the deep shell ionization thresholds, ignoring the wide hierarchy of the many-particle effects.

In this chapter, we develop the nonrelativistic *many-particle* quantum theory of the X-ray photon scattering process in the energy region of the atom and the atomic ion deep shell ionization thresholds.

In Part 2.1, the analytic structure of the process cross-section is represented. The analytic form factor structure of the open-shell atom in the ground state and the calculation data for a number of such atoms are given in Part 2.6. In Part 2.2, the hierarchy of the many-particle effects is analyzed. In Part 2.3, the process amplitude is physically interpreted and the question regarding photon scattering phase and number is examined. In Part 2.4, the computational algorithm for the process cross-section is represented. In Part 2.5, the correlation structure of the atom form factor in the X-ray scattering region is studied. In Part 2.7, the calculation data of the scattering cross-sections for a number of atoms are represented in the context of the theory developed in Parts 2.1–2.6. In Part 2.8, the theory is adapted to the cross-section construction of the anomalous elastic X-ray photon scattering by an atomic ion. In Part 2.9, the elastic scattering indicatrix in the anomalous dispersing X-ray photon energy region is studied. At the end of the chapter the findings are represented.

2.1 Analytic Structure of the Differential Process Cross-Section

We shall construct the differential cross-section (1.1) in *four stages*. At the first stage, we shall construct the process amplitude. The construction is realized in the context of the multiconfiguration wave functions conception of scattering states. In order to expound the developing theory, we reproduce

the results of the quantum scattering theory [62–64]. At the second stage, we shall concretize the scattering amplitude structure as it is presented in the *secondary quantization* of the electromagnetic field. At the third stage, we shall examine the analytic form factor structure of the closed-shell atom in the ground state. Finally, at the fourth stage, we shall note the resultant expression for the differential process cross-section.

2.1.1 Construction of the Process Probability Amplitude

Let us find the probability of the elastic photon scattering by an atom. For this purpose, we shall ascertain the solution of the Schrödinger equation:

$$i\frac{\partial}{\partial t}\psi = \hat{H}(t)\psi,$$
$$\widehat{H}(t) = \widehat{H}_a + \widehat{V}(t), \tag{2.1}$$

for the weight factors a_m of the wave functions of the orthonormal basic states in the complete wave function in the form of

$$\psi = |j_t\rangle + \sum_m a_m |m_t\rangle;$$
$$|j_t\rangle = |O_t\rangle \cdot \hat{a}_f^+ |O_f\rangle, \quad t \in [0; \infty). \tag{2.2}$$

In (2.1) the Hamiltonian of the atom

$$\hat{H}_a = -\sum_{n=1}^{N}\left(\Delta_n/2 + r_n^{-1}Z\right) + \sum_{k>n}^{N}|\mathbf{r}_k - \mathbf{r}_n|^{-1}$$

and the atom-external electromagnetic field interaction operator are determined (see Part 1.1.1)

$$\widehat{V}(t) = \widehat{H}_1(t) + \widehat{H}_2(t); \tag{2.3}$$
$$\widehat{H}_1(t) = -(1/c)\sum_{i=1}^{N}(\mathbf{p}_i \cdot \mathbf{A}_i); \quad \mathbf{A}_i \equiv \mathbf{A}(\mathbf{r}_i; t);$$
$$\widehat{H}_2(t) = (1/2c^2)\sum_{i=1}^{N}(\mathbf{A}_i)^2.$$

In (2.2), the summation is over all basic states of an atom + radiation quantum system, including the radiative vacancy decay channels in the $|m_t\rangle$ − state structure. The symbols are also introduced: $|O_t\rangle$ − is the wave function of the atom ground state (Fermi vacuum); $|O_f\rangle$ − is the wave function of the photon vacuum; $\hat{a}_f^+$ − is the photon creation operator.

Meeting the conditions

$$i\frac{\partial}{\partial t}\left|O_t\right\rangle = \hat{H}_a\left|O_t\right\rangle; \tag{2.4}$$

$$i\frac{\partial}{\partial t}\left|m_t\right\rangle = \hat{H}\left(0\right)\left|m_t\right\rangle, \tag{2.5}$$

we extract from (2.1) and (2.2) the differential equation for the weight factors:

$$i\frac{d}{dt}a_m = \left\langle m_t\right|\hat{V}\left(t\right)\left|j_t\right\rangle + \sum_n a_n\left\langle m_t\right|\hat{V}\left(t\right) - \hat{V}\left(o\right)\left|n_t\right\rangle. \tag{2.6}$$

Let us solve it rough, setting aside the sum and including the perturbance (ω is the absorbed photon energy)

$$\hat{V}(t) \rightarrow \hat{V}^{\lambda}(t) = \hat{V}(0)\exp\left(-i\omega t + \lambda t\right), \quad \lambda > o.$$

Let us factor the wave functions of the basic states in time:

$$\left|O_t, m_t\right\rangle \rightarrow \left|O, m\right\rangle\exp\left(-iE_{o,m}t\right).$$

Then passing to the limit $\lambda \rightarrow 0$, we obtain the well-known *Fermi golden rule* for the transition probability of an atom + radiation quantum system from the state $\left|j\right\rangle$ to the state $\left|m\right\rangle$:

$$W_{mj} = \frac{d}{dt}\left|a_m\right|^2 = 2\pi\left|Q_{mj}\right|^2\delta\left(E_m - E_0 - \omega\right). \tag{2.7}$$

The expression (2.7) holds the amplitude structure of the photon scattering by an atom:

$$Q_{mj} = <m\left|\hat{V}\left(0\right)\right|j>; \ \left|j\right\rangle = \left|j_{t=0}\right\rangle. \tag{2.8}$$

Let us define concretely the amplitude structure (2.8). For this purpose, we shall find the wave function of the state $\left|m\right\rangle$ in the form of

$$\left|m\right\rangle = \left|j\right\rangle + \mathop{S}_{n>f}\beta_{nj}\left|n\right\rangle, \quad \mathop{S}_{n>f} \equiv \sum_{n>f}^{\infty}\int_0^{\infty}dn, \tag{2.9}$$

where the fulfillment of the conditions is required

$$\hat{H}(0)\left|m\right\rangle = E_m\left|m\right\rangle; \tag{2.10}$$
$$\hat{H}_a\left|j\right\rangle = E_0\left|j\right\rangle; \tag{2.11}$$
$$\hat{H}^*\left|n\right\rangle = E_n\left|n\right\rangle; \quad \hat{H}^* = \hat{H}_a + \hat{H}_1(0). \tag{2.12}$$

However we did not require the fulfillment of the conditions (2.11) and (2.12) on the Hamiltonian of an atom + radiation quantum system. As a result, the states $\left|j\right\rangle$ and $\left|n\right\rangle$ turn out to be virtual (nonobservable) in the elastic scattering process.

In order to find the weight factors β_{nj} in (2.9) we have to determine the expression for the energy of the $|n\rangle$ − state. We shall find the wave function of this state in the form of:

$$|n\rangle = |n_0\rangle + \underset{\alpha,b}{S}\, \eta^b_{\alpha n} \left|\alpha^b\right\rangle + \underset{R,l}{S}\, q^l_{Rn} \left|R^l\right\rangle . \tag{2.13}$$

The following is here determined: the wave functions of the excitation/ionization $|n_0\rangle$ − states of the atom nl-shell, of the $\left|\alpha^b\right\rangle$ − states of the Auger (b-channel) decay of the nl-vacancy with the weight factors $\eta^b_{\alpha n}$, and of the $\left|R^l\right\rangle = \left|R^l_a\right\rangle \cdot \hat{a}^+_{fl} |O_f\rangle$ − states of the radiative (l-channel) decay of the nl-vacancy with the weight factors q^l_{Rn}, $\left|R^l_a\right\rangle$ − is the atom part of the wave function, $\hat{a}^+_{fl}$ − is the creation operator of the photon with a f-frequency on the l-channel decay.

We shall neglect the intrachannel confounding in (2.13). It will lead to diagonal energy matrices on the $\widehat{H}^*$ − operator

$$\langle n_o| \widehat{H}^* |m_o\rangle = E^{(0)}_n \delta_{nm};$$
$$\left\langle\alpha^b\right| \widehat{H}^* \left|\beta^c\right\rangle = E^b_\alpha \delta_{\alpha\beta} \delta_{bc}; \tag{2.14}$$
$$\left\langle R^l\right| \widehat{H}^* \left|L^k\right\rangle = E^l_R \delta_{RL} \delta_{lk}.$$

Taking into consideration the known operator equation $\underset{\varepsilon \to 0}{\lim} (x \pm i\varepsilon)^{-1} =$ $\mathrm{P}\left(1/x\right) \mp i\pi\delta\left(x\right)$, for the energy of the $|n\rangle$ – state we obtain from (2.12)–(2.14) the expression:

$$E_n = \mathrm{Re}\, E_n - i\Gamma_n/2; \tag{2.15}$$
$$\mathrm{Re}\, E_n = E^{(0)}_n + \mathrm{P}\left\{ S_{\alpha,\beta} \frac{\left|h^b_\alpha\right|^2}{E_n - E^b_\alpha} + S_{R,l} \frac{\left|\xi^l_R\right|^2}{E_n - E^l_R} \right\};$$
$$h^b_\alpha = \langle n_o| \widehat{H}^* \left|\alpha^b\right\rangle; \quad \xi^l_R = \langle n_o| \widehat{H}^* \left|R^l\right\rangle;$$
$$\Gamma_n = \Gamma^A_n + \Gamma^R_n;$$
$$\Gamma^A_n = 2\pi \sum_b \left|h^b_\alpha\right|^2,\ E_n = E^b_\alpha;\ \Gamma^R_n = 2\pi \sum_l \left|\xi^l_R\right|^2,\ E_n = E^l_R.$$

The Auger (A) and radiative (R) components of the total decay width of the $|n_0\rangle$ − state vacancy are here determined.

Returning to the wave function (2.9) and taking into consideration (2.10)–(2.12) and (2.15) for β_{nj} we obtain the equation:

$$\beta_{nj}\left(E_j - \mathrm{Re}\, E_n + i\Gamma_n/2\right) \cong V_{nj}, \tag{2.16}$$
$$V_{nj} = \langle n_0| \hat{V}(0) |j\rangle .$$

Considering (2.9) and (2.16), we have the desired analytic expression for the scattering amplitude (2.8) in the form of:

$$Q = \langle j | \hat{V}(0) | j \rangle + \underset{n>f}{S} \frac{V_{jn} V_{nj}}{E_j - \mathrm{Re}\, E_n + i\Gamma_n/2}. \qquad (2.17)$$

The formula (2.17) *reconstitutes* the known result of the quantum scattering theory [62–64].

Let us pass on to the second stage of the construction. We shall define concretely the amplitude (2.17) in the context of the *secondary quantization* of the electromagnetic field (1.7).

We shall take into consideration the structure of the perturbation operator (2.3) and of the expression for the matrix elements of the photon creation and annihilation operators in the context of the occupation $n_{k\eta}-$numbers [12]:

$$\langle n_{k\eta} - 1 | \hat{a}_{k\eta}^- | n_{k\eta} \rangle = \sqrt{2\pi c^2 n_{k\eta}/\omega V},$$

$$\langle n_{k\eta} + 1 | \hat{a}_{k\eta}^+ | n_{k\eta} \rangle = \sqrt{2\pi c^2 (n_{k\eta} + 1)/\omega V}.$$

Then, to the *dipole* approximation for the Fourier components of the field operator (1.7), we obtain:

$$Q = (\boldsymbol{e}_1 \cdot \boldsymbol{e}_2) \left\{ F(\theta; \omega) + a \underset{n>f}{S} \omega_n \sigma(\omega_n) (C_{1n} - i\pi C_{2n}) \right\}; \qquad (2.18)$$

$$(\boldsymbol{e}_1 \cdot \boldsymbol{e}_2) F(\theta; \omega) = \left\langle j \left| \hat{H}_2(O) \right| j \right\rangle;$$

$$C_{1n} = \frac{\Delta \omega_n}{(\Delta \omega_n)^2 + \gamma_n^2} - \frac{1}{\omega + \omega_n};$$

$$C_{2n} = (\gamma_n/\pi) \left[\frac{1}{(\Delta \omega_n)^2 + \gamma_n^2} + \frac{1}{(\omega + \omega_n)^2} \right];$$

$$\omega_n = \mathrm{Re}\, E_n - E_o; \quad \Delta \omega_n = \omega - \omega_n;$$

$$\gamma_n = \Gamma_n/2; \quad a = \left(4\pi^2 c r_o \right)^{-1}.$$

In (2.18), we considered the connection of the length and speed forms for the radiative transition operator [65] and the expression for the cross-section of the phototransition [10] (length form) from the $|m\rangle$-state with the energy E_m to the $|n\rangle$-state with the energy E_n:

$$\sigma(\omega_{nm}) = (4/3)\, \pi^2 \alpha a_0^2 \frac{1}{q_m} \omega_{nm} \left| \langle n | \sum_{i=1}^{N} \boldsymbol{r}_i | m \rangle \right|^2;$$

$$\omega_{nm} = E_n - E_m; \qquad (2.19)$$

where q_m is the statistical weight of the $|m\rangle$-state.

In our study, we shall mainly examine the elastic X-ray photon scattering by an atom (an ion) with the $^1S_0$ -term of the ground state. In this situation, we shall find the probability amplitude of the single excitation/ionization of the atom $n_1 l_1 -$ shell. We shall keep in mind the structure of the matrix

element of the radiation transition $Q^{(k)}$-operator to the approximation of the LS-bonding [66]:

$$\left\langle n_1 l_1^{N_1}, LSJ \left\| Q^{(k)} \right\| n_1 l_1^{N_1-1} n_2 l_2 L_1' S_1', L'S'J' \right\rangle$$

$$= (-1)^{l_2+L_1'-S-J'} \sqrt{N_1 [L, L', J, J']} \delta_{SS'} \left(l_1^{N_1} LS \left\| l_1^{N_1-1} (L_1' S_1') l_1 \right. \right) \cdot$$

$$\left\{ \begin{matrix} l_1 & L & L_1^l \\ L' & l_2 & k \end{matrix} \right\} \left\{ \begin{matrix} L & J & S \\ J' & L_2 & k \end{matrix} \right\} \left\langle n_1 l_1 \left\| Q^{(k)} \right\| n_2 l_2 \right\rangle .$$

Then, if we define concretely the values

$$k = 1; N_1 = 4l_1 + 2; LSJ \to {}^1 S_0; \ L'S'J' \to {}^1 P_1; \ L_1' S_1' \to {}^2 l_1;$$

$$\left(l_1^{4l_1+2} 00 \left\| l_1^{4l_1+1} ({}^2 l_1) l_1 \right. \right) = 1;$$

$$\left\langle n_1 l_1 \left\| Q^{(1)} \right\| n_2 l_2 \right\rangle = (-1)^{l_1+g} \sqrt{l_{\max}} \{l_1 1 l_2\} \left\langle n_1 l_1 \left| \hat{r} \right| n_2 l_2 \right\rangle;$$

$$\left\{ \begin{matrix} 0 & 0 & 0 \\ 1 & 1 & 1 \end{matrix} \right\} = \frac{1}{\sqrt{3}}; \quad \left\{ \begin{matrix} l_1 & 0 & l_1 \\ 1 & l_2 & 1 \end{matrix} \right\} = \frac{1}{\sqrt{3(2l_1+1)}} \cdot (-1)^{l_1+l_2+1};$$

we obtain for the desired amplitude

$$\left\langle n_1 l_1^{4l_1+2}, {}^1 S_0 \left\| Q^{(1)} \right\| n_1 l_1^{4l_1+1} n_2 l_2, {}^1 P_1 \right\rangle = (-1)^{l_1+g} \sqrt{2l_{\max}} \left\langle n_1 l_1 \left| \hat{r} \right| n_2 l_2 \right\rangle .$$

The following is denoted here: $[x] \equiv 2x + 1$, $l_{\max} = \max(l_1, l_2)$, $2g$ is the even-numbered condition and $\{l_1 1 l_2\}$ − is the *triad* ones.

The expression for the cross-section $n_1 l_1 \to n_2 l_2$ of the phototransition (2.19) assumes the form:

$$\sigma(\omega) = (4/3) \pi^2 \alpha a_0^2 \omega \, (Ry) \, l_{\max} \left| \langle n_1 l_1 \left| \hat{r} \right| n_2 l_2 \rangle \right|^2 .$$

For the general nl-shell of the atom, the use of the length or speed forms of the radiation transition operator should be followed by taking into consideration the correlation influence (if it is appreciable) of the random phase approximation with an exchange (see Part 2.2.3) for the theoretical scattering amplitudes (2.18).

2.1.2 Form Factor of the Closed-Shell Atom

To complete the statement we shall reproduce the result (1.4) as the third stage for the construction of the elastic scattering differential cross-section by using the methods of the irreducible tensor operator theory.

Let us write the exponent expansion in (1.3) by the $C_p^{(t)}$ -spherical functions ($t \geq 0$, $p = -t, \ldots, t$):

$$\exp[i(\boldsymbol{q} \cdot \boldsymbol{r})] = \sum_{t,p} (-1)^p i^t (2t+1) j_t(qr) C_{-p}^{(t)}(\boldsymbol{q}) C_p^{(t)}(\boldsymbol{r}) . \qquad (2.20)$$

We consider the Wigner–Eckart theorem for the matrix element $T_p^{(t)} = C_p^{(t)}(r) j_t(qr)$ of the operator:

$$\langle \gamma_2 J_2 M_2| T_p^{(t)} |\gamma_1 J_1 M_1\rangle = \varphi \begin{pmatrix} J_2 t\, J_1 \\ -M_2 p M_1 \end{pmatrix} \langle \gamma_2 J_2 | \left\| T^{(t)} \right\| |\gamma_1 J_1\rangle ; \quad (2.21)$$

$$\phi = (-1)^{J_2 - M_2} .$$

We also consider that $C_0^{(0)} = 1$ and for the scalar $(t = 0)$ operator $\langle \gamma_2 J_2| |j_0(qr)| |\gamma_1 J_1\rangle \to \sum\limits_{nl} N_{nl} \langle nl| j_0(qr) |nl\rangle$, is realized, where the following is determined: $|nl\rangle$ is the radial part of the wave function of the nl-electron and N_{nl} is the occupation number of the atom nl-shell.

Then, from (1.3) we obtain (1.4), where $\sin(kr)/kr = j_0(kr)$.

In (2.20), the $j_t(qr)$-spherical t-order Bessel function of the first kind is determined. In (2.21), the γ-set of quantum numbers, that characterizes along with JM the atomic state.

We realize the fourth stage of the construction and write the differential cross-section in the form we shall use in the following.

Inserting the expression (2.18) into (1.1), we obtain finally:

$$\frac{d\sigma}{d\Omega} = r_0^2 (\boldsymbol{e}_1 \cdot \boldsymbol{e}_2)^2 \left\{ \left(F(\theta; \omega) + \eta \sum_{nl \leq f} R_{nl} \right)^2 + \left(\eta \sum_{nl \leq f} I_{nl} \right)^2 \right\}; \quad (2.22)$$

$$R_{nl} = \sum_{m>f} A_{nl,m} W_{Rm}^{nl} + \sum_{k=1} \int_0^\infty dD_{nl}^k W_{Rk}^{nl}; \quad (2.23)$$

$$I_{nl} = \sum_{m>f} \omega_m A_{nl,m} W_{mI}^{nl} + \gamma_{nl} \sum_{k=1} \int_0^\infty dD_{nl}^k W_{Ik}^{nl}; \quad (2.24)$$

$$W_{Rm}^{nl} = \omega_m \varepsilon_m \left(1 + \varepsilon_m^2\right)^{-1} - \gamma_{nl} (1 + \omega/\omega_m)^{-1};$$

$$W_{Rk}^{nl} = \Delta\omega_k[(\Delta\omega_k)^2 + \gamma_{nl}^2]^{-1} - (\omega + \omega_k)^{-1};$$

$$W_{mI}^{nl} = \left(1 + \varepsilon_m^2\right)^{-1} + \gamma_{nl}^2 (\omega + \omega_m)^{-2};$$

$$W_{Ik}^{nl} = [(\Delta\omega_k)^2 + \gamma_{nl}^2]^{-1} + (\omega + \omega_k)^{-2};$$

$$dD_{nl}^k = (\omega_k/\pi) \sigma_{nl}^k \prod_{i=1}^k d\varepsilon_i;$$

$$\varepsilon_m = \Delta\omega_m/\gamma_{nl}; \quad \Delta\omega_k = \omega - \omega_k; \quad \gamma_{nl} = \Gamma_{nl}/2;$$

$$\omega_k = \operatorname{Re} E(\varepsilon_1....\varepsilon_k) - E_o; \quad \eta = 1,4327 \cdot 10^{-2} \left(eV^{-1} \times Mb^{-1}\right).$$

For the transitions to the discontinuous spectrum, the value $A_{nl,m} = \sigma_{nl}(\omega_m)/\pi\gamma_{nl}$ is here determined and the ionization k-repetition factor is denoted too. $E(\varepsilon_1....\varepsilon_k) -$ is the energy of state, $\sigma_{nl}^k \equiv \sigma_{nl}(\varepsilon_1....\varepsilon_k) -$ is the cross-section of the atom k-divisible photoionization.

In (2.22) the expression in the braces is dimensionless, but the dimension of the elastic scattering differential cross-section is r_0^2/sr.: $r_0^2 = 7,941 \cdot 10^{-26} cm^2$; $d\Omega = \sin\theta d\theta d\varphi$, $\theta \in [0;\pi]$, $\varphi \in [0;2\pi]$. $\theta-, \varphi-$ are angles of the spherical coordinate system. They are interpreted from the physical standpoint as the scattering angle and the angle between the axle OX and the scattering plane (the plane going through the wave vectors of the incident and scattering photon).

2.2 Anomalous Dispersion Kramers–Heisenberg–Waller Terms: Qantum Interference of the Many-Particle Effects

The interference of the scattering amplitudes does not lead the total scattering cross-section to be represented as a sum of partial (atom shell) cross-section. So, theoretically describing the cross-section of the elastic photon scattering by an atom, we face the quantum interference of all the many-particle effects hierarchy forming the probability amplitude of the process.

In this part of our treatise, we present the physical state and the methods for the theoretical description of the mentioned many-particle effects hierarchy when scattering the X-ray photon in the energy region of the atom deep shell ionization thresholds.

2.2.1 Electron Shells Radial Rearrangement Effect

It is found that the main many-particle effect having influence on the theoretical photon absorption cross-section in the energy region of the atom deep shell ionization threshold, is the effect of the radial relaxation of the atomic core electron shells in the field of the deep vacancy [67].

The appearance of the deep nl-vacancy mainly leads the *outer* shells of the atomic core to react (decreasing distinctly their midradius) to the destruction of the nl^{4l+2}−"screen" between them and the atomic core. The shifting of the electron density of the atomic core shells to the atomic centre is accompanied by the additional *de*localization of the photoelectron wave function. The result of such delocalization is the photoionization probability amplitude contraction.

Adding the effect of the radial relaxation presupposes two problems to be solved – the computation of the one-electron wave functions of the initial and final phototransition states and the matrix elements of the physical quantities operators.

So, the problem algorithm can be divided into two steps. Let us describe them step by step.

Computation of the one-particle states wave functions. We shall write down the $\psi-$ wave function of the N-electron atom in the form of the antisymmetrized product of the one-electron $\phi_\alpha-$ wave functions:

$$\psi = (N!)^{-1/2} \det \|\phi_\alpha\|. \tag{2.25}$$

Then solving the problem of minimizing the energy functional of the atomic state we arrive at the Hartree-Fock equation [10]:

$$\left(\hat{h} - 2Q_{nl} - \varepsilon_{nl}\right)|nl\rangle = X_{nl} + L_{nl}, \tag{2.26}$$

for $|nl\rangle \equiv P_{nl}(r)$ radial part of the $\phi_\alpha-$ wave function (Y is an angular and χ is a spin parts)

$$\phi_{nls}^{m_l m_s} = \frac{1}{r} Y_{m_l}^l (\theta; \varphi) \chi_{m_s}^s (\sigma) |nl\rangle, \tag{2.27}$$

$$\langle nl | n'l' \rangle = \delta_{nn'} \delta_{ll'}. \tag{2.28}$$

In (2.26) ε_{nl} – is the energy of the nl-electron and the functionals are determined:

$$L_{nl} = \frac{2}{N} \sum_{n' \neq n} \lambda_{nl,n'l} |n'l\rangle, \tag{2.29}$$

$$rQ_{nl} = \frac{1}{N} \sum_k \Phi_{nl}^{(k)} - Z, \tag{2.30}$$

$$\Phi_{nl}^k = \sum_{n'l'} (1 + \delta_{nl,n'l'}) f_{ll'}^{(k)} Y_{n'l',n'l'} \tag{2.31}$$

$$rX_{nl} = \frac{2}{N} \sum_k \sum_{n'l' \neq nl} g_{ll'}^{(k)} Y_{nl,n'l'}^{(k)} |n'l'\rangle, \tag{2.32}$$

and the differential as well

$$\hat{h} = d^2/dr^2 - l(l+1)/r^2. \tag{2.33}$$

The functionals (2.30) and (2.32) accordingly define the straight (local) and exchange (nonlocal) parts of the electrostatic potential for the nl-electron.

The nondiagonal Lagrange multiplier λ in (2.29) ensures the fulfillment of the condition (2.28).

In (2.30)–(2.32) the radial integral

$$Y_{nl,n'l'}^{(k)} = \left(\int_0^r [r_1/r]^k + \int_r^\infty [r/r_1]^{k+1}\right) P_{nl}(r_1) P_{n'l'}(r_1) dr_1$$

is indicated, Z is the nuclear charge, $f_{ll'}^{(k)}-, g_{ll'}^{(k)}-$ are the angular coefficients.

The (2.26) equation is solved numerically, since the analytical solution by modern mathematical methods is impossible, if the number of electrons in the atom $N > 2$. The main difficulty in getting an analytical solution is determined by the *nonlocality* of the *exchange* part (3.32) of the Hartree–Fock potential.

In order to consider the correlation effects, the atom wave function can be built in the form of the linear combination of the wave function (2.25) with the wave functions of the excitation/ionization states of the atom:

$$\Phi_{LS} = S_n \alpha_n^{LS} \psi_n^{LS}.\tag{2.34}$$

The solution of the variational problem with the wave function (2.34) leads to the Hartree–Fock–Jucys multiconfiguration equation [68] for the nl-orbital. The solution of this equation is an exceptionally intricate problem. One of the ways to simplify it is by the *method of the configuration mixing*. In this situation the one-electron wave functions are determined not by the solution of the Hartree–Fock–Jucys equation, but by the solution of the equations (2.26) for each configuration from the $\{\psi_n^{LS}\}$ – set in (2.34). The simplified version of this method – the approximation of the "frozen core" – is the most-used. In this approximation, the orbitals obtained for the wave function of some fixed ψ_n^{LS} – configuration are "frozen" and used for building of all basic set in (2.34).

In our work we shall turn to the multiconfiguration approximation in the context of the method of configuration mixing (Chaps. 2–4).

The variation principle as applied to the study of the upper state ψ_n faces the challenge of the condition agreement (2.28) and the orthogonality claim

$$\langle \psi_n | \, \psi_m \rangle = 0 \tag{2.35}$$

of the state ψ_n to the state ψ_m of *the same* symmetry if $E_m < E_n$, where $E_{n,m}$ is the energy states $\psi_{n,m}$.

The rejection of the condition (2.28) for the orbitals of one symmetry from different configurations leads to using the *nonorthogonal orbitals*. In this case, the Hartree–Fock–Jucys equations are appreciably complicated. To keep the orthogonality ψ_n to ψ_m without turning to the solution of the Hartree–Fock–Jucys equations we can use the Gram–Schmidt orthogonalization algorithm [69, 70]. According to this algorithm, if we want to meet the condition (2.35), we have to change from the radial orbitals $P_{kl}^{(n)}$ to the radial orbitals:

$$\tilde{P}_{kl}^{(n)} = \alpha_{kk'}^{nm} \left(P_{kl}^{(n)} - \left\langle P_{kl}^{(n)} \middle| P_{k'l}^{(m)} \right\rangle P_{k'l}^{(m)} \right);$$

$$\alpha_{kk'}^{nm} = \left[1 - \left\langle P_{kl}^{(n)} \middle| P_{k'l}^{(m)} \right\rangle^2 \right]^{-1/2}; \tag{2.36}$$

that fulfils the orthogonality condition $\left\langle \tilde{P}_{kl}^{(n)} \middle| P_{k'l}^{(m)} \right\rangle = 0$.

Calculation of the transition probability amplitudes. Using the nonorthogonal orbitals makes the analytical structure of the radiation transition lose simplicity. Such structure was determined for the first time in the work [71] and is of the form of (length form):

$$\langle \psi_a | \sum_{i=1}^{N} \hat{r}_i | \psi_b \rangle = (D_{aa} D_{bb})^{-1/2} \sum_{i,j=1}^{N} \langle a_i | \hat{r} | b_j \rangle D_{ab} (a_i b_j). \tag{2.37}$$

In (2.37) the wave functions of the transition states are defined through the one-electron orbitals:

$$|\psi_a(x_1, x_2, ... x_N)\rangle = (D_{aa}N!)^{-1/2} \det \|a_i(x_j)\| \,;$$
$$|\psi_b(x_1, x_2, ... x_N)\rangle = (D_{aa}N!)^{-1/2} \det \|b_i(x_j)\| \,;$$

where $D_{ab} = \det \|\langle a_i| b_j\rangle\|$ is the determinant of the orbital overlap integral and $D_{ab}(a_i b_j) -$ is the algebraic complement to the element $\langle a_i| b_j\rangle$ in the determinant D_{ab}.

In the scheme of the genealogical coefficients [65, 66], when constructing the wave functions of the transition states, the result (2.37) was confirmed in the works [72, 73]. In accordance with the formula (2.37) the authors of these works obtained for the transition amplitude (length form):

$$R_{n_1 l_1 n_2 l_2} = S \sum_{n_i} \sum_{n_j} (-1)^{2-\delta_{n_1 n_i}-\delta_{n_2 n_j}} C_{ij}^{12} Q_j; \qquad (2.38)$$

$$C_{ij}^{12} = \langle n_i l_1| \hat{r} | n_j l_2\rangle \frac{\langle n_1 l_1| n_i l_1\rangle \langle n_j l_2| n_2 l_2\rangle}{\langle n_i l_1| n_i l_1\rangle \langle n_j l_2| n_j l_2\rangle}; \qquad (2.39)$$

$$Q_j = 1 - \sum_{n_i \neq n_j, l} \frac{\langle n_j l| n_i l\rangle \langle n_i l| n_j l\rangle}{\langle n_i l| n_i l\rangle \langle n_j l| n_j l\rangle}; \qquad (2.40)$$

$$S = \prod_i \langle n_i l_i| n_i l_i\rangle^{q_i};$$

$$\langle n_1 l| n_2 l\rangle = \int_0^\infty P_{n_1 l}(r) P_{n_2 l}(r) dr; \quad \langle n_1 l_1|\hat{r}|n_2 l_2\rangle = \int_0^\infty P_{n_1 l_1}(r) P_{n_2 l_2}(r) r dr;$$

$\delta_{\alpha\beta}$ – is the Kronecker–Weierstrass symbol; q_i – is the smaller of numbers of shell occupation of transition configurations.

Both the nonrelativistic and the relativistic calculations of the matrix elements of the physical quantities operators using the methods of the nonorthogonal orbitals theory demonstrate (see Part 2.7.1) that the value (2.40) can be saved out to a high degree of precision as:

$$Q_j \to 1. \qquad (2.41)$$

2.2.2 Multiple Atomic Excitation/Ionization Effect

In the energy region of the atom deep shell ionization threshold, the effect of the radial relaxation results in the decrease of the photoabsorption intensity value, calculated on the basis of wave functions of the *un*reconstructed atomic core electrons. The losing of intensity in such a way can be first reconstructed by considering the process of multiple excitation/ionization of the atomic ground state. We shall restrict ourselves in our work to the analysis of the excitation/ionization process of $\kappa = 2$ multiplicity. The reason is as follows.

In the works [74–79], the near-edge photoabsorption fine structure spectra were experimentally ascertained first for the atoms ^{10}Ne [74] (KL_{23}-structure), ^{11}Na [75, 76] (KM_1-structure), ^{18}Ar [77] (KM_{23}-structure) and ^{36}Kr [78,79] (KN_{23}-structure). In the works [80–82], the results of these experiments ([80] ^{10}Ne, [80, 81] ^{11}Na, [80] ^{18}Ar, [82] ^{36}Kr) were first interpreted in theory and it was demonstrated that the processes of $\kappa = 2$ multiplicity contribute significantly to the intensity of the multiple excitation/ionization. The scientific works that followed (see, e.g., [83, 84]) confirmed this result.

In order to describe in theory the cross-section of the double excitation/ionization of the atomic ground state that belongs to the scattering cross-section structure (2.22), we have to solve two problems -1) to construct the wave functions of the double excitation/ionization states and 2) to calculate the photoabsorption cross-section.

We shall describe this algorithm for the radiation transitions to the states with a deep $1s$-vacancy and a vacancy in the valence n_1l_1-shell $1\,s^{-1}n_1l_1^{-1}$ $n_2l_2n_3l_3$ ($n_1 = f;\ n_{2,3} > f$). These transitions will exactly play a leading part when describing the near-edge fine structure of the scattering cross-sections of the atoms studied in our work.

Constructing the wave functions of the final states. It consists of two stages. At the first stage the radial orbitals of the core and excited electrons are found out by solving the Hartree–Fock (2.26) for each configuration from the set $\{1\,s^{-1}n_1l_1^{-1}n_2l_2n_3l_3\}$. At the second stage the base wave functions are constructed:

$$|\alpha LS\rangle = \left|1s^{-1}n_1l_1^{-1}\left(L_0S_0\right)n_2l_2n_3l_3\left(\bar{L}\bar{S}\right);LS\right\rangle; \qquad (2.42)$$

where as α the totality of the intermediate moments and configurations is denoted. Finally, by solving the defining equation

$$\sum_{\alpha'} a_{\alpha\alpha'}\left\{\langle\alpha'LS|\,\hat{W}\,|\alpha LS\rangle - \left(E - E_k\right)\delta_{\alpha\alpha'}\right\} = 0; \qquad (2.43)$$

the energies of steady-state conditions and their wave functions are found out

$$|ELS\rangle = \sum_{\alpha} a_{\alpha E}\,|\alpha LS\rangle. \qquad (2.44)$$

In (2.43) $\hat{W} = \hat{H}_c - \hat{V}\left(K\right),\ \hat{H}_c-,\ \hat{V}\left(K\right)-$ are operators of the Coulomb interaction and Hartree–Fock potential of K configuration.

Let us define the described algorithm concretely for the atoms studied in our work. The wave function (2.44) for the closed-shell atoms in the ground state is obtained in the form:

$$\psi\left(^1P_1\right) = \sum_{n_{1,2}>f}\sum_{LS}\sum_{l_{1,2}}a_{12}^{LS}\left|1s^{-1}fp^{-1}\left(^{2S+1}P\right)n_1l_1n_2l_2\left(LS\right);{}^1P_1\right\rangle. \quad (2.45)$$

In case of an argon atom the region of absorption K-spectrum in the photon energy $\omega \leq 3228\,\text{eV}$ is described through the wave function (2.45).

If $\omega \geq 3237\,\text{eV}$, the fine structure spectrum is mainly determined through radiation transition to the final state with a wave function of the form:

$$\Psi\left({}^1P_1\right) = \sum_{n_{1,2}>f} \left\{ \sum_{LS} a_{12}^{LS} \left|A_{12}^{LS}\right\rangle + \sum_{n>f} b_{12}^n \left|B_{12}^{LS}\right\rangle \right\}; \qquad (2.46)$$

$$\left|A_{12}^{LS}\right\rangle = \left|1s^{-1}3s^{-1}\left({}^{1,3}S\right)n_1sn_2p\,(LS)\,;{}^1P_1\right\rangle;$$

$$\left|B_{12}^{LS}\right\rangle = \left|1s^{-1}3p^{-2}\left({}^1D\right)nd[{}^2S]n_1sn_2p;{}^1P_1\right\rangle.$$

The configuration mixing in (2.46) describes the so-called dynamic dipole polarization effect [85] of the valence $3p$-shell through the excitations $3p^2 - 3snd$.

In (2.45), for a neon atom (for atoms ^{18}Ar and ^{36}Kr the main quantum numbers of the valence fp-shell and the excited s-, p- electrons are increased by one and two correspondingly) the excitations are taken into consideration:

$$n_1l_1n_2l_2 = \left\{ \begin{array}{c} 3p3p \\ 3p4p \\ 3p5p \end{array} \right\}, \left\{ \begin{array}{c} 3s3d \\ 3s4d \end{array} \right\}, \left\{ \begin{array}{c} 3d3d \\ 3d4d \end{array} \right\}, \left\{ \begin{array}{c} 3s3s \\ 3s4s \end{array} \right\}. \qquad (2.47)$$

In the intermediate and short-wave region of the near-edge scattering fine structure K-spectra the radiation transitions to the constant spectrum state are considered as well:

(a) excitation/ionization

$$1\,sfp - np\varepsilon p \;\left({}^{10}Ne,\; {}^{18}Ar,\; {}^{36}Kr,\; {}^{54}Xe\right);$$
$$1\,sfs - np\varepsilon s, \, ns\varepsilon p \;\left({}^{11}Na\right); \qquad (2.48)$$

(b) double ionization

$$1\,sfp - \varepsilon p\varepsilon' p \;\left({}^{10}Ne,\; {}^{18}Ar,\; {}^{36}Kr,\; {}^{54}Xe\right). \qquad (2.49)$$

The states (2.46) are submerged in the constant spectrum of the states (2.48) and (2.49), but their interference is not taken into consideration in our work.

The calculation of the wave functions of photoabsorption final states for a natrium atom differs from that for neon, argon, and krypton atoms. The difference is connected with the fact that the main contribution to the photoexcitation intensity in the region of the near-edge scattering fine structure K-spectrum of the natrium atom is made by excitations of the peripheral $3s$-electron. Then, while calculating we can restrict ourselves to considering the configurations with three $1\,s$-, n_1l_1-, n_2l_2-incomplete shells:

$$\psi\left({}^2P_{3/2}\right) = \sum_{n_{1,2}>f} \sum_{LS} a_{12}^{LS} \left|1s^{-1}n_1l_1\,(LS)\,n_2l_2;{}^2P_{3/2}\right\rangle; \qquad (2.50)$$

$$l_1l_2 = \{sp\}, \, \{pd\}.$$

In the defining (2.43), the state energy of the K-configuration is calculated from the formula:

$$E_K \rightarrow E_{12}^{LS} = E_{12} - \left\langle \hat{W}_{12} \right\rangle + W_{12}^{LS} - \tilde{E}. \tag{2.51}$$

E_{12} is the state energy of the K-configuration which is averaged over the term values of $(n_1l_1n_2l_2)$-pairs of excited electrons; $\left\langle \hat{W}_{12} \right\rangle$ is the averaged over the terms interaction energy of the excited electron pairs; W_{12}^{LS} is the energy of electron-electron interaction depending on term; $\tilde{E}-$ is the energy of the arbitrarily fixed state, where the energy count starts (2.51).

Then, the energies of the photon absorbed by an atom are calculated from the formula:

$$\omega \rightarrow \omega_{12}^{LS} = E_{12}^{LS} - \left(E(0) - \tilde{E} \right); \tag{2.52}$$

where $E(0)$ is the energy of the atomic ground state.

Account for the correlation effects leads to the *decrease* of electron–electron interaction and as a result to the "compression" on the energy scale of the photoabsorption theoretical spectrum. For neon, argon, and krypton atoms such decrease is equivalent to the conversion of values E_{12}^{LS} from (2.52) and nondiagonal $W_{\alpha\alpha'}^{LS} \equiv \left\langle \alpha'LS \left| \hat{W} \right| \alpha LS \right\rangle -$ elements in (2.43):

$$E_{12}^{LS} \rightarrow m^{-1}E_{12}^{LS} + \left(\frac{1-m}{m} \right) \left(E_{12} - \tilde{E} \right); \quad W_{\alpha\alpha'}^{LS} \rightarrow m^{-1} W_{\alpha\alpha'}^{LS}; \tag{2.53}$$

where $m = 1,5$; $1,4$ and $1,3$ for neon, argon, and krypton correspondingly.

For the natrium atom the decrease of the electron–electron interaction is not deduced from the formula (2.53), but calculated [87] by methods of the correlation Feynman diagrams [88].

Photoabsorption cross-section. The probability amplitude of the phototransition to the states (2.44)

$$A_{ELS} = \sum_{\alpha} a_{\alpha E} \left\langle \alpha LS | Q^{(1)} | 0 \right\rangle \tag{2.54}$$

as a matrix element of the operator

$$Q^{(1)} = e \sum_{i=1}^{N} \boldsymbol{r}_i \tag{2.55}$$

determines the intensity of the double photoexcitation of the atom

$$I_{ELS} (\omega) = 2\sigma_{ELS} (\omega) / \pi \Gamma_{n_1l_1};$$
$$\sigma_{ELS} (\omega) = \frac{4}{3}\pi^2 \alpha a_0^2 \omega \left| A_{ELS} \right|^2; \tag{2.56}$$

where $\Gamma_{n_1l_1}-$ is the total width of the n_1l_1- vacancy decay.

In case of excitation/ionization the value $\sigma_{ELS} (\omega)$ in (2.56) coincides with the process cross-section, and in case of double ionization it determines the integrand in the expression for the cross-section of the atom double

photoionization:

$$\sigma_{ELS}(\omega) = \int\limits_{0}^{\omega - IP_{12}} \sigma_{ELS}(\omega; \varepsilon)\, d\varepsilon; \qquad (2.57)$$

where $IP_{12}-$ is the energy of the atom double ionization threshold.

The angular and radial structures of the matrix elements of the transition operator (2.55) in the amplitude (2.54) are obtained in the works [80,82]. If we consider the radial relaxation effect and the approximation of the LS-connection, these structures have in the dipole approximation the form:

1. for $1\,snp \to npn'p$ transitions in the atoms ^{10}Ne, ^{18}Ar, ^{36}Kr and ^{54}Xe:

$$\left\langle n_1 l_1^{4l_1+1} n_2 l_2^{4l_2+1} (LS)\, nl_2 n'l_2\, (L'S),\, {}^1P_1 \left\| Q^{(1)} \right\| O, {}^1S_0 \right\rangle$$
$$= (-1)^{l_1+l_2+S}\, N \sqrt{l_{\max}[L, L', S]\,(1+\delta_{nn'})^{-1}} \cdot \begin{Bmatrix} l_2 & L' & l_2 \\ 1 & l_1 & L \end{Bmatrix} \cdot$$
$$\cdot \left[\left(nl_2 \left\| \hat{d} \right\| n_1 l_1 \right) \langle n'l_2 \mid n_2 l_2 \rangle + (-1)^{L'+S} \left(n'l_2 \left\| \hat{d} \right\| n_1 l_1 \right) \langle nl_2 \mid n_2 l_2 \rangle \right];$$

2. for $1\,sns \to npn's$ transitions in the atom ^{18}Ar:

$$\left\langle n_1 l_1^{4l_1+1} n_2 l_1^{4l_1+1} (LS)\, nl_2 n'l_1\, (L'S),\, {}^1P_1 \left\| Q^{(1)} \right\| O, {}^1S_0 \right\rangle$$
$$= (-1)^{l_1+l_2+S}\, N \sqrt{l_{\max}[L, L', S]} \cdot \begin{Bmatrix} l_1 & L' & l_2 \\ 1 & l_1 & L \end{Bmatrix} \cdot$$
$$\cdot \left[\left(nl_2 \left\| \hat{d} \right\| n_1 l_1 \right) \langle n'l_1 \mid n_2 l_1 \rangle + (-1)^{L+S} \left(nl_2 \left\| \hat{d} \right\| n_2 l_1 \right) \langle n'l_1 \mid n_1 l_1 \rangle \right];$$

3. for $1\,s3s \to npn's$ transitions in the atom ^{11}Na:

$$\left\langle n_1 l_1^{4l_1+1} n'l_1 (LS)\, nl_2,\, {}^2\bar{L} \left\| Q^{(1)} \right\| n_1 l_1^{4l_1+2} n_2 l_1,\, {}^2l_1 \right\rangle$$
$$= (-1)^{l_1+l_2+L}\, N \sqrt{\frac{1}{2} l_{\max}[L, \bar{L}, S]} \cdot \begin{Bmatrix} l_1 & l_2 & 1 \\ \bar{L} & l_1 & L \end{Bmatrix} \cdot \left(nl_2 \left\| \hat{d} \right\| n_1 l_1 \right)$$
$$\langle n'l_1 \mid n_2 l_1 \rangle + N \sqrt{2 l_{\max}[l_1]}\, \delta_{SO}\, \delta_{LO} \left(nl_2 \left\| \hat{d} \right\| n_2 l_1 \right) \langle n'l_1 \mid n_1 l_1 \rangle.$$

The following values are here determined: N is the product of the overlap integrals of the wave functions of the electrons that are not involved in the transition; $\left| O, {}^1S_0 \right\rangle$ is the wave function of the atom ground state; $[x] \equiv 2x+1$; $l_{\max} = \max(l_1, l_2)$ the matrix element of the transition one-electron operator (the length form)

$$\left(n_2 l_2 \left\| \hat{d} \right\| n_1 l_1 \right) = \langle n_2 l_2 \left| \hat{r} \right| n_1 l_1 \rangle - \sum_{n_1 \angle n \angle f} \frac{\langle n_2 l_2 \mid nl_2 \rangle \langle nl_2 \left| \hat{r} \right| n_1 l_1 \rangle}{\langle nl_2 \mid nl_2 \rangle}.$$

2.2.3 Correlation Effects of the Random Phase Approximation with Exchange and Auger and Radiative Decay of the Deep Vacancy

In the energy region of the atom deep shells ionization thresholds the autoionization effects (without photon radiation) of two types play important roles: the correlation effect of the *random phase approximation with exchange* (RPAE) [67], the deep vacancy Auger decay effect [89], and the deep vacancy radiative (with photon radiation) decay effect as well [90].

The RPAE correlations are determined through the electrostatic interaction of the atom deep nl-shell excitation/ionization channel with the atom core $m(l \pm 1)-$ shells ionization channels. At the same time, the RPAE correlations keep the deep vacancy as the metastable state of the atom + radiation quantum system. The observable state of this system is already realized through the Auger and radiative decays of the deep shell.

As already mentioned in the introduction to Part 2.2, the RPAE correlations and the effects of the deep shells Auger and radiative decays during elastic photon scattering by an atom interfere at the virtual level.

The degree of this interference is determined by the vacancy position in the atomic core. So, the Auger and radiative vacancy decay widths in the outer shells do not exceed 10^{-6} eV. In this case, we can neglect the Auger and radiative decay effects when constructing the transition amplitudes and consider only the RPAE correlations. But if we have for example, atoms with a nuclear charge $Z \geq 10$, the strong spatial and energy apartness of the deep $1s$-shell from the other shells of the atomic core permits neglect of the RPAE correlations influence on the theoretical cross-section of the photon absorption by the atomic $1s$-shell.

The situation can be changed in a workmanlike manner if $n = m$. Precisely this case is realized if we deal with the $2s$-shell photoionization of the argon atom [91, 92]. The spatial and energy nearness of the deep $2s$- and $2p$-shells here make the RPAE correlations **interfere** distinctly with both $2s$-vacancy Auger and radiative decay effects and with the electron shells radial relaxation effect in the field of the $2s$-vacancy. This case is analyzed in Part 2.7 of our treatise when we describe in theory the elastic X-ray photon scattering cross-section in the energy region of the $2s$-shell ionization threshold of the argon atom.

The correlation effect of the random phase approximation with exchange. The differential cross-section of the atom nl-shell photoionization in the RPAE methods has the form [67] for example in case of the linear polarization of the absorbed photon:

$$\frac{d\sigma_{nl}(\omega)}{d\Omega} = \frac{4\pi^2 N_{nl}}{c\,\omega\,(2l+1)} \sum_{l_{1,2}} D_{ll_1} D_{ll_2} \psi_{l_1 l_2} F_{l_1 l_2}(\theta, \phi); \qquad (2.58)$$

$$\psi_{l_1 l_2} = i^{l_1 - l_2} \exp[i(\delta_{l_1} - \delta_{l_2})]; \quad l_{1,2} = l \pm 1;$$

$$F_{l_1 l_2}(\theta, \phi) = \sum_m \begin{pmatrix} l_1 & 1 & l \\ -m & 0 & m \end{pmatrix} \begin{pmatrix} l_2 & 1 & l \\ -m & 0 & m \end{pmatrix} Y_m^{l_1}(\theta, \phi) Y_m^{l_2}(\theta, \phi).$$

The ionization amplitude here is in accord with the integral equation:

$$D_{ll_1} = d_{ll_1} + \frac{1}{3} \left(\underset{\alpha \leq f, \beta > f}{S} - \underset{\alpha > f, \beta \leq f}{S} \right) D_{\alpha\beta} U_{ll_1}^{\alpha\beta} E_{\alpha\beta}^{-1}. \tag{2.59}$$

In the expressions (2.58) and (2.59) the following values are defined: ω is the absorbed photon energy; c is the velocity of light; Ω is the solid angle; θ, φ are the angles of the spherical coordinate system; δ_{l_1} – is the elastic scattering phase of the εl_1-electron in the atomic core field; N_{nl} – is the electron number in the absorbing shell; the matrix element of the radiative transition one-electron operator (length form)

$$d_{ll_1} = \omega[(2l+1)(2l_1+1)]^{1/2} \cdot \begin{pmatrix} l & 1 & l_1 \\ 0 & 0 & 0 \end{pmatrix} \langle nl | \hat{r} | \varepsilon l_1 \rangle;$$

the matrix element of the electron-electron interaction $\widehat{V}$-operator (if $j \to l$)

$$U_{jn}^{i\gamma} = 2 \left(ij \left\| \hat{V}_l \right\| \gamma\eta \right) - (2l+1) \sum_{l' \geq 0} (-1)^{l+l'} \begin{Bmatrix} l_i & l & l_\gamma \\ l_j & l' & l_\eta \end{Bmatrix} \left(ij \left\| \hat{V}_{l'} \right\| \gamma\eta \right); \tag{2.60}$$

the energy denominator

$$E_{\alpha\beta} = \varepsilon_\alpha - \varepsilon_\beta + \omega + i(1 - 2n_\beta)\Delta;$$
$$\Delta \to 0; \quad n_\beta = \{1, \beta \leq f; \ 0, \beta > f\}.$$

The physical interpretation of the amplitude (2.59) in the Goldstone–Hubbard–Feynman diagrams formalism is presented in the work [67] (see the work [94] for the matrix element (2.60) too).

The deep vacancy Auger and radiative decay effects. The vacancy lifetime in the atom deep nl-shell

$$\tau_{nl} = \hbar \Gamma_{nl}^{-1}; \quad \Gamma_{nl} = \Gamma_{nl}^A + \Gamma_{nl}^R; \tag{2.61}$$

is in inverse proportion to the total width of its Auger and radiative channels decay

$$\Gamma_{nl}^A = 2\pi \sum_i \left| \langle nl^{-1} | \hat{H} | A_i \rangle \right|^2;$$

$$\Gamma_{nl}^R = 2\pi \sum_j \left| \langle nl^{-1} | \hat{P} | R_i \rangle \right|^2. \tag{2.62}$$

In (2.62) the following is defined: $\hat{P} = \sum\limits_{k=1}^{N} \hat{\boldsymbol{p}}_k -$ is the radiative transition operator, $\left|nl^{-1}\right\rangle -$ is the wave function of the state with an nl-vacancy, $|A_i\rangle -$ and $|R_j\rangle -$ are the wave functions of the Auger and radiative nl-vacancy decay states and the summation is over the decay channel number.

According to construction in Part 2.1, the value (2.61) determines the non-zero imaginary part of the energy denominator of the elastic scattering amplitude (2.17). In that way, from the mathematical standpoint the role of the virtual deep vacancy Auger and radiative decay effects during the elastic X-ray photon scattering by an atom consists in the fact that they remove the singularities of the real (2.23) and imaginary (2.24) parts of the scattering probability amplitude during photon resonance (see $\Delta\omega_k = 0$ in (2.22)) absorbing by an atom.

We constructed the theory of the elastic photon scattering by an atom in Part 2.1 to the approximation when the following effects are ignored: (a) the effects of the radial reconstruction of the photoelectron wave function when transiting from the atom deep shell excitation/ionization state to the deep vacancy Auger and radiative decay state; (b) the effects of the electrostatic photoelectron-Auger-electron interaction. These effects are combined in scientific literature under the common name of the **post-collisional interaction effect**. Chapter 3 of our treatise is dedicated to the problem of theoretical description of this effect and to argumentation of the approximation we made.

2.3 Physical Interpretation of the Process Probability Amplitude

The scattering (2.17) amplitude structure constituents can be interpreted from the physical standpoint as follows.

The probability amplitude $\left\langle j \left| \hat{V}(0) \right| j \right\rangle$ determines the form factor structure of the atom (1.3). The amplitude of such elastic scattering type can be explained as the probability amplitude of the photon-atom *contact* interaction (two photon lines converge to the Goldstone–Hubbard–Feynman diagram vertex), that is described through the quadratic part regarding the electromagnetic field operator

$$\hat{H}_2(0) = \left(1/2c^2\right) \sum_{i=1}^{N} \left(\boldsymbol{A}_i\right)^2; \quad \boldsymbol{A}_i \to \boldsymbol{A}\left(\boldsymbol{r}_i; 0\right);$$

of the complete Hamiltonian of the atom + radiation quantum system.

The probability amplitude

$$\underset{n>f}{S} V_{jn} V_{nj} \left(E_j - \operatorname{Re} E_n + i\Gamma_n/2\right)^{-1} \tag{2.63}$$

describes the elastic photon scattering by an atom in its *reorganizing* on the virtual level and determines the structure of the anomalous dispersion Kramers–Heisenberg–Waller terms of the scattering overall amplitude. The amplitude of such elastic scattering type can be interpreted as the probability amplitude of formation and following disappearance of the endless set of the atom + radiation quantum system excitation/ionization *virtual* states. This amplitude is described through the linear part regarding the electromagnetic field operator

$$\hat{H}_1 (0) = -\frac{1}{c} \sum_{i=1}^{N} (\boldsymbol{p}_i \cdot \boldsymbol{A}_i); \quad \boldsymbol{A}_i \to \boldsymbol{A} (\boldsymbol{r}_i; 0);$$

of the complete Hamiltonian of the atom + radiation quantum system.

In the energy region of the incident photon $E_j \to \operatorname{Re} E_n$, the amplitude (2.63) becomes the dominant part of the scattering overall amplitude. So, the inner structure of the mentioned endless set determines the main features of the *anomalous* elastic X-ray photon scattering by an atom.

2.3.1 Goldstone–Hubbard–Feynman Diagrams Formalism

Considering the endless set of the atom + radiation quantum system excitation/radiation, virtual states presupposes the summation of the endless *functional* series of the evolution $\widehat{S}$-operator expansion [7, 12] in electromagnetic interaction constant $\alpha = e^2/\hbar c = 1/137$. In the modern stages of the quantum electrodynamics development, the solution of such problem seems to be impossible. But considering the many-particle effects in the elastic X-ray photon scattering by an atom is meant to solve exactly **this** problem.

In the works [95–99] the following approximation to the solution of this problem is formulated. If we continue to be in the context of the perturbation theory for the scattering amplitude (2.17), we can consider the many-particle effects in twostages. In the first stage we transit from the wave functions one-electron basis of the atom ground states configuration to the basis that is nonorthogontal to it. This basis is reconstructed in the field of one (or more) vacancy (Parts 2.2.1, 2.2.2). In the second stage the configuration mixing method is realized (Part 2.2.1). In this way, the summation of the mentioned series is unnecessary, because the required transition amplitudes (and the Goldstone–Hubbard–Feynman diagrams corresponding with them) appear by themselves.

Actually, let us consider the values V_{jn} in (2.63) in the Goldstone–Hubbard–Feynman diagrams formalism [100]. Then we obtain the diagram representation in Fig. 2.1 for the anomalous dispersion part (2.63) of the scattering amplitude (1.2). This representation shows all main topological types of the many-particle correlations diagrams: (a) the F_1 block describes the interference of the RPAE correlations and the electron shells radial relaxation
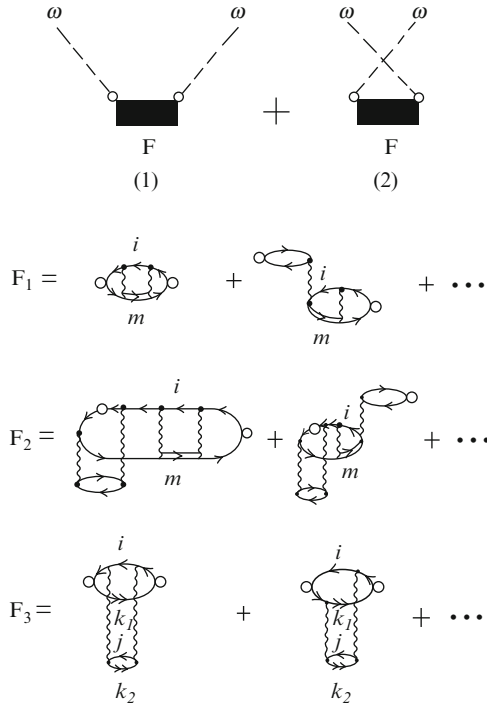
Fig. 2.1. The direct (1) and exchange (2) parts of the anomalous dispersion amplitude of the photon scattering (2.17) by an atom in Goldstone–Hubbard–Feynman diagrams representation [97]; ω is the scattering photon energy; $F = F_1 + F_2 + F_3 + \ldots$; *line* – the state is obtained in the configuration field of the atom ground state; *double line* – the state is obtained in the i-vacancy field; *the double arrows line* – the state is obtained in the i- and j-vacancy field. The $F_{1,2,3}$ structures are explained from the physical standpoint in the text. The time-sequential routine of the virtual processes is from left to right. The points stand for the infinite diagrams series

effect in the i-vacancy field; (b) the F_2 block describes the *interference* of the radial relaxation effects and the vacuum correlations (excitation/ionization of Fermi-vacuum before the photon absorbing by an atom); (c) the F_3 block describes the effects of the atom ground state multiple excitation/ionization $|0\rangle + \omega \rightarrow i^{-1}j^{-1}k_1k_2$.

Keep in mind that ignoring the photon exchange process (see the diagrams block (2) in Fig. 2.1) in the $f'-$ real component of the scattering amplitude (1.16) leads to appreciable errors in calculating the scattering cross-section (2.22). So, the calculation for the neon atom [95, 96] showed that the calculation error in the photon energy region $400 \div 800$ eV (the energy of the $1s$-shell ionization threshold is $I_{1s} = 870, 10$ eV) amounts to 40%. The magnitude of calculation error does not exceed 1% in the case of $f''-$ imaginary component.

2.3.2 About the Scattered Photon Phase and Number

We shall finish our review of Part 2.3 with marking the problem of scattered photons phase and number measurement.

Describing the process of the elastic photon scattering by an atom we can come to a conclusion (in contrast to the classical description [101,102]), that it is impossible to measure some physical quantities *simultaneously*. We describe this fact as applied to the problem of the scattered photon phase and number measurement.

In the work [103] (see also [104, 105]), for the variables {photon phase is (φ); photon number (N)} the following equivocation correlations are first determined:

$$\Delta N \cdot \Delta C \geq \frac{1}{2} \langle S \rangle ; \tag{2.64}$$

$$\Delta N \cdot \Delta S \geq \frac{1}{2} \langle C \rangle . \tag{2.65}$$

The hermitian operators of the cosine and sine of the photon phase and number are here defined

$$\widehat{C} = \frac{1}{2} \left(\widehat{E}_- + \widehat{E}_+ \right) = \widehat{C}^+ ; \quad \widehat{S} = \frac{1}{2} \left(\widehat{E}_- - \widehat{E}_+ \right) = \widehat{S}^+ ; \tag{2.66}$$

$$\widehat{E}_- = \left(\widehat{N} + 1 \right)^{-1/2} \widehat{a}; \quad \widehat{E}_+ = \widehat{a}^+ \left(\widehat{N} + 1 \right)^{-1/2}; \tag{2.67}$$

$$\widehat{N} = \widehat{a}^+ \widehat{a}; \tag{2.68}$$

in the eigen wave functions $(\alpha, \alpha' -$ are normalization factors$)$

$$|\psi_c\rangle = \alpha \sum_{n=0}^{\infty} \sin \left[(n+1) \varphi \right] |n\rangle; \tag{2.69}$$

$$|\psi_s\rangle = \alpha' \sum_{n=0}^{\infty} [e^{i(n+1)\phi} - e^{-i(n+1)(\phi-\pi)}] |n\rangle; \tag{2.70}$$

$$|n\rangle = (n!)^{-1/2} \left(\widehat{a}^+ \right)^n |0\rangle ; \quad \langle n \mid n \rangle = 1; \tag{2.71}$$

$$\langle \psi_c \mid \psi_c' \rangle = \langle \psi_s \mid \psi_s' \rangle = \delta \left(\phi - \phi' \right) ;$$

with eigenvalues:

$$\widehat{C} |\psi_c\rangle = \cos \varphi \cdot |\psi_c\rangle ; \quad \widehat{S} |\psi_s\rangle = \sin \varphi \cdot |\psi_s\rangle ; \quad \widehat{N} |n\rangle = n |n\rangle ;$$

$$\widehat{a} |n\rangle = n^{1/2} |n-1\rangle ; \quad \widehat{a}^+ |n\rangle = (n+1)^{1/2} |n+1\rangle . \tag{2.72}$$

However, the linear hermitian operator cannot be compared [105] with the photon phase in the Hilbertian space. So, the elastic scattered photon phase turns out to be physically nonobservable (immeasurable) and defines only

the mathematical structure of the weighting factor of n-photon states in the photon systems wave functions (2.69) and (2.70). In (2.64), (2.65) the following is denoted: $\langle C \rangle$, $\langle S \rangle$ − are the matrix elements of the operators (2.66)–(2.68) in the states (2.69) and (2.70); $\hat{a}^{+}$ $(\hat{a})$ − is the photon birth (annihilation) operator. In (2.71) and (2.72), $|n\rangle$ − is the wave function of the $n-$photon states of the *Fock space* and $|0\rangle$ − is the wave function of the photon vacuum.

According to (2.64) and (2.65), the transition from the classical to the quantum description is followed by the *loss* of the possibilityof measuring *simultaneously* the quantities N and φ. Actually, if we try to measure for example the scattered photon phase ($\Delta C \to 0$; $\Delta S \to 0$), we can lose all information about the scattered photon number ($\Delta N \to \infty$). Let us state here that the equivocation correlation in the form of $\Delta N \cdot \Delta \varphi \geq 1/2$ discussed in early works (Dirac (1927) [106], Heitler (1956) [102]; see also the work by Louis de Broglie (1986) [107]) turns out to be *false*, as is demonstrated in the work [103].

2.4 Calculation Algorithm of the Process Differential Cross-Section

Let us take a detailed look at the numerical and analytical aspects of the calculation algorithm of the scattering differential cross-section (2.22).

2.4.1 Calculation of the Integral Amplitude Terms

The main structural constituent of the expressions (2.23) and (2.34) is the photoabsorption σ_{nl}^{k}− cross-section (2.19) for each nl-shell of the studied atom. The cross-section (2.19) is built on the wave functions of the transition states obtained by computational solution of the Hartree–Fock equation (2.26). From here on, for calculating the integral terms in (2.23) and (2.24) the following is used:

(a) Lagrange second kind polynomial representation of the function $\sigma_{nl}^{k}(x)$:

$$L_{n}^{(2)}(x) = a_{n}x^{2} + b_{n}x + c_{n} \tag{2.73}$$

on the partial interval $x \in [x_{2n-1}, x_{2n}, x_{2n+1}]$ of the final domain of integration $x \in [x_{1}, x_{2N+1}]$, $n = 1, 2, \ldots N$, N is the polynomial number;

(b) asymptotic of the function $\sigma_{nl}^{k}(x)$ on the infinite interval of integration $x \in [x_{2N+1}, \infty)$:

$$\sigma_{nl}^{k}(x) \to c_{2}x^{-2} + c_{3}x^{-3} + c_{4}x^{-4}. \tag{2.74}$$

The constant coefficients are here out of the condition of "lacing" of the function (2.74) with the polynomial (2.73) if $n = N$.

2.4.2 Asymptotic Problem of the Partial Photoionization Cross-Sections

The only *analytical* result obtained presently for the atomic photoionization cross-section in the *ultra* relativistic limit – the result for a hydrogen atom – leads to the *logarithmic divergence* of the real part (2.23) of the scattering amplitude. Actually, the photoionization cross-section of the hydrogen-like atom in the ultra relativistic limit $\omega >> m_e$ takes the form of [7]:

$$\sigma\left(\omega\right) \propto 2\pi Z^5 \alpha^4 r_0^2 \omega^{-1}; \tag{2.75}$$

where Z is the atom nuclear charge, α is the fine structure constant. Then, if we substitute (2.75) in (2.23) on the interval of the integration $x \in [x_{2N+1}, \infty)$, we obtain:

$$\int_{x_{2N+1}}^{\infty} \frac{x\left(\omega - x\right)\sigma_{nl}\left(x\right)}{\left(x - \omega\right)^2 + \Gamma_{nl}^2/4}dx \ \propto \ln[(x-\omega)^2 + \Gamma_{nl}^2/4]\,_{x_{2N+1}}^{\infty} = \infty.$$

Let us remark that in the work [108] the *analytical* result is obtained for asymptotic of the photoionization cross-section of the *multielectron* atom nl-shell in the limit $I_{nl} << \omega << m_e$ (I_{nl} is the ionization threshold energy of the studied atomic nl-shell):

$$\sigma_{nl}\left(\omega\right) \propto \omega^{-\eta};\ \eta = 7/2\ (l = 0)\,; 9/2\ (l \neq 0)\ .$$

But in the *ultra* relativistic limit $\omega >> m_e, I_{nl}$ we are interested in, the issue of the analytical structure of the asymptotic of the *multielectron* atom photoionization cross-section remains open.

In such a situation, the empirical choice of the asymptotic of the atomic photoionization cross-section is unavoidable. This choice is mainly determined by three circumstances: (a) the calculated and proved by experiment [109,110] absolute values of the atomic photoionization cross-sections in the far post threshold energies of the absorbed photon must be reproduced to a high degree of precision $(1 \div 3\%)$; (b) the singularities of the scattering amplitude must be absent; (c) the following analytical integration must be simple. The choice of asymptotic in the form of (2.74) meets these conditions.

2.4.3 Calculation of the Double Photoionization Channels

If calculating the double photoionization channels in the expressions (2.23) and (2.24), the double improper integral of the first kind appears. We shall demonstrate that this integral can be transformed [96] to the singlefold integral of the expression containing the double photoionization cross-section (2.57). Let us take a look at the integral of the form:

$$\iint_D dxdy\,\Phi\left(x, y\right) = \iint_{D'} d\alpha d\beta\,|I|\,\Phi\left(\alpha, \beta\right) \tag{2.76}$$

in the rectangular $D : (x, y) \in [0; \infty)$ and curvilinear D' integration domain. Let us transform the coordinates:

$$x\left(\alpha, \beta\right) = \alpha - \beta - a; \quad y\left(\alpha, \beta\right) = \beta; \qquad (2.77)$$

where a is one constant. According to (2.77) for the Jacobian of mapping we obtain:

$$I = \det \left\| \partial \left(x, y\right) / \partial \left(\alpha, \beta\right) \right\| = 1.$$

Then, for the right member (2.76) we have an expression:

$$\iint\limits_{D'} d\alpha d\,\beta \Phi\left(\alpha, \beta\right) = \lim_{\Delta \to \infty} \left(\int\limits_{a}^{n} \int\limits_{0}^{m} + \int\limits_{n}^{n+\Delta} \int\limits_{m-\Delta}^{\Delta} \right) d\alpha d\,\beta \Phi\left(\alpha, \beta\right); \qquad (2.78)$$

where $n = a + \Delta, m = \alpha - a$. We consider that the external integral in the addend of (2.78) goes to zero for the regular functions $\Phi\left(\alpha, \beta\right) \propto \alpha^{-\eta}$ with $\eta \geq 2$. Then, we obtain for (2.76):

$$\int\limits_{0}^{\infty} \int\limits_{0}^{\infty} dx dy \Phi\left(x, y\right) = \int\limits_{a}^{\infty} d\alpha \int\limits_{0}^{\alpha-a} d\,\beta \Phi\left(\alpha, \beta\right). \qquad (2.79)$$

Let us hold fix the variables of integration in (2.77):

$$\alpha = IP_{12} + \varepsilon + \varepsilon'; \; \beta = \varepsilon'; \; a = IP_{12}. \qquad (2.80)$$

Then instead of (2.79) we obtain the desired singlefold integral of the double photoionization cross-section (2.57). This cross-section appears in (2.79) in the interior integration on the energy surface $\varepsilon + \varepsilon' = \alpha - IP_{12}$. Remember (Part 2.2.2) that in (2.80) $\varepsilon-, \varepsilon'-$ are energies of the continuous spectrum photoelectrons, $IP_{12}-$ is the energy of the atomic double ionization threshold.

2.5 Correlation Abnormalities of the Atomic Form Factor

In this part of our treatise we investigate the role of the *correlation effects* when describing in theory the atomic form factor. As a subject of inquiry we chose the ^{10}Ne atom.

2.5.1 Correlation Structure of the Atomic Form Factor

We determine the analytical structure of the atomic form factor with the $^{1}S_{0}-$ term of the ground state *outside* the one-configuration Hartree–Fock approximation. We transform the form factor of the atom (1.4) to the form:

$$F_0 = \int_0^\infty q(r) j_0(kr) dr; \tag{2.81}$$

$$q(r) = \sum_{nl} N_{nl} P_{nl}^2(r); \quad k = \frac{2\omega}{c} \sin\left(\frac{\theta}{2}\right),$$

where $q(r)$ is the function of the electronic charge radial distribution in the atom.

In the work [111], the correlation structure of the ground state wave function of the ^{10}Ne atom was analyzed. The modified ground state wave function is obtained in the form of:

$$\left|\psi\left(^1S_0\right)\right\rangle = \alpha_0 \left|0; {}^1S_0\right\rangle + \left|\psi_c\left(^1S_0\right)\right\rangle, \tag{2.82}$$
$$\left|\psi_c\left(^1S_0\right)\right\rangle = \sum_{m \leq f} \sum_{n_{1,2}} \sum_{LS} \beta_m^{12}(LS) \left|(m, LS) n_1 l_e n_2 l_e'; {}^1S_0\right\rangle.$$

The summation here is made over the two-particle *(m,LS)*- excitation of the atomic core shells into the states described by so-called *natural orbitals* (index "*e*") [10, 71]; α_0-, $\beta_m^{12}(LS)-$ are the weighing coefficients of the basis states in the modified wave function structure and $LS =^1 S$, ^3P, ^1D. After substitution of (2.82) for (1.3) we derive the *desired* expression for the modified form factor of ^{10}Ne atom:

$$F = F_0 + \int_0^\infty \Delta q(r) j_0(kr) dr; \tag{2.83}$$

where $\Delta q(r)$ is the change function of the electronic charge radial distribution in the atom when allowing for the correlations.

We shall define concretely the basis states in (2.82):

$$(m, LS) \to 2p^4(LS), n_1 l_e n_2 l_e' \to n l_e^2, l \geq 0.$$

We consider the expression for the matrix element of the transition $Q^{(k)}$ – operator [66]:

$$\left\langle n_1 l_1^{N_1} n_2 l_2^{N_2} \gamma_1 \gamma_2 LSJ \left\| Q^{(k)} \right\| n_1 l_1^{N_1} n_2 l_2^{N_2} \gamma_1' \gamma_2' L'S'J' \right\rangle$$
$$= (-1)^{L_1 + S + J'} \delta_{SS'} \sqrt{[L, L', J, J']} \begin{Bmatrix} L & J & S \\ J' & L' & k \end{Bmatrix}$$
$$\left[(-1)^{L_2 + L + L'} A_{12}^{(k)} + (-1)^{L_2'} A_{21}^{(k)} \right];$$

$$A_{12}^{(k)} = \delta\left(\gamma_2, \gamma_2'\right) \delta\left(S_1, S_1'\right) [S_1]^{-1/2} \left\{ \begin{matrix} L_1 & L & L_2 \\ L' & L_1' & k \end{matrix} \right\} B_1^{(k)};$$

$$B_1^{(k)} = \left(l_1^{N_1} \gamma_1 \left\| u^k \right\| l_1^{N_1} \gamma_1' \right) \left(n_1 l_1 \left\| q^{(k)} \right\| n_1 l_1 \right);$$

$$\gamma_1 \equiv \alpha_1 L_1 S_1; \ [x] \equiv 2x + 1; Q^{(k)} = \sum_{i=1}^{N} q_i^{(k)}; \ q_i^{(k)} = C^{(k)} j_k\left(kr_i\right).$$

We also consider that:

$$\left(l \left\| C^{(0)} \right\| l' \right) = [l]^{1/2} \cdot \delta\left(l, l'\right); \ \left(nl \left\| q^{(0)} \right\| nl \right) = [l]^{1/2} \cdot \langle nl \left| j_0 \right| nl \rangle;$$

$$\left(l^N \gamma \left\| u^0 \right\| l^N \gamma' \right) = N[L, S]^{1/2}[l]^{-1/2} \cdot \delta\left(\gamma, \gamma'\right);$$

$$\left\{ \begin{matrix} 0 & 0 & 0 \\ 0 & 0 & 0 \end{matrix} \right\} = 1; \ \left\{ \begin{matrix} L & 0 & L \\ 0 & L & 0 \end{matrix} \right\} = [L]^{-1/2}.$$

Then, if $k = 0$, $LSJ = L'S'J' \rightarrow {}^1S_0, L_1S_1 = L_2S_2, L_1'S_1' = L_2'S_2'$, we derive from (1.3) the analytical representation for the $\Delta q\left(r\right)-$function:

$$\Delta q\left(r\right) = 2 \sum_{n, LS} \left| \beta_n\left(LS\right) \right|^2 \left[P_{nl_e}^2\left(r\right) - P_{2p}^2\left(r\right) \right].$$

Let us remark here that if the scattering angle is *zero* (forescattering), the Bessel's function $j_0\left(kr\right) \rightarrow 1$ and the modified form factor of an atom coincide with (2.81).

2.5.2 Calculation Results: ^{10}Ne Atom

For characterizing the influence of the correlation effects on the theoretical value of the form factor of the ^{10}Ne atom we defined and examined numerically the function of the correlation abnormalities:

$$\Delta\left(\%\right) = \left(\frac{F}{F_0} - 1 \right) \cdot 100\left(\%\right). \qquad (2.84)$$

We calculated the F_0 value in the wave functions of the atomic core electrons that were obtained by solving the Hartree–Fock equations for the ground state configuration of the neon atom $1s^2 2s^2 2p^6 \left({}^1S_0\right)$. The $\Delta q\left(r\right)$ function is calculated in the work [111] in the natural orbitals with $n \in [3, 11]$ and $l \in [0, 10]$. The natural orbitals of the basis states $1s^2 2s^2 2p^4 \left(3p^2, 3d^2\right)$, contributing significantly to (2.82), are represented in Table 2.1.

Comparing the midradius of the neon atom valence $2p$-shell $r_{2p} = 0,51$ $\mathring{A}$ with the midradiuses of the natural orbitals from Table 2.1 we can disclose the following. The electron configurations lead to a small charge redistribution from the interior of domain of the atomic ground state described in the one-configuration Hartree–Fock approximation to its periphery [112]. As a result, the function of the correlation abnormalities (2.84) becomes different from zero and oscillates in the limit from -0.15% to $+0.15\%$ (Fig. 2.2).

Table 2.1. Weighting coefficients β_m^{12} and midradiuses r_{nl} of the natural orbitals of the dominant basis states in the wave function (2.82)

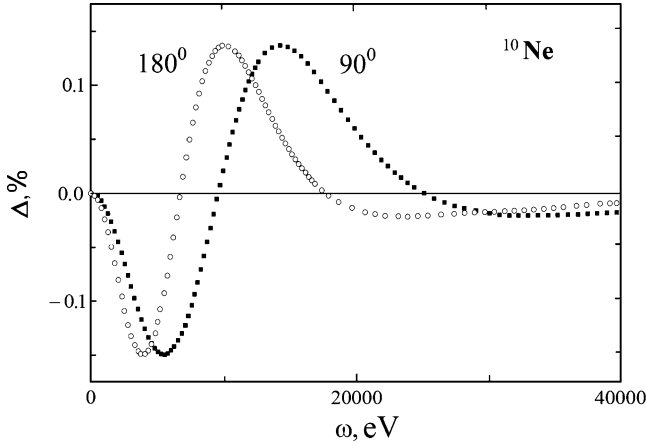| nl_e	$-\beta_m^{12}$			r_{nl}, Å		
	^1S	^3P	^1D	^1S	^3P	^1D
$3p$	0,046	0,069	0,077	0,694	0,714	0,706
$3d$	0,044	0,062	0,049	0,550	0,563	0,558

Fig. 2.2. Dependence of the function of the correlation abnormalities (2.84) for the neon atom on the energy of the elastic scattered X-ray photon (ω) if the scattering angles are 90°, 180°

2.6 Form Factor of the Open-Shell Atom

The form factor of the atom with an arbitrary $^{2S+1}L_J-$ term of the $|LSJ\rangle$ electron configuration of the ground state is defined in the following manner (Part 1.1.1):

$$F = \langle LSJ | \sum_{i=1}^{N} \exp\{i\,(\boldsymbol{q} \cdot \boldsymbol{r}_i)\} | LSJ\rangle. \tag{2.85}$$

If we have a *closed*-shell atom in the ground state, the expression (2.85) takes the form:

$$F_0 = \sum_{nl \leq f} N_{nl} \langle nl | j_0 | nl\rangle. \tag{2.86}$$

As was mentioned in Chap. 1, the formula (2.86) or its relativistic generalization is traditionally extended to an *arbitrary* atom. If we can apply such approximation it should be theoretically proved. But in published works there are still no theoretical and experimental investigations dealing with the influence of the aspheric effects of the open-shell atom in the ground state on the

form factor (2.86) magnitude. In this part of our treatise we study such influence for the first time, confining ourselves to the atoms with one open-shell and the total ground-state momentum $J = 0, 1/2, 3/2$ [113].

2.6.1 Analytic Structure of the Form Factor

We shall determine the angular and radial structure of the expression (2.85) for an arbitrary term of the atomic ground state.

Considering the quantum interference effect of the contact elastic photon scattering amplitudes by the series ($M = -J, \ldots, J$) of the atomic $|\gamma J M\rangle -$ ground state, we can represent its form factor as ($J_1 = J_2 = J$):

$$F = \frac{1}{2J+1} \sum_{M_1=-J_1}^{J_1} \sum_{M_2=-J_2}^{J_2} \left\langle \gamma_1 J_1 M_1 \left| \sum_{i=1}^{N} \exp\{i\,(\boldsymbol{q} \cdot \boldsymbol{r}_i)\} \right| \gamma_2 J_2 M_2 \right\rangle. \quad (2.87)$$

In (2.87) we summed over the M_2-projections of the J_2-total momentum in the final atomic state, averaged over the M_1-projections of the J_1-total momentum in the initial atomic state, and indicated the $\gamma-$ set of quantum numbers characterizing the atomic state with the JM.

We shall expand the exponent in spherical functions according to (2.20), use the Wigner–Eckart theorem (2.21) and consider that $\left(l\,\|C^{(2n+1)}\|\,l\right) = 0$ is realized if $n = 0, 1, 2, \ldots$ Then we obtain the desired analytic structure from (2.87):

$$F = F_0 + \frac{1}{2J+1} \sum_{n=1}^{\infty} \langle \gamma J | \left| Q^{(2n)} \right| \| \gamma J \rangle \, \psi_J^{(n)}. \quad (2.88)$$

In (2.88), the spherically symmetrical ($n = 0$) part of the atomic form factor is distinguished and the following is defined:

(a) the *contact* transition operator

$$Q^{(2n)} = \sum_{k=1}^{N} C^{(2n)}(\boldsymbol{r}_k)\, j_{2n}(q r_k); \quad (2.89)$$

forcing on the pair of the nonrecurring electron shells of the $|\gamma J\rangle -$ configuration. If we have the odd number of the electron shells in the configuration, the virtual electron shell with a zero occupation number and $^1S_0$ term is added;

(b) angle function

$$\psi_J^{(n)} = \sum_{M_1=-J}^{J} \sum_{M_2=-J}^{J} \sum_{p=-2n}^{2n} R_{-p}^{(2n)}(\boldsymbol{q}) \begin{pmatrix} J & 2n & J \\ -M_2 & p & M_1 \end{pmatrix}; \quad (2.90)$$

$$R_{-p}^{(2n)}(\boldsymbol{q}) = (-1)^n\,(8n+2)^{1/2}\,\Theta_{2n,-p}(\alpha)\exp\left(-ip\varphi\right).$$

In (2.90), α and φ are the spherical angles of the scattering vector $\boldsymbol{q}$ and $\Theta_{2n,-p}$ are the associated Legendre polynomials [65].

The matrix element in (2.88) in the approximation of the LS-bonding can be calculated from the formula:

$$\left\langle n_1 l_1^{N_1} n_2 l_2^{N_2} T_1 T_2; LSJ \left\| Q^{(k)} \right\| n_1 l_1^{N_1} n_2 l_2^{N_2} T_1' T_2'; LSJ \right\rangle =$$

$$= (-1)^{L_1+L_2+S+J} [L,J] \begin{Bmatrix} L & J & S \\ J & L & k \end{Bmatrix} \left(A_{12}^{(k)} + A_{21}^{(k)} \right); \tag{2.91}$$

$$A_{12}^{(k)} = [S_1]^{-1/2} \begin{Bmatrix} L_1 & L & L_2 \\ L & L_1 & k \end{Bmatrix} B_1^{(k)};$$

$$B_1^{(k)} = D_k (N_1, l_1, T_1) \left(l_1 \left\| C^{(k)} \right\| l_1 \right) \langle n_1 l_1 | j_k | n_1 l_1 \rangle;$$

$$D_k (N, l, T) = N[L][S]^{-1/2} \sum_{T_1} (-1)^{L_1+L+l+k} |G_{TT_1}|^2 \begin{Bmatrix} l & l & k \\ L & L & L_1 \end{Bmatrix}; \tag{2.92}$$

$$D_k (4l+2-N, l, T) = (-1)^{k+1} D_k (N, l, T); \tag{2.93}$$

where $G_{TT_1}-$ are the genealogical coefficients and $T \equiv \gamma LS, [x] \equiv 2x+1$, is indicated.

The expression (2.91) is a consequence of the general result of the work [66] for the matrix element of the transition operator (2.89).

2.6.2 Calculation Results: Atoms of ^{17}Cl, ^{21}Sc, ^{23}V, ^{35}Br, ^{39}Y, ^{73}Ta.

As a subject of inquiry we chose the atoms with *one* open shell and the total momentum of the ground state $J = 0, 1/2, 3/2$. Three groups of terms correspond with them: $^3P_0$, $^5D_0$, $^7F_0$ group, $^2S_{1/2}$, $^2P_{1/2}$ group, and $^4S_{3/2}$, $^2P_{3/2}$, $^2D_{3/2}$, $^4F_{3/2}$ group.

For the first ($J = 0$) and the second ($J = 1/2$) group of terms there is *no* sum in (2.88) and the expression (2.86) remains for the form factors of atoms. For example for the $^2S_{1/2}-$ term $J_1 = J_2 = 1/2$ and from the condition $|J_2 - J_1| \leq t \leq J_1 + J_2$ we obtain $0 \leq t \leq 1$. Since $\left(l \left\| C^{(1)} \right\| l \right) = 0$, in the expansion by the t-multipolarity for the form factor (2.87), only the item with Wigner coefficient remains non-zero:

$$\begin{pmatrix} J_2 & 0 & J_1 \\ -M_2 & 0 & M_1 \end{pmatrix} = (-1)^{J_2-M_2} \frac{1}{\sqrt{2J_1+1}} \delta_{J_1 J_2} \delta_{M_1 M_2}. \tag{2.94}$$

Considering (2.94) for (2.87), we have:

$$F = (2J_1+1)^{-1/2} \left\langle \gamma_2 J_2 \left\| \sum_{k=1}^{N} C^{(0)} (\boldsymbol{r}_k) j_0 (qr_k) \right\| \gamma_1 J_1 \right\rangle. \tag{2.95}$$

After all, considering (2.91) if

$$J = 1/2, \, L = 0, S = 1/2, L_1 S_1 = L_1' S_1' = (0,0) \, ,$$
$$L_2 S_2 = L_2' S_2' = (0, 1/2) \, ,$$
$$\left\{ \begin{matrix} 0 & 1/2 \, 1/2 \\ 1/2 & 0 \quad 0 \end{matrix} \right\} = -\frac{1}{\sqrt{2}}, \quad \left(l \left\| C^{(0)} \right\| l' \right) = (2l+1)^{1/2} \, \delta_{ll'},$$

we obtain the expression (2.86) for the form factor.

For the third $(J = 3/2)$ group of terms the sum in (2.88) contains one $(n = 1)$ item. In this case, we have for the function (2.90):

$$\psi_{3/2}^{(1)} = \frac{1}{\sqrt{5}} f(\theta); \quad f(\theta) = 1 + 2\cos\theta; \tag{2.96}$$

where θ is the scattering angle. From (2.92) and (2.93) it follows that $D_2 \left(1, d, {}^2 D \right) = - D_2 \left(5, p, {}^2 P \right) = \sqrt{2}$. We took the values $D_2 \left(3, p, {}^4 S \right) = 0$, $D_2 \left(3, d, {}^4 F \right) = - 2\sqrt{6}/5$ from the work [66]. Finally, calculating the matrix elements (2.91) we obtain for the form factors of atoms from the third group of terms considering (2.96):

$$F \left({}^4 S_{3/2} \right) = F_0;$$

$$F \left({}^2 P_{3/2} \right) = F_0 - \frac{1}{2} f(\theta) \langle np | j_2 | np \rangle \, ;$$

$$F \left({}^2 D_{3/2} \right) = F_0 + \frac{17}{14} f(\theta) \langle nd | j_2 | nd \rangle \, ;$$

$$F \left({}^4 F_{3/2} \right) = F_0 - \frac{6}{35} f(\theta) \langle nd | j_2 | nd \rangle \, ;$$

$$j_2(x) = \left(\frac{3}{x^3} - \frac{1}{x} \right) \sin x - \frac{3}{x^2} \cos x; \quad x = qr; \quad \lim_{x \to 0, \infty} j_2(x) = 0.$$

To describethe atom aspheric effects we defined and investigated numerically the asphericity function:

$$\Delta(\%) = \left(\frac{F}{F_0} - 1 \right) \cdot 100(\%). \tag{2.97}$$

We calculated the function (2.97) for the atoms (the open shell and the ground state term are given in brackets) $^{17}Cl \left(3p^5; {}^2 P_{3/2} \right)$, $^{21}Sc \left(3d; {}^2 D_{3/2} \right)$, $^{23}V \left(3d^3; {}^4 F_{3/2} \right)$, $^{35}Br \left(4p^5; {}^2 P_{3/2} \right)$, $^{39}Y \left(4d; {}^2 D_{3/2} \right)$ and $^{73}Ta \left(5d^3; {}^4 F_{3/2} \right)$, if the energies of the scattered photon are $\omega = \omega_{1s} \pm 0,5$ (keV). We took the energy values of the atom $1s-$ shell ionization thresholds from the work [10]: ω_{1s} (keV) $= 2,83$ (Cl); $4,49$ (Sc); $5,47$ (V); $13,48$ (Br); $17,04$ (Y); $67,42$ (Ta). The calculation results by the example of atoms of ^{21}Sc and ^{39}Y are represented in Fig. 2.3.

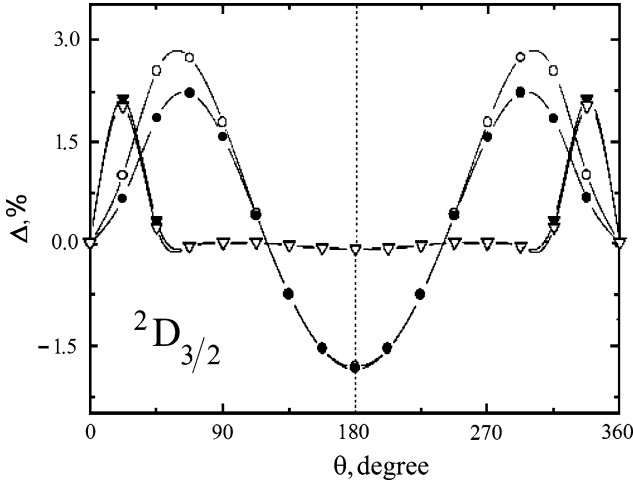We formulate the received results for the atoms with the total momentum of the ground state $J = 3/2$.

Fig. 2.3. The asphericity function (2.97) for the atoms of ^{21}Sc (*filled circle, open circle*) and ^{39}Y (*filled inverted triangle▼, open inverted triangle▽*). The *black circle(triangle)*: $\omega = \omega_{1s} - 0,5\,(keV)$; *the light circle(triangle)*: $\omega = \omega_{1s} + 0,5\,(keV)$. ω is the scattered photon energy, θ is the scattering angle, ω_{1s} is the energy of the atom 1s-shell ionization threshold

1. The behavior of the aspericity function (2.97) on the interval of the scattering angles $[0°; 180°]$ has an oscillation character. The absolute value of the function is situated in the limits from –2% to +3%.
2. If the nuclear charge of the atom increases, the oscillation number of the function (2.97) increases too. At the same time, the values of its extreme points are located on the interval of the scattering angles $[0°; 45°]$.

The calculation results represented in Fig. 2.3 demonstrate that corrections for atom aspericity in the energy region of the $1s-$ shell ionization threshold $(-2\% \div +3\%)$ seem to be the same values as corrections for the *correlation effects* ($^{10}Ne : -0,15\% \div +0,15\%$; [54–58]: $1\% \div 2\%$). As a consequence, the approximation (2.86) traditionally used in scientific literature turns out to be quite acceptable if describing in theory the experimental results with measurements errors $\sim \pm 5\%$.

2.7 Differential Cross-Sections of the Anomalous Elastic X-Ray Photon Scattering by an Atom

In this part of our treatise, we set forth the results of the first theoretical studies dealing with the role of *many-particle effects* in the elastic X-ray photon scattering by an atom and an atomic ion in the energy region of their deep shells ionization thresholds [95–99, 112–118].

2.7.1 Closed-Shell Atoms in the Ground State: ^{10}Ne, ^{18}Ar, ^{36}Kr, ^{54}Xe

We shall examine the calculation results for the cross-sections of the anomalous elastic X-ray photon scattering by a closed-shell atom in the ground state in the energy region of its deep $1s$ (Ne,Ar,Kr,Xe)-, $2s$ (Ar)- and $2p$ (Xe)- shells ionization thresholds.

Atom of ^{10}Ne: scattering in the $1s$-shell ionization threshold region. The matrix elements of the radiation transition operator and the photoabsorption cross-section (2.19) are obtained in two approximations.

Approximation 1: without considering the radial relaxation effect in the $1s$-vacancy field. The wave function of the np-photoelectron is derived by solving the Hartree-Fock equation for the configuration $1s_0^1 2s_0^2 2p_0^6 np\,(^1P_1)$. The wave functions of the atomic core electrons are deduced by solving the Hartree–Fock equations for the $1s_0^2 2s_0^2 2p_0^6\,(^1S_0)$ − configuration of the atomic ground state. In this approximation, the matrix elements of the radiation transition operator contain only the first items in the sums (2.38) with $S = 1$ and the probabilities of the multiple excitation/ionization of the atomic ground state are equal to zero.

Approximation 2: considering the radial relaxation effect in the $1s$-vacancy field. The wave function of the np-photoelectron is derived by solving the Hartree–Fock equation for the configuration $1s^1 2s^2 2p^6 np\,(^1P_1)$. The wave functions of the atomic core electrons are deduced by solving the Hartree–Fock equations for the configuration $1s^1 2s^2 2p^6\,(^2S_{1/2})$. By this means, we managed to consider the atomic core relaxation in the $1s$-vacancy field. In this case, the matrix elements of the radiation transition operator take the form (2.38) with $S < 1$. For example, considering the approximation (2.41) and the orthogonality of the wave function of the $1s^1 np$ state to the wave function of the $2s^1 np$ state of the same symmetry, the expression (2.38) takes the form (*length form*) in case of the $1s$-np transition:

$$R_{1snp} = S_{1s} \left(\langle 1s_0\, |\hat{r}|\, np \rangle - \langle 1s_0\, |\hat{r}|\, 2p \rangle \cdot \frac{\langle 2p_0|\, np \rangle}{\langle 2p_0|\, 2p \rangle} \right);$$
$$S_{1s} = \langle 1s_0|\, 1s \rangle^1 \, \langle 2s_0|\, 2s \rangle^2 \, \langle 2p_0|\, 2p \rangle^6.$$

We calculated the radiation transition amplitudes in the length form, since the RPAE correlations change the values of amplitudes with a $1s$-shell for not more than 0,5%. Calculating the scattering discrete subspectrum, we considered only the most intensive radiation transitions to the $3p$-, $4p$- states of the photoelectron (the calculation results for $n \in [3; \infty)$ are represented in the next Part). The main resonances of the scattering cross-sections in the photon energy region $\omega \cong 870 \pm 3\,\text{eV}$ in Fig. 2.4 are determined through the transitions to these states. For the value of the total width of the $1s$-vacancy decay we accepted the value $\Gamma_{1s} = 0,65\,\text{eV}$ measured in
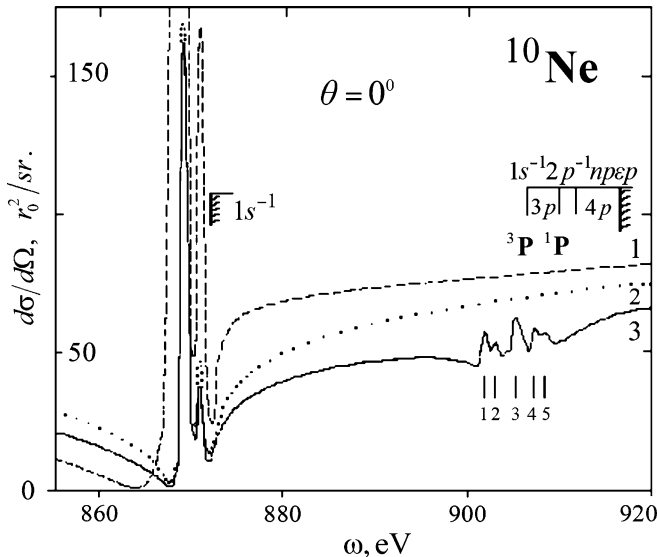
Fig. 2.4. The differential cross-section of the anomalous elastic nonpolarized X-ray photon scattering by neon atom (scattering resonance area): 1 – without considering the radial relaxation effect (RRE); 2 – RRE without considering the double excitation/ionization processes; 3 – RRE with considering the double excitation/ionization processes. The identification of the resonances indicated by numerals is given in the text. θ is the scattering angle, Ω is the solid angle, ω is the energy of the scattered photon. The calculated relativistic values for threshold energies of the K (872,32 eV)- and KL_{23} (916,00 eV)-ionization of the neon atom are indicated

the experimental spectrum of the neon atom K-photoabsorption [74]. Along with $1s$-np excitation/ionization in the second approximation we considered the double excitation/ionization of the neon atom ground state. The double photoexcitation amplitudes are described in the Hartree–Fock multiconfiguration approximation with intermediate states of the form (2.45). The algorithm for deriving the wave functions of these states is represented in Part 2.2.2. Here: (a) the wave functions of the electron-excited are derived by solving the Hartree–Fock term-averaged equations for the configuration $1s^1 2s^2 2p^5 \left(^{1,3}P\right) n_1 l_1 n_2 l_2 \, (LS)$; (b) the wave functions of the atomic core electrons are calculated by solving the Hartree–Fock $^{1,3}P$-term-averaged equations for the configuration $1s^1 2s^2 2p^5$. The amplitudes of the double excitation/ionization and the double ionization are described in the Hartree–Fock one-configuration approximation through the transitions to the states:

$$1s^1 2s^2 2p^5 \left(np\varepsilon \, p, \ \varepsilon \, p\varepsilon' \, p\right), \quad n = 3, 4. \tag{2.98}$$

At the same time, for the first ($n = 3$) channel we considered the electrostatic splitting of the ^1P- and ^3P- terms of the atomic core $1s^1 2p^5 \left(^{1,3}P\right)$. The
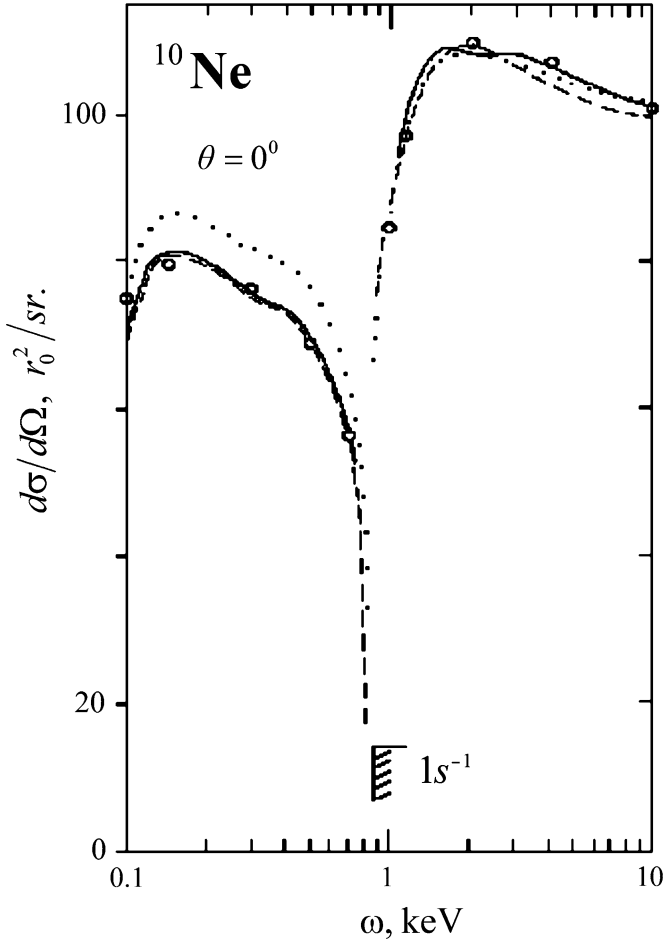
Fig. 2.5. The differential cross-section of the anomalous elastic nonpolarized X-ray photon scattering by neon atom (near-threshold scattering region): the circles indicate the calculation (the Kissel–Pratt relativistic algorithm) of the work [29]; the other symbols are the same as in **Fig. 2.4**. The details of the scattering resonance region are not given. The energy scale is given in the logarithmic scale

channels (2.98) are open if the X-ray photon energies are $906, 82 \, (^3P), 909, 81$ $(^1P), 911, 70$ and $916,00 \, \text{eV}$ correspondingly.

The calculation results for the cross-section of the nonpolarized X-ray photon zero-angle scattering (2.22) by neon atom in the energy region of the $1s$-shell ionization threshold are represented in Fig. 2.4, 2.5, and in Table 2.2.

The radiation transitions to the double photoexcitation states correspond with the most intense resonancesin the near fine structure area of the

Table 2.2. Spectral characteristics of the main resonances of the differential cross-section of the elastic nonpolarized X-ray photon zero-angle scattering by neon atom in the ionization K-threshold areas in approximations 1,2 and 3 (see **Fig. 2.4**)

nl	ω, eV		$d\sigma/d\Omega$, $r_0^2/sr.$		
	1	2,3	1	2	3
$3p$	$868, 64$	$869, 40$	$1900, 00$	$170, 00$	$162{,}50$
$4p$	$870, 96$	$871, 10$	$167, 60$	$47, 26$	$37{,}53$

scattering cross-section in Fig. 2.4:

$$|1\rangle = \gamma_3 \, 3\,p^2[0, 97 \, (^3P)];$$
$$|2\rangle = \gamma_1[0, 90\,3s3d \, (^1D) - 0, 50\,3p^2 \, (^1D)];$$
$$|3\rangle = \gamma_1 \, 3\,p^2 \left[0, 70 \, (^1D) + 0, 60 \, (^1S)\right];$$
$$|4\rangle = \gamma_1 \, 3\,p4\,p \left[0, 90 \, (^1D)\right];$$
$$|5\rangle = \gamma_1 \, 3\,p5\,p \left[0, 80 \, (^1D)\right];$$

where $\gamma_{1,3} = 1s^1 2p^5 \, (^{1,3}P)$ and the terms with $\left|a_{12}^{LS}\right| \geq 0, 50$ are deducted in the full structure of the wave function (2.45).

We obtained the cross-sections of the $2s$- and $2p$-photoabsorption considering the radial relaxation effect and the RPAE correlations. However, since the $1s$-shell is significantly separated spatially and energy-wise from the $2s$-and $2p$-shells of the atomic core, the influence of the radial relaxation effect and the RPAE correlations in $2s$- and $2p$-photoabsorption on the theoretical scattering cross-section in the energy region of the ionization K-threshold turned out to be insignificant.

According to the results represented in Fig. 2.4, 2.5, and in Table 2.2, we can arrive at the following conclusions. The electron shell radial relaxation effect in the $1s$-vacancy field leads (a) to a strong intensity rejection and to a shift to shorter wavelengths of the resonance energies of scattering cross-sections calculated without considering this effect and (b) to the redistribution of the scattering intensity, calculated without considering this effect, between short-wave and long-wave regions of the scattering spectrum. The magnitude and direction of the redistribution of the scattering intensity are essentially determined by considering the double excitation/ionization processes both in the region of the scattering resonances, and in the region of near-threshold scattering. *Outside* the anomalous dispersing scattering area the results of our calculation coincided almost with the theoretical results of the *independent particles approximation* in the work [29].

Considering the set completeness of the photoexcitation one-particle states. In this part we turn to the problem of considering the *set completeness* [119] of the excitation/ionization one-particle states of the quantum system "atom⊕photon" if constructing the scattering cross-section.

We have two methods before us. The first approach is to spread the methods well known in literature (*the correlation functions technique* [120–123]) to the resonance region of the scattering spectra. The second is to develop an *alternative* method for considering the set completeness of the photoexcitation one-particle states of the quantum system "atom⊕photon". In our treatise, we chose the *second* method and solved the problem by the example of the simple many-electron systems with ground state $^1S_0$ - term of the ^{10}Ne atom (present Part) and of its ion Ne^{6+} (Part 2.8).

Let us turn directly to the quantum-mechanical *observed value* – the differential cross-section of the scattering (2.22). We shall transform (2.22) to the form:

$$d\sigma/d\Omega = r_0^2 \left(\boldsymbol{e}_1 \cdot \boldsymbol{e}_2\right)^2 \left\{\left(F\left(\theta;\omega\right) + f'\right)^2 + \left(f''\right)^2\right\};$$

$$f' = \eta \sum_{nl \leq f} R_{nl}; \quad f'' = \eta \sum_{nl \leq f} L_{nl};$$

$$R_{nl} = \sum_{m \geq f}^{k-1} B_m \left(\frac{\Delta_m}{1 + \Delta_m^2} - \delta_m\right) + R_k;$$

$$L_{nl} = \sum_{m \geq f}^{k-1} B_m \left(\frac{1}{1 + \Delta_m^2} + \delta_m^2\right) + L_k;$$

$$\Delta_m = \left(\omega - \omega_m\right)/\gamma; \quad \delta_m = \gamma/\left(\omega + \omega_m\right); \quad \omega_m = I_{nl} - \varepsilon_m;$$

$$B_m = \left(\frac{4}{3}\pi\alpha\, a_0^2/\gamma\right)\omega_m^2 A_m; \quad A_m = \left|D_m\right|^2; \quad \gamma = \Gamma_{nl}/2.$$

Here, from the full structures of the real (f') and imaginary (f'') components of the scattering amplitude we extracted *only* the sums of the one-particle excitations with the principal quantum number $m \in [f;\infty)$. Additional to the symbols indicated earlier in (2.22), we introduced the following symbols: R_k and L_k are the remainders of the ($m \in [k;\infty)$) functional series for the R_{nl}- and L_{nl}-functions; D_m is the amplitude of the radiation $nl \to m\,(l \pm 1)$ transition; I_{nl} is the energy of the atomic nl-shell ionization threshold; ϵ_m is the energy module of the $m\,(l \pm 1)$-photoelectron.

We shall sum the functional series in the context of the *quasiclassical approximation* of quantum mechanics [124] for the singly and highly excited states $m \in [k \gg f;\infty)$:

$$A_m = \left(\frac{k-1}{m}\right)^3 A_{k-1}, \quad \varepsilon_m = \left(\frac{k-1}{m}\right)^2 \varepsilon_{k-1}.$$

Let us turn from summing to integrating under the condition $\omega_{k+1} - \omega_k \propto 10^{-\lambda}$eV, $\lambda \geq 4$ and consider the equality:

$$arctg(x) - arctg(y) = arctg\left(\frac{x-y}{1+xy}\right), \quad xv > -1.$$

Then, for the R_k - and L_k - remainders of series we obtain the expressions closed in the elementary functions:

$$R_k = \pi\mu\{\omega\ln(1 + 2\beta/a) - 2\varepsilon_k + \gamma\rho\};$$

$$L_k = \mu\left(\frac{\gamma\varepsilon_k}{c - \varepsilon_k} + c\rho\right); \quad c > \varepsilon_k;$$

$$\rho = arctg\left(\frac{\gamma\varepsilon_k}{a + \beta}\right); \quad \mu = \frac{(k-1)}{2c\varepsilon_{k-1}} \cdot \gamma\, I_{nl} A_{k-1};$$

$$a = b^2 + \gamma^2; \; \beta = b\varepsilon_k; \quad b = \omega - I_{nl}; \; c = \omega + I_{nl}.$$

In that way, the following algorithm is realized for calculating the cross-section (2.22) for $m \in [f; \infty)$. If $m \in [f; k\text{-}1]$, we perform calculations in the Hartree-Fock wave functions of the transition states. If $m \in [k >> f; \infty)$, we use the quasiclassical approximation. The selection criterion for the natural numbers λ and k is determined through the computer-based experiment: their following increase does not change the values of the cross-section (2.22) calculated at the previous step.

The calculation results for the cross-section (2.22) and the $f'-, f''-$ components of the scattering amplitude with provision for the set completeness and *many-particle effects* (see previous Part) are represented in Fig. 2.6, 2.7. The linear-polarized photon is examined: $e_{1,2} \perp P$ are scattering planes passing through the wave vectors of the incident and scattered photons. In calculating we used the experimental values (in eV) of the energies of atomic shell ionization thresholds [125] 870.230 ($1s$), 48.445 ($2s$), 21.613 ($2p$), and the total widths of the atom vacancies decays 0.230 ($1s$) [126], 0.050 ($2s$) [127], 10^{-17} ($2p$) (estimate on evidence derived from the work [128]). In the previous part we considered only the most intensive transitions from the $1s$-shell to the photoelectron $3p$-, $4p$- states. As could be expected (see Fig. 2.6), considering the set completeness of the photoexcitation mp-states makes the nonphysical minimum of the theoretical scattering cross-section in the ionization K-threshold region disappear. We shall state the good compliance of calculation results with results of synchrotron experiments [129, 130] dealing with measuring the cross-section of the photon absorption by ^{10}Ne atom in the ionization K-threshold region. So, considering the **optical theorem** (1.13) according to information from Fig. 2.7, for example, if $\omega = 870$ eV, we obtain $\sigma = 0.356$ Mb, whereas the experimental work [130] gives us $\sigma = 0.376$ Mb.

Atom of ^{18}Ar: scattering in the $1s$-shell ionization threshold region. The cross-section calculation (2.22) is performed in two approximations that are analogous to the approximations for neon atom. In Approximation 2, additional to the radial relaxation effect and the double excitation/ ionization processes we considered the many-particle *effect of the vacuum correlations* [100]. In this case, this effect is determined through the radiation transitions from $3p_0^2 \rightarrow m_1\,(p, d)\,m_2\,(p, d)$ states of excitation/ionization of the ground state to the initial state of argon atom K-photoabsorption.
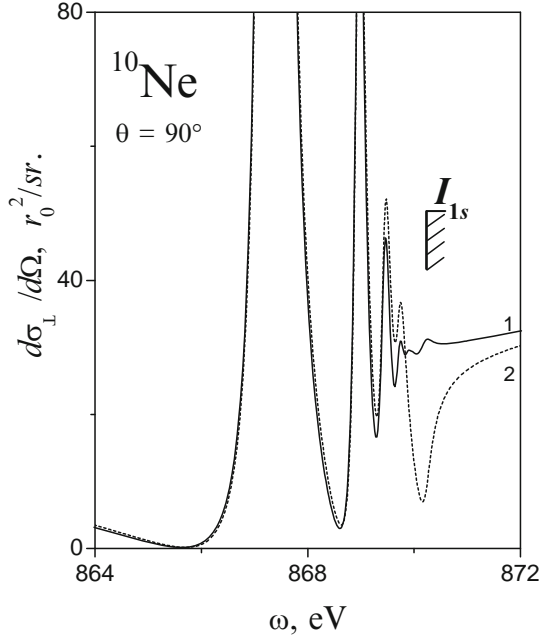
Fig. 2.6. The differential cross-section of the anomalous elastic linear polarized (at right angle to scattering plane) X-ray photon scattering by neon atom: $1 - 1s \rightarrow [3; \infty)p$ photoexcitations are considered; 2 – only $1s \rightarrow [3; 6]\, p$ photoexcitations are considered. θ is the scattering angle, ω is the scattered photon energy. The position of the $1s$-shell ionization threshold energy $I_{1s} = 870.230$ eV is marked off

In calculating the resonant part of the scattering spectrum in all approximations we considered only the transitions to the $4p$-, $5p$-, $6p$- states of the photoelectron. We did not solve the problem of considering the np-states for $n \in [7; \infty)$. This problem is a subject for future studies.

The calculated value of the ionization K-threshold energy $\omega_{1s} = 3205,65$ eV agrees well with the experimental value $3206{,}26$ eV [84]. In this connection we considered the relativistic correction $10{,}0$ eV [131] to the threshold energy. For the $1s$-vacancy decay width we accepted the value $\Gamma_{1s} = 0{,}69$ eV [132].

To describe the near fine structure of the scattering cross-section in the energy region of the ionization K-threshold we considered the transitions to the states with the wave functions (2.45) and (2.46) in Part 2.2.2 of our treatise. The channels of excitation/ionization and of the double ionization $1s^1 3p^5 (np\, \varepsilon p, \varepsilon p\, \varepsilon' p)$, $n = 4, 5$ are open, if the energy of the scattered photon is 3228.50, 3232.40 and 3237.40 eV correspondingly.

The radiation transitions to the double photoexcitation states correspond with the *brightest* resonances in the region of the near fine structure of the
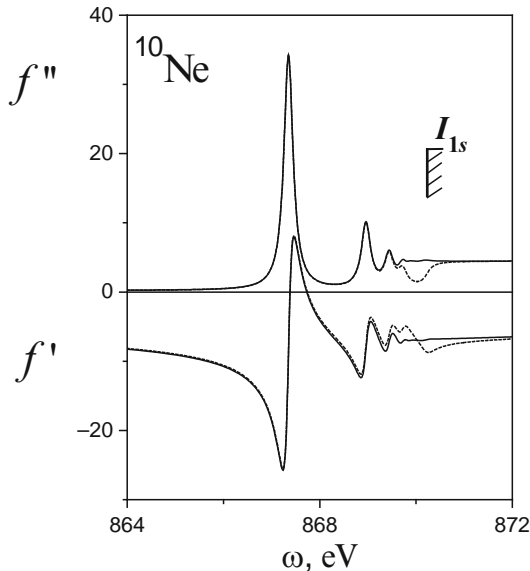
Fig. 2.7. The anomalous dispersing f'- and f''- components of the elastic scattering amplitude for the neon atom. The symbols are the same as in **Fig. 2.6**

scattering cross-section:

$$|1\rangle = 0,60\,\gamma_1\,4p^2(^1S) - 0,50\,\gamma_1 3d^2(^1S); \tag{2.99}$$
$$|2\rangle = -\gamma_3\,4p5p[0,60(^3P) + 0,50(^3D)];$$
$$|3\rangle = 0,80\gamma_1 4p5p(^1D);$$
$$|4\rangle = 0,86\left|1s^13s^1(^3S)4s4p(^3P)\right\rangle + 0,50\left|1s^13p^43d4s4p\right\rangle; \tag{2.100}$$

where $\gamma_{1,3} \equiv 1s^13p^5\left(^{1,3}P\right)$ is indicated and the items with the mixing coefficients $\left|a_{12}^{LS}\right| \geq 0,50$ are deducted in the wave function structure (2.45) and (2.46). In the argon atom, the $d-$symmetry of the excited states is *collapsible* [133]. This results in a strong electrostatic mixing of the $1s3p$-$4p4p$, $3d3d$ excitations in the state (2.29) and in the dynamic *dipole polarization effect* [85] of the $3p$-shell through the $3p^2 - 3s3d$ excitation in the state (2.100).

   The many-particle effects play a significant role only in the region of the ionization threshold through the atomic nl-shell. The ionization threshold energies of the $n\,(s,p)$-shells $(n = 2,3)$ of the argon atom are strongly separated from the ionization $K-$threshold energy (for example, $\omega\,(K) - \omega\,(L_1) = 2,88\,\text{keV}$). So, the cross-sections of the $2s$-, $2p$-, $3s$-, $3p$- photoabsorption are calculated to the approximation of the atomic core that is unreconstructed in the fields of these vacancies.

   The radiation transition amplitudes are calculated in the *length form*, since the RPAE correlations change the amplitude values with $1s$-shell not more than 1% [134].
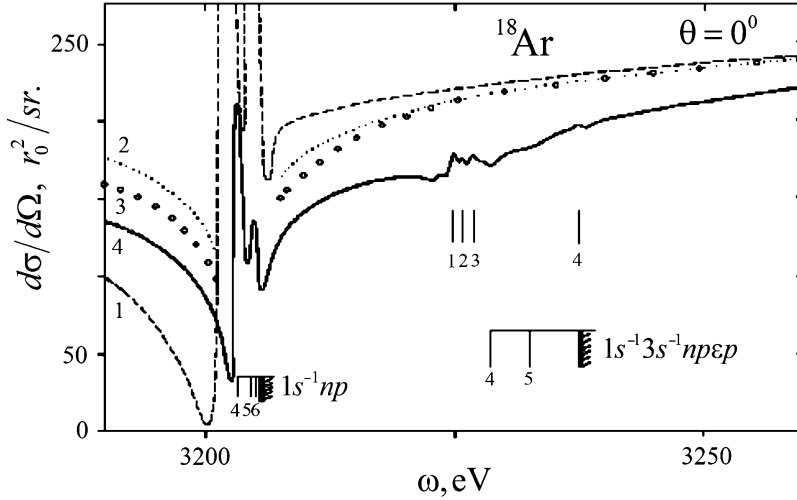
Fig. 2.8. The differential cross-section of the anomalous elastic nonpolarized X-ray photon scattering by argon atom (scattering resonance region): 1 – without considering the radial relaxation effect (RRE) for electron shells in the $1s$-vacancy field; 2 – with considering RRE; 3 – RRE + vacuum correlations; 4 – approximation 3 + double excitation/ionization processes. The resonances indicated by numerals are interpreted in the text. θ is the scattering angle, Ω is the solid angle, ω is the scattered photon energy. The calculated energy values of the argon ionization K (3205, 65 eV) and KM_{23} (3237,40 eV) thresholds are marked off

The calculation results for the argon atom are given in Fig. 2.8, 2.9, and in Table 2.3 [98]. The conclusions that follow from the obtained results are similar to the results for the neon atom.

Atom of ^{18}Ar: scattering in the $2s$-shell ionization threshold region. This part of the treatise aims at researching the influence of the RPAE correlations on the elastic scattering cross-section. As a subject of inquiry we chose the differential cross-section of the elastic X-ray photon scattering in the energy region of the argon atom $2s$-shell ionization threshold. The choice is determined by the fact that the absolute values and the cross-section form of the $2s$-photoabsorption by argon atom are found out to high precision during the synchrotron experiment [135] and they are appreciably determined by the RPAE correlations [91, 92].

The $2s$-photoabsorption cross-section is obtained to three approximations.

Approximation 1: without considering the effect of the radial electron shells relaxation in the $2s$-vacancy field. The states of the single excitation/ionization $2s^1 (m, \varepsilon) p$, $m \leq 9$ are considered.

Approximation 2: the effect of the radial electron shells relaxation in the $2s$-vacancy field is considered.
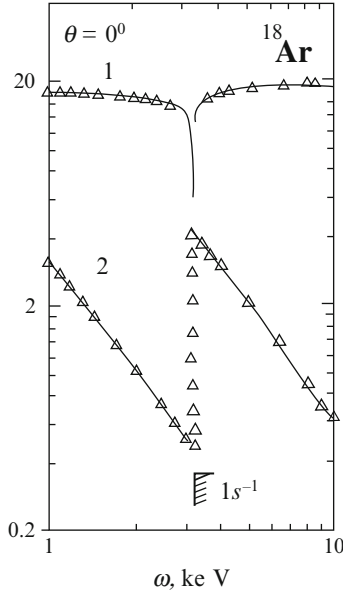
Fig. 2.9. The real (1) and imaginary (2) parts of the probability amplitude of the anomalous elastic nonpolarized X-ray photon scattering by argon atom: unbroken line indicates the radial relaxation effect (RRE) + vacuum correlations + double excitation/ionization process; triangles denote the theory (nonrelativistic form factor approximation without considering RRE) in the work [26]. The calculated energy value of the argon atom $1s$-shell ionization threshold $I_{1s} = 3205, 65$ eV is indicated. The details of the scattering resonance region are not given. The coordinate axis scales are given in the logarithmic scale

Table 2.3. Spectral characteristics of the main resonance for the differential cross-section of the elastic nonpolarized X-ray photon scattering by argon atom in the ionization K-threshold region to the 1,2,3 and 4 approximations (see **Fig. 2.8**)

ω, eV		$(d\sigma/d\Omega)\, 10^{-2}, r_0^2/sr.$			
1	2,3,4	1	2	3	4
3202,19	3203,26	24,910	2,341	2,397	2,106

Approximation 3: Approximation 2 including the mixing of the $2s^1\,(m,\varepsilon)\,p$ and $2p^5\varepsilon d$ configurations (the RPAE correlations are considered).

The effect of such mixing leads to the following analytical structure of the transition amplitude [92]:

$$A_n = L_n^{1/2} \left(a_n + \int\limits_0^\infty d\varepsilon \, L_\varepsilon \, \psi_{n\varepsilon} \, f_{n\varepsilon} \right). \qquad (2.101)$$

In (2.101), the following values are defined:

$$L_n = (\Delta_{2s}/\pi) \left[(\omega - \omega_n)^2 + \Delta_{2s}^2 \right]^{-1};$$
$$L_\varepsilon = (\Delta_{2p}/\pi) \left[(\omega - \omega_\varepsilon)^2 + \Delta_{2p}^2 \right]^{-1};$$
$$f_{n\varepsilon} = b_\varepsilon + c_{n\varepsilon};$$
$$b_\varepsilon = \left(\frac{\omega - \omega_\varepsilon}{\Delta_{2p}} \right) \left[\frac{\pi}{2} + arctg \left(\omega_\varepsilon / \Delta_{2p} \right) \right]; \qquad (2.102)$$
$$c_{n\varepsilon} = (\pi/\Delta_{2s}) \, (\omega - \omega_n) + \ln \left[\omega \left(\omega_\varepsilon^2 + \Delta_{2p}^2 \right)^{-1/2} \right]; \qquad (2.103)$$
$$a_n = \langle 0 | \hat{D} | n \rangle ; \quad \psi_{n\varepsilon} = \langle 0 | \hat{D} | \varepsilon \rangle \langle \varepsilon | \hat{H} | n \rangle ;$$
$$|0\rangle = \left| 2s^2; {}^1 S_o \right\rangle ; \quad |n\rangle = \left| 2s^1 np; {}^1 P_1 \right\rangle ; \quad |\varepsilon\rangle = \left| 2p^4 \varepsilon d; {}^1 P_1 \right\rangle ;$$

where ω is the absorbed photon energy; ω_ε is the $2p - \varepsilon d$ transition energy; ω_n is the $2s - np$ transition energy; $2\Delta_{2s,2p} = \Gamma_{2s,2p}$ are widths of the 2s- and 2p-vacancy decays. The problem of considering the mp-states for $m \in [10; \infty)$ is not solved and is the subject for future inquiries.

The integral term in (2.101) describes the effect of the RPAE correlations. The calculation results in Fig. 2.10 demonstrate the *strong influence* of the RPAE correlations on the 2s-photoabsorption cross-section. We can see that considering the $2p^5\varepsilon d$-states determines the formation of the *asymmetric* resonance profile instead of symmetric Cauchy–Lorentz ones.

In the same figure, the amplitude (2.101) is interpreted from the physical standpoint in the Goldstone–Hubbard–Feynman diagrams representation (at time *forward*). The first diagram is in accord with the first term in the amplitude, while the second (direct) and the third (exchange) diagrams correspond with the integral term. Let us remark here that the time-*back*-diagrams describe the *vacuum correlation effect* which we did not consider in this contest. Considering this effect is the subject of future inquiries.

When constructing the cross-section in Fig. 2.10, we used the calculated value of the 2s-shell ionization potential being equal to 324,90 eV and the value of the 2s-vacancy decay width being equal to 2,04 eV. These values fit well with the experimental values $326,25 \pm 0,05$ eV and $2,25 \pm 0,15$ eV in the work [136].

The appearance of the value Δ_{2p} in (2.102) and (2.103) was interpreted by the authors of the work [137] as the effect of the nonzero widths of the RPAE states vacancy decay. If we consider this effect mathematically, we can discover that the integrals of the *singular* functions are not presented in the photoabsorption amplitude structure. From the practical standpoint, this effect can turn out to be appreciable for very heavy atoms, where the decay widths of the deep 2p-vacancy amount to 9,60 eV, for example, for the atom
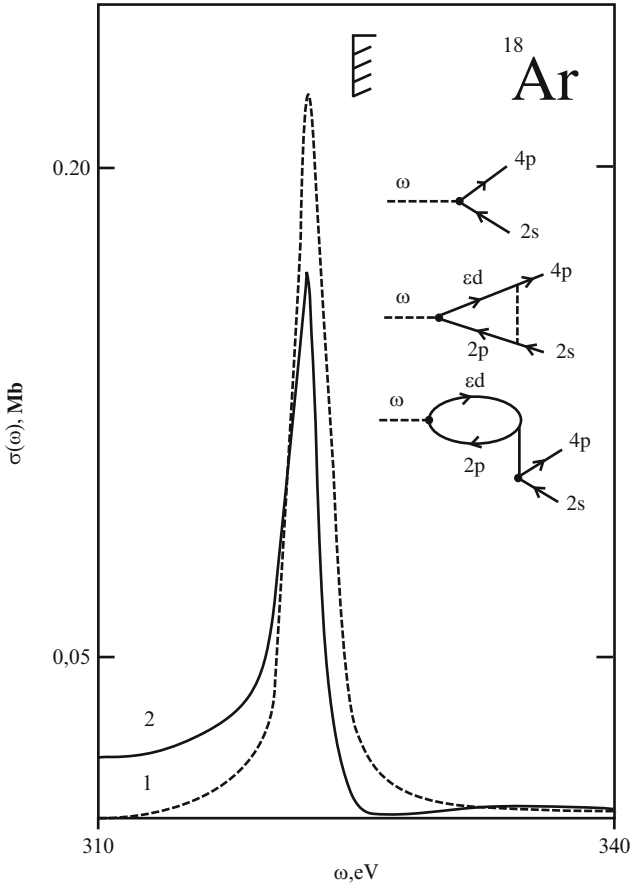
Fig. 2.10. $2s$-$4p$ photoexcitation cross-section for argon atom: 1 – Approximation 2; 2 – Approximation 3. ω is the absorbed photon energy. The calculated location of the $2s$-shell ionization threshold energy $I_{2s} = 324, 90$ eV is indicated. The interpretation of the transition amplitude (2.101) in the Goldstone–Hubbard–Feynman diagrams representation is inserted

of uranium $\left(^{92}\mathrm{U}\right)$ [61]. For the atoms of argon $(\Gamma_{2p} = 0, 13$ eV [138]), krypton $(\Gamma_{2p} = 1.26$ eV [60]), and xenon $(\Gamma_{2p} = 3.25$ eV [60]), its influence on the $2s$-photoabsorption cross-section did not exceed 1% [92, 137].

The calculation results for the scattering cross-section for the atom of argon in the energy region of the ionization L_1-threshold at the scattering angle 60° are represented in Fig. 2.11 [114]. It follows from Fig. 2.11 that the radial relaxation effects and the RPAE correlations ones are the effects *of the same order*. By this means, if calculating and interpreting the scattering spectrum, these effects must be considered simultaneously.
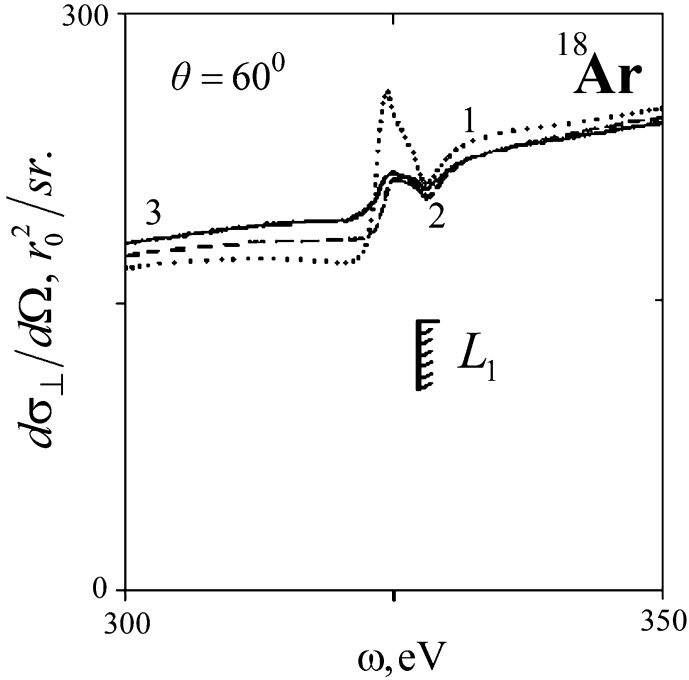
Fig. 2.11. Differential cross-section of the anomalous elastic linear polarized (at right angle to the scattering plane) X-ray photon scattering by argon atom in the energy region of the ionization L_1-threshold: 1, 2, 3 – Approximations 1, 2, 3. θ is the scattering angle, Ω is the solid angle, ω is the scattered photon energy. The measured in the work [136] location of the $2s$-shell ionization threshold energy $I_{2s} = 326, 25 \pm 0, 05 \, \mathrm{eV}$ is indicated

X-ray photon scattering by a heavy atom. Let us summarize the results obtained for *light* atoms in the case of elastic X-ray photon scattering by *heavy* atoms.

Atom of ^{36}Kr: scattering in the $1s$-shell ionization threshold region. We obtained the differential cross-section (2.22) to two approximations which are similar for the atom of neon. The ionization threshold energy of the krypton $1s$-shell is significantly segregated from the ionization threshold energy of other atomic core shells (for example, $\omega_{1s} - \omega_{2s} = 12, 646 \, \mathrm{keV}$). For this reason, the scattering amplitudes for these shells are taken to Approximation 1.

To identify the photoabsorption processes we studied the cross-section of the X-ray photon absorption by the atom of krypton in the energy region of the $1s$-shell ionization threshold:

$$\sigma_{1s}\left(\omega\right) = \left(4\pi^2/3c\right) \underset{m>f}{S} \, L_{1s}\left(\omega,\omega_m\right)\omega_m \left|A_{1s}^{mp}\right|^2 + \sigma_{1s}^{XANES}\left(\omega\right);$$

$$L_{1s}\left(\omega,\omega_m\right) = \left(\Gamma_{1s}/2\pi\right)\left[\left(\omega-\omega_m\right)^2 + \Gamma_{1s}^2 \, / \, 4\right]^{-1}, \qquad (2.104)$$

where A_{1s}^{mp} is the probability amplitude, ω_m is the $1s$-mp transition energy, Γ_{1s} is the width of the $1s$-vacancy decay, ω is the absorbed photon energy, c is the light speed, and $\sigma_{1s}^{XANES}\left(\omega\right)$ is the cumulative cross-section of the double excitation/ionization processes (the calculation method – see Part 2.2.2). To all approximations in (2.104) we considered only the radiative transitions into $5p$-, $6p$-, $7p$- states of the photoelectron (Fig. 2.12). These transitions determine the broad resonance of the scattering cross-section in the photon energy region $\omega \cong 14325 \pm 3$ eV (Fig. 2.13). The problem of considering the mp-states for $m \in [8;\infty)$ is not solved and will be the subject for future inquiries.

The calculated energy value of the $1s$-shell ionization threshold amounted to 14325,911 eV. This value corresponds well with the experimental one – 14327,190 eV [125]. For the total width of the $1s$-vacancy decay we took the theoretical value 2,69 eV [60].

The discrete part of the near fine structure of the absorption spectrum (Fig. 2.12, 2.13) is determined through the radiative transitions to the states [82]:

$$|1\rangle = -0,8\,\gamma_3\,5p^2\left(^3P\right) + 0,5\,\gamma_1\,4d^2\left(^1D\right);$$
$$|2\rangle = 0,7\,\gamma_1\,5p^2\left(^1D\right) - 0,5\,\gamma_3\,4d^2\left(^3P\right);$$
$$|3\rangle = 0,5\,\gamma_3\,5p6p\left(^3D\right);$$
$$|4\rangle = 0,7\,\gamma_1\,5p6p\left(^1D\right);$$
$$|5\rangle = 0,5\,\gamma_1\,4d5d\left(^1D\right).$$

$\gamma_{1,3} \equiv 1s^14p^5\left(^{1,3}P\right)$ is indicated here and the terms with the mixing coefficient $\left|a_{12}^{LS}\right| \geq 0,50$ are deducted in the structure of the wave functions (2.45). The components $1s^14p^5n_1dn_2d$, $1s^14p^5n_1sn_2\,(s,d)$ of the states (2.45) are "*shadow*" components, since they do not contribute to the radiative transition amplitude to the *dipole* approximation. Actually, the rules of the orbital quantum number l selection do not allow transiting to the states $1s^14p^5n_1dn_2d$. The transitions to the states $1s^14p^5n_1sn_2\,(s,d)$ are not allowed by reason of the orthogonality demand of the wave functions of these transitions for the wave functions of the states with the same symmetry situated below on the energy scale (see Part 2.2.2). The channels of the double excitation/ionization and of the double ionization of the krypton ground-state $1s^14p^5\left(np\,\varepsilon\,p;\varepsilon p\,\varepsilon'p\right)$, $n = 5,6$ are open, if the energies of the scattered photon are 14344,70, 14348,21, and 14351,97 eV correspondingly.

The calculation results for the scattering cross-section are represented in Fig. 2.13, 2.14, and in Table 2.4 [97]. According to these results, the conclusions we made with reference to the role of the radial relaxation effect and the
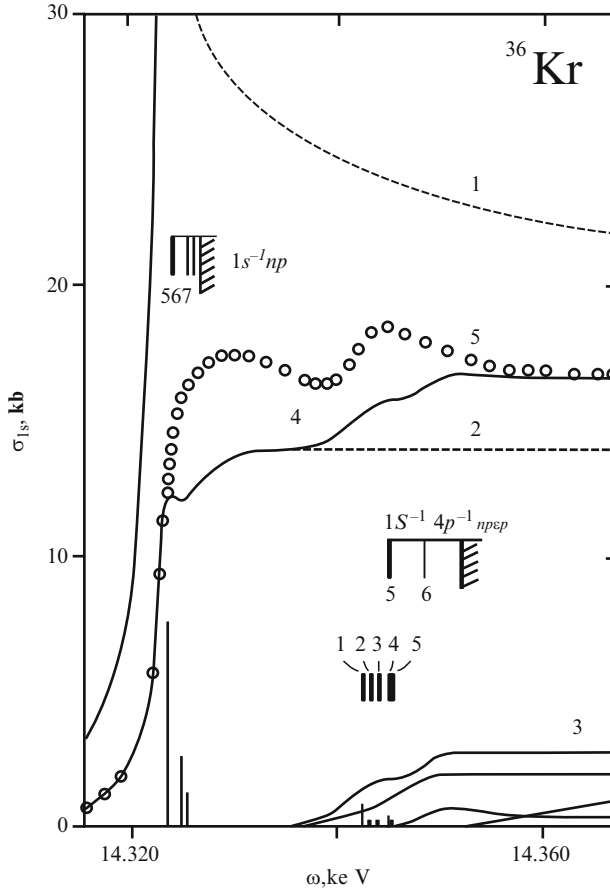
Fig. 2.12. Cross-section of X-ray photon absorption by krypton $1s$-shell: 1 – Approximation 1; 2 – the radial relaxation effect is considered; 3 – the cumulative cross-section of the double excitation/ionization; the curves under the curve 3 are partial cross-sections of the double excitation/ionization for $n = 5, 6$ and ε correspondingly; 4 – Approximation 2 (sum spectrum); 5 – synchrotron experiment in the work [139]. The states of the double photoexcitation marked by numbers are identified in the text. The width of the $1s$-vacancy decay is $\Gamma_{1s} = 2,69\,\text{eV}$ [60]. ω is the absorbed photon energy. The calculated energy locations of the krypton ionization thresholds $K\,(14325,911\,\text{eV})$ and $KN_{23}\,(14351,970\,\text{eV})$ are indicated

double excitation/ionization processes are similar to the conclusions for the light atoms.

Let us formulate the *additional* obtained results:

1. If increasing the scattering angle, we notice the profound influence both of the radial relaxation effect of the electron shells in the $1s$-vacancy field
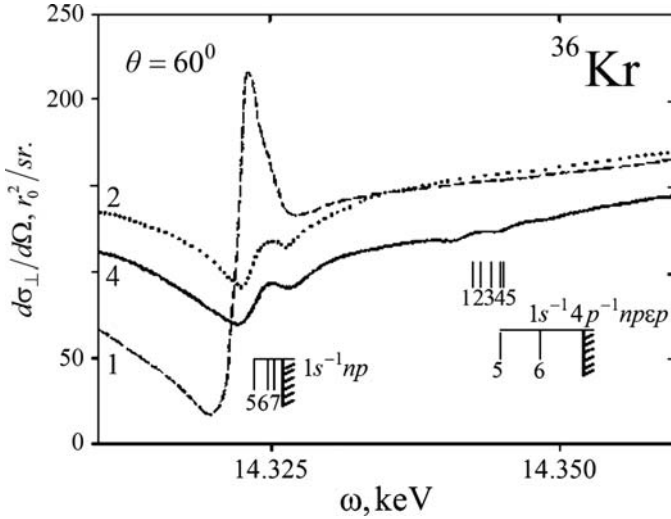
Fig. 2.13. Differential cross-section of the elastic linear polarized (at right angle to the scattering plane) X-ray photon scattering by krypton atom in the energy region of the 1s-shell ionization threshold. The symbols are the same as in **Fig. 2.12**. ω is the scattered photon energy, Ω is the solid angle, θ is the scattering angle

and double excitation/ionization processes on the theoretical scattering cross-section. To demonstrate this result we shall define the value:

$$\eta_\perp\,(\omega;\theta) = (d\sigma_\perp/d\Omega)_2 \,/\, (d\sigma_\perp/d\Omega)_1\,, \tag{2.105}$$

which characterizes the degree of suppression or increase in theoretical elastic scattering intensity, when transiting from Approximation 1 (index 1) to Approximation 2 (index 2). In Table 2.4, the scattering angle dependence of the value (2.105) is represented, when the photon energy is equal to the energy of 1s-shell ionization threshold for krypton atom.

2. If increasing the atom nuclear charge, the domain of appreciable influence of many-particle effects on the theoretical elastic scattering cross-section corresponds with the large scattering angles. We obtain this result as a consequence of the previous conclusion considering the fact that the atom form factor agrees with the atom nuclear charge, if the scattering angle is zero.

By this means, predicting the theoretical models for heavy atoms based on the approximation of "independent particles" [8, 43] (without considering the radial relaxation effect) should distinctly disagree with experimental data, first of all, if the scattered angles are *large*. While arguing for this statement we can mention the fact that $20\% \div 70\%$ disagreements are discovered between the values of the elastic large-angle scattering cross-section by a number of heavy atoms measured and calculated to approximation of "independent particles"
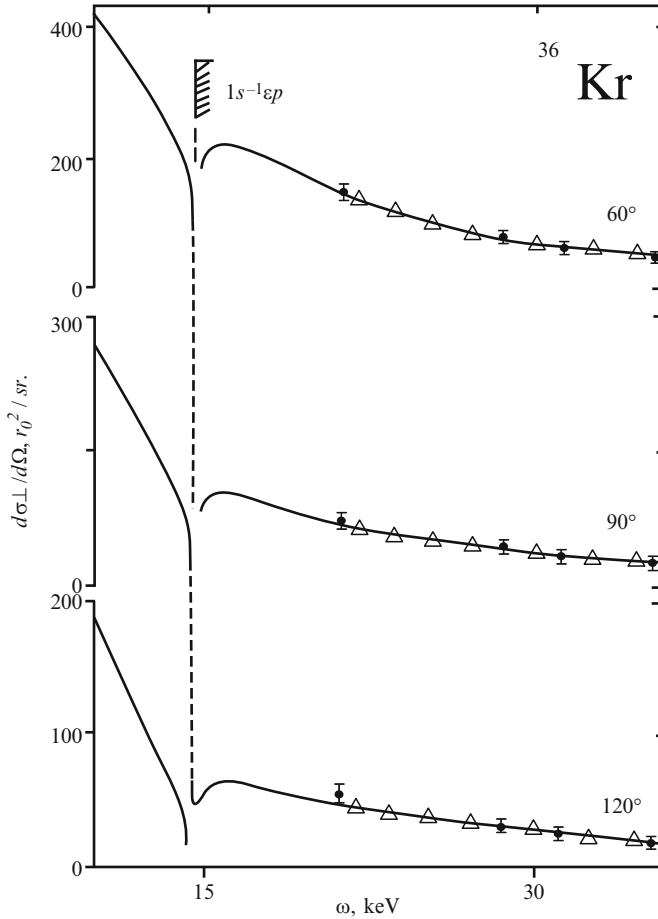
Fig. 2.14. Differential cross-section of the anomalous elastic linear polarized (at right angle to the scattering plane) X-ray photon scattering by krypton atom at the angles $60°$, $90°$, and $120°$. The points and triangles indicate the synchrotron experiment and theory (the relativistic Kissel-Pratt algorithm) in the work [43]; the continuous curve indicates the theory of present work (Approximation 2). Ω is the solid angle, ω is the scattered photon energy. The energy location of the krypton $1s$-shell ionization threshold $I_{1s} = 14325,911\,\mathrm{eV}$ is represented

in the works [41] (the atoms of ^{30}Zn, ^{42}Mo, ^{50}Sn, ^{73}Ta, ^{79}Au, ^{82}Pb) and [44] (the atoms of ^{82}Pb, ^{83}Bi).

Atom of ^{54}Xe: scattering in the $1s$-shell ionization threshold region. The calculation method for the scattering cross-section (2.22) and the conclusions as well are the same as for krypton atom. For this reason we shall present only the calculation results. They are given in Fig. 2.15, 2.16 [99].

Table 2.4. Scattering angle dependence of the value (2.105) for krypton atom when X-ray photon energy is $I_{1s} = 14325,911$ eV

θ , degree	0^0	30^0	60^0	90^0	120^0
$\eta_\perp\,(\omega_{1s};\theta)$	0,90	0,81	0,64	0,39	0,23

The calculation results for K-photoabsorption cross-section (2.104) are represented in Fig. 2.15. At all approximations only the most intensive transitions to the $6p$-, $7p$- and εp- states of the photoelectron are considered. The problem of considering the np-states for $n \in [8; \infty)$ is not solved and it is a subject for future inquiries. The calculated energy value for $1s$-shell ionization threshold amounted $I_{1s} = 34564,21$ eV. In this connection we considered the relativistic correction for the threshold energy 1309,50 eV [131]. The obtained value corresponds well with the experimental ones 34565,40 eV represented in the work [140]. As a width of the $1s$-vacancy decay we took the theoretical value 11,49 eV from the work [141].

The channels of the double excitations/ionization and the double ionization $1s^15p^5\,(np\,\varepsilon p;\,\varepsilon p\,\varepsilon'p)$ are open, if the scattered photon energies are 34580,21 $(n = 6)$, 34583,32 $(n = 7)$, and 34587,03 eV. The channels of the double excitation make a small vanishing contribution to the photoabsorption intensity and we did not consider them when calculating the scattering cross-section.

The amplitudes of the radiative $1s$-shell-assisted transitions are calculated in the length form, since the RPAE correlations change them not more than 1% [142].

For comparison, the results of the cross-section calculation are represented for the $1s$-shell ionization of xenon atom from the work [142] in Fig. 2.15. It is specified in this work that considering the *spinor* structure of the electron wave functions (curve **5**) leads to $10\% \div 12\%$ value decrease of ionization cross-section at nonrelativistic approximation (curve **2**). Considering this effect for compound nonrelativistic ionization cross-section (transition from curve **4** to curve **6**) makes the theory agree significantly with the experiment (curve **7**).

As widths of the $nl \neq 1s$ vacancy decay (in eV) we took the following values: $4,00\,(2s)$, $3,25\,(2p)$, $5,50\,(4s)$, $3,00\,(4p)$, $0,09\,(4d)$ [60], $11,70\,(3s)$ [143], $5,16\,(3p)$, $0,68\,(3d)$ [144], and $0,19 \cdot 10^{-7}\,(5s)$ [145]. There is no information about the width of $5p$-vacancy decay in the literature, and so we accepted it to be equal to the width of the $5s$-vacancy decay. For the energies of $nl \neq 1s$ shells ionization thresholds we took the values represented in the works [125, 146].

Atom of ^{54}Xe: scattering in the $2p$-shell ionization threshold region. Let us study the influence of *spin-orbit splitting* effect of the atom deep shell on the theoretical scattering cross-section. As a subject of inquiry we took the cross-section of the elastic X-ray photon scattering in the energy region of the $2p$-shell ionization threshold for xenon atom. The choice is conditioned by the fact that the form of $2p$-photoabsorption spectrum for
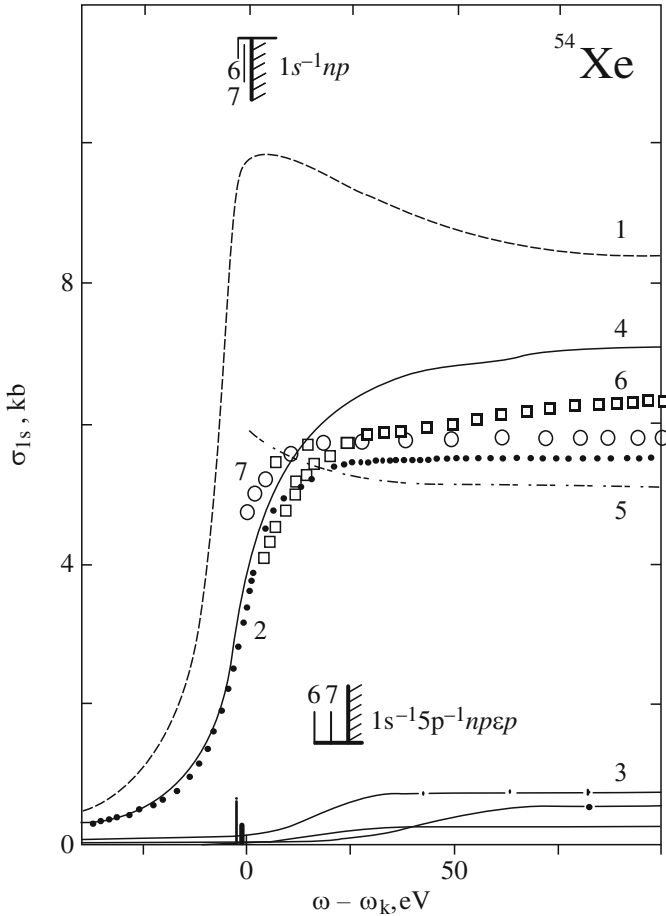
Fig. 2.15. Cross-section of the X-ray photon absorption by xenon atom $1s$-shell: 1 – Approximation 1; 2 – Approximation 2; 3 – partial cross-sections of double excitation/ionization for $n = 6, 7$ and ε correspondingly; 4 – Approximation 2 (sum spectrum); 5 – the theory from the work [142]; 6 – Approximation 2 considering the result [142]; 7 – the synchrotron experiment from the work [149]. The width of the $1s$-vacancy decay $\Gamma_{1s} = 11, 49 \, \text{eV}$. ω is the absorbed photon energy. The calculated energy locations for xenon atom ionization thresholds K (34564, 21 eV) and KO_{23} (34587,03 eV) are marked

xenon atom is mainly determined through the spin-orbit splitting effect of the $2p_{1/2,3/2}$ - shell [147, 148].

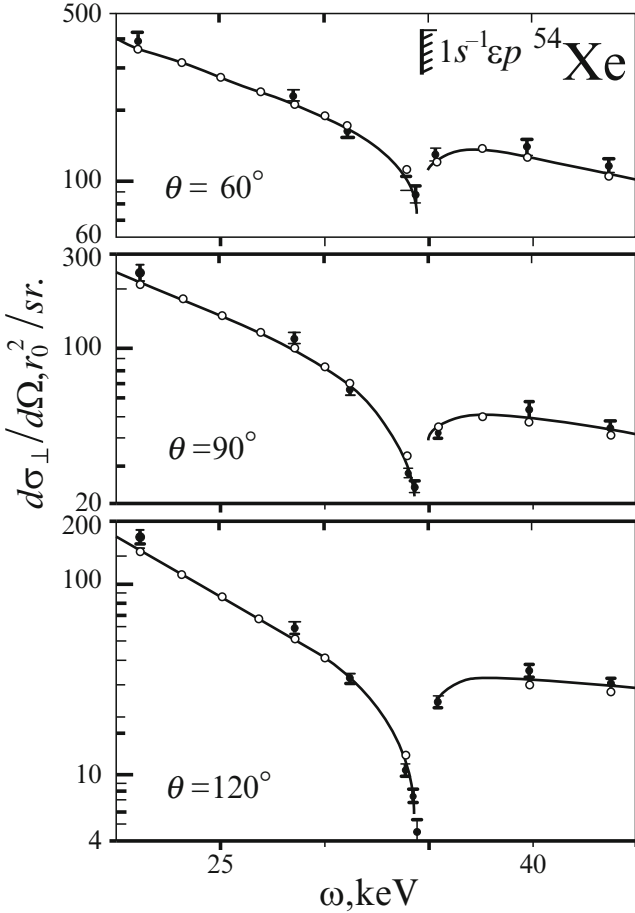The radiative transition amplitude and the $2p$-photoabsorption cross-section are obtained at two approximations.

Fig. 2.16. Differential cross-section of the anomalous elastic linear polarized (at right angle to the scattering plane) X-ray photon scattering by xenon atom. The points and light circles demonstrate the synchrotron experiment and theory (the relativistic Kissel-Pratt algorithm) in the work [43]; the continuous curve presents the theory of this work (Approximation 2). θ is the scattering angle, Ω is the solid angle, ω is the scattered photon energy. The calculated energy location of the $1s$-shell ionization threshold for xenon atom $I_{1s} = 34564, 21$ eV is indicated. The scale of cross-sections is given in logarithmic scale

Approximation 1: without considering the radial relaxation effect for electron shells in the $2p$-vacancy field. The states of single excitation/ionization $2p^5 (m, \varepsilon) (s, d)$, $m \leq 7$ are considered.

Approximation 2: the radial relaxation effect for electron shells in the $2p$-vacancy field is considered.

The amplitudes of the $2p$-shell-assisted transitions are calculated in the length form, since the RPAE correlations change their values not more than 1%.

The problem of considering the $m(s, d)$-states for $m \in [8; \infty)$ is not solved and it is a subject for future inquiries.

To consider the spin-orbit splitting effect of the $2p$-shell at all approximations, we determined the wave functions of the final states in two stages.

At the *first* stage we obtained the wave functions of the single excitation/ionization states having used the energy matrix diagonalization of the spin-orbit splitting operator [10] at the LSJ-bonding approximation:

$$|nJ\rangle = \sum_{LS} a_{LSJ} \left|2p^5 n\,(s, d)\,;\, {}^{2S+1}L_J\right\rangle;\qquad (2.106)$$

where a_{LSJ} are the coefficients of term mixing.

At the *second* stage we considered the wave functions (2.106) mixing with the wave functions of the $|\,mJ\,;\,i\rangle$-channels of the $2p$-vacancy Auger-decay:

$$|\omega nJ\rangle = \rho_{n\omega}^{1/2}\left(|nJ\rangle + \sum_{i=1}^{N} \underset{m>f}{S}\,\beta_{nm}^{iJ}(\omega)\,|mJ;\,i\rangle\right);\qquad (2.107)$$

$$\langle \omega nJ|\,\omega'n'J'\rangle = \delta_{nn'}\delta_{JJ'}\delta\left(\omega - \omega'\right);$$

$$\rho_{n\omega} = \left(\Gamma_{2p}/2\pi\right)\left[\left(\omega - \omega_n\right)^2 + \Gamma_{2p}^2/4\right]^{-1}.$$

The following values are defined in (2.107): Γ_{2p} is the width of the $2p$-vacancy Auger-decay, ω_n is the energy of $2p$-$n\,(s, d)$ transition, ω is the absorbed photon energy. The calculated energy values for the $2p_{1/2,3/2}$- shell ionization thresholds $4791{,}54\,\mathrm{eV}$ (L_3-threshold) and $5089{,}44\,\mathrm{eV}$ (L_2-shell) correspond well with the experimental [125] ones $4782{,}16\,\mathrm{eV}$ and $5106{,}72\,\mathrm{eV}$. The widths of the $2p$-vacancy decay we took from the graphic data represented in the works [60, 61]: $\Gamma_{2p}\,(L_3) = 3{,}00\,\mathrm{eV}$ and $\Gamma_{2p}\,(L_2) = 3{,}25\,\mathrm{eV}$.

The near-edge $2p$-photoabsorption fine structure spectrum of xenon atom observed in the experiment [147] in the photon energy region $\omega \geq 4806\,\mathrm{eV}$ is determined through the excitation/ionization of the outer $4d$-, $5s$- and $5p$- shells in the ground state. This structure is not analyzed in the present treatise.

The calculation results for the cross-section of the X-ray photon scattering by xenon atom in the energy region of $2p$-shell ionization thresholds are represented in Fig. 2.17 [114]. It follows from them that the radial relaxation effect of electron shells (against the "background" of the spin-orbit $2p$-shell splitting effect) changes significantly the results of Approximation 1. Actually, we have to deal with redistribution of scattering intensity from L_2-threshold region into L_3-threshold region, suppression of resonance intensity, and minimum shift to the short-wave region of the theoretical elastic scattering cross-section.
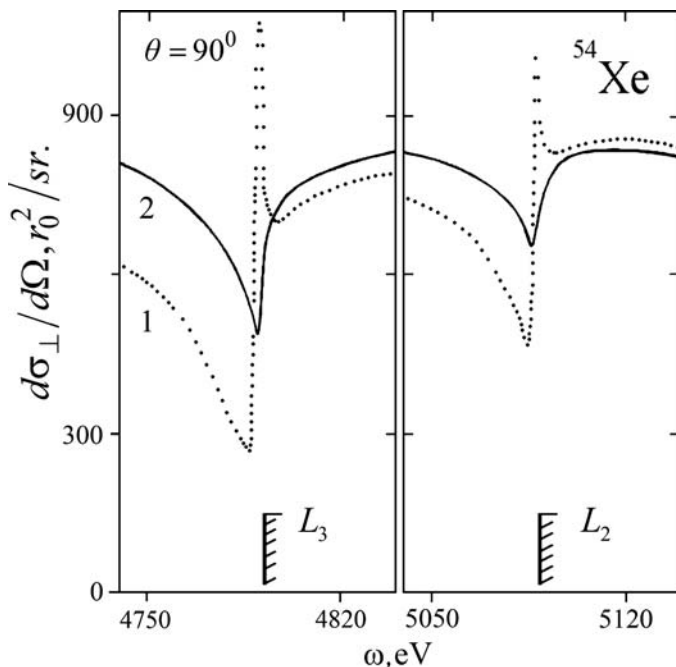
Fig. 2.17. Differential cross-section of the elastic linear polarized (at right angle to the scattering plane) X-ray photon scattering by xenon atom in the energy region of the ionization L_3- and L_2-thresholds: 1, 2 – Approximations 1, 2. ω is the scattered photon energy, θ is the scattering angle, Ω is the solid angle. The calculated energy location of the ionization thresholds $I\left(L_3\right) = 4791,54\,\mathrm{eV}$ and $I\left(L_2\right) = 5089,44\,\mathrm{eV}$ is indicated

2.7.2 Open-Shell Atoms in the Ground State: ^{11}Na,^{42}Mo

Let us take a look at the results of theoretical investigations dealing with the cross-section of elastic X-ray photon scattering by an *open*-shell atom in the ground state in the energy region of its deep $1\,s$-shell ionization threshold. As subjects of inquiry we chose the atoms of sodium and molybdenum. Such choice is conditioned by the following reasons. The atom of sodium is a simple many-electron system having one$(3s)$ electron *outside* the filled shells of the ground state configuration. The near-threshold structure of the sodium K-photoabsorption spectrum has been analyzed enough theoretically [80, 81, 87] and experimentally [75, 76]. The atom of molybdenum is presently the only one element of the Mendeleev's table, for the experimental data [42], obtained for the *absolute* values of the differential cross-section of the elastic X-ray photon scattering in the immediate vicinity of the 1s-shell ionization energy.

Atom of ^{11}Na: scattering in the *1s*-shell ionization threshold region. The elastic scattering (2.22) for the $1\,s$-shell is calculated at two approximations.

Approximation 1: the radial relaxation effects of the electron shells in the $1s$-vacancy field and the $^{1,3}S$-term splitting effects of the $1s^1 3s^1 [^{1,3}S] mp^1 \, (^2P)$ photoabsorption states are not considered.

Approximation 2: the radial relaxation effects of the electron shells in the $1s$-vacancy field and the mentioned splitting effects are considered.

At all approximations we considered only the most intensive transitions to the photoelectron $3p$-, $4p$- and $5p$- states. The problem of considering the np-states for $n \in [6; \infty)$ is not solved and it is a subject for future inquiries.

The radiative $1s$-shell-assisted transitions amplitudes are calculated in the length form, since the RPAE correlations change their values not more than 1%.

For the width of the $1s$-vacancy decay and the energy of the $1s$-shell ionization threshold we used the values $\Gamma_{1s} = 0,80\,\text{eV}$ for $m = 3$, $\Gamma_{1s} = 0,55\,\text{eV}$ for $m = 4, 5$ and $I_{1s} = 1079,10\,\text{eV}$, measured in the experimental photoabsorption spectrum [76]. We did not analyze such significant distinctions for the widths of the $1s$-vacancy decay when changing the main quantum number of the mp-photoelectron. It is a subject for future inquiries.

Along with the $1s$-mp transitions we considered the radiative transitions to the double excitation/ionization states (2.48) and (2.50) in Approximation 2. The radiative transitions to the photoabsorption states show the best correlation with the resonances in the region of the near-edge scattering cross-section fine structure in Fig. 2.18:

$$|1\rangle = 0,99\,\gamma\,4s\,\left(^{1,3}S\right)\,3p;$$
$$|2\rangle = 0,93\,\gamma\,5s\,\left(^{3}S\right)\,3p;$$
$$|3\rangle = 0,80\,\gamma\,4p\,\left(^{3}P\right)\,3d + 0,50\,\gamma\,4s\,\left(^{3}S\right)\,4p; \qquad (2.108)$$
$$|4\rangle = -0,50\,\gamma\,4p\,\left(^{1}P\right)\,3d + 0,80\,\gamma\,4s\,\left(^{1}S\right)\,4p; \qquad (2.109)$$
$$|5\rangle = -0,80\,\gamma\,4s\,\left(^{3}S\right)\,4p.$$

Here $\gamma \equiv 1s^1 2s^2 2p^6$, and the terms with $\left|a_{12}^{LS}\right| \geq 0,50$ are deducted in the wave functions (2.50) structure. The "shadow" $1s^1 n_1 p \left(^{1,3}P\right) n_2 d$ components of the states (2.108) and (2.109) do not contribute to the radiative transition amplitude at the dipole approximation and appear in the scattering spectrum through the mixing with $1s^1 n_1 s \left(^{1,3}S\right) n_2 p$ components. The channels of the double excitation/ionization $1s3s \rightarrow 3p\varepsilon s, 4s\varepsilon p$ are open when the scattered photon energies are 1084,76 eV and 1089,02 eV correspondingly.

The energies of the $2s$-, $2p$-, $3s$- shell ionization thresholds are significantly far removed from the energy of the $1s$-shell ionization threshold (for example, $\omega_{1s} - \omega_{2s} \cong 1\,\text{keV}$). For this reason, the scattering amplitudes for the $nl \neq 1s$ shells are calculated at Approximation 1.

The main conclusions [116] are the same as for atoms of neon and argon. We shall add only one new condition. The presence of the open $3s^1$-shell in the ground state does not disturb (see Part 2.6 for $^2S_{1/2}$-term of the atomic ground state) the analytical structure of its form factor (1.4). But the
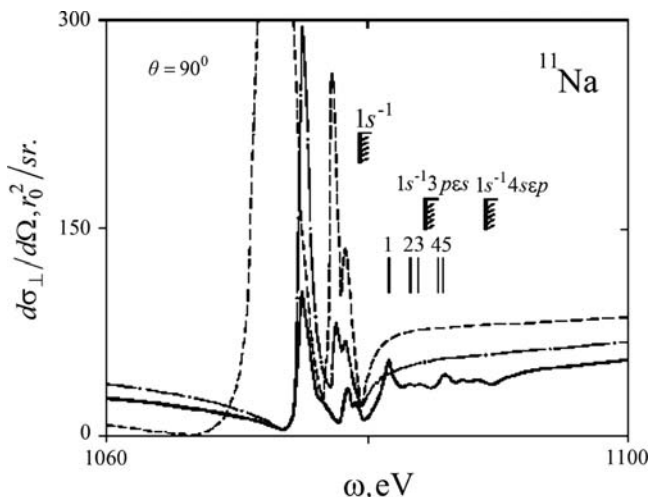
Fig. 2.18. Differential cross-section of the elastic linear polarized (at right angle to the scattering plane) X-ray photon scattering by atom of sodium in the energy region of the $1s$-shell ionization threshold. The broken curve indicates Approximation 1; the continuous curve indicates Approximation 2; the chain curve – the radial relaxation effect of the electron shells in the $1s$-vacancy field is considered without $^{1,3}S$-terms splitting of the $1s^1 3s^1[^{1,3}S]mp^1$ (^2P) states. The scattering resonances marked by numbers, and the values of the indicated energy locations of the ionization thresholds are identified in the text. ω is the scattered photon energy, Ω is the solid angle, θ is the scattering angle

$^{1,3}S$-term splitting effect of the $1s^1 3s^1$ $[^{1,3}S]$ mp^1 (^2P) photoabsorption states results in complication of the scattering cross-section resonance structure.

Atom of ^{42}Mo: scattering in the *1s*-shell ionization threshold region. The form factor of molybdenum atom is calculated in the wave functions of electrons obtained by solving the Hartree-Fock equation for the ground state configuration $1s_0^2 4d_0^5 5s_0^1$ $(^7S_3)$. We did not study the influence of the two *open*-shells field on its form factor structure, and restricted ourselves to the spherically symmetric representation (1.4).

The scattering cross-sections (2.22) for the $1s$-shell are obtained at two approximations.

Approximation 1: the radial relaxation effect of the electron shells in the deep $1s$-vacancy field is not considered.

Approximation 2: the radial relaxation effects of the electron shells in the deep $1s$-vacancy field and the effects of the excitation/ionization and double ionization to states:

$$\left|1s^1 4d^5 \left(6s\varepsilon p;\ \varepsilon s5p;\ \varepsilon s\varepsilon'p\right)\right\rangle; \qquad (2.110)$$

$$\left|1s^1 4d^4 5s^1 \left(5d\varepsilon p;\ \varepsilon d5p;\ \varepsilon d\varepsilon'p\right)\right\rangle, \qquad (2.111)$$

are considered. We did not considered the *double* excitation states, since their contribution to the scattering amplitude had turned out to be vanishingly small as compared to the contribution of the states (2.110) and (2.111).

When calculating the amplitudes of the 1s-np photoexcitation, we considered only the states with $n = 5, 6, 7$. It is the subject of future inquiries to consider the states for $n \in [8; \infty)$. The radiative 1s-shell-assisted transitions amplitudes are calculated in the length form, since the RPAE correlations do not change their values more than 1%.

The calculated energy value for the 1s-shell ionization threshold of molybdenum atom amounted to 20007,473 eV. It corresponds well with the experimental [150] value 20008 ± 2 eV. For the width of 1s-vacancy decay we used the theoretical value 6,00 eV [60]. The widths of the $nl \neq 1s$, 4d, 5s vacancies decays are taken from the graphic data of the work [61]. The widths of the 4d-, 5s- vacancies decays are not available in the published works, and we accepted them as equal to 10^{-9} eV.

The 1s-shell ionization threshold for molybdenum atom is significantly far removed from the ionization thresholds of other atomic core shells (for example, $\omega_{1s} - \omega_{2s} \cong 17$ keV). For this reason, the scattering amplitudes for the $nl \neq 1s$ shells are calculated at Approximation 1.

The calculation results for the cross-section and the *real* component of the scattering amplitude from (1.11),

$$f' = \sum_{nl} \operatorname{Re} A_{nl} \qquad (2.112)$$

are represented in Fig. 2.19, 2.20 [117]. When calculating the value (2.112), we did not consider the radiative transitions to the single excitation states.

The transition from Approximation 1 to Approximation 2 can be theoretically interpreted as follows. The electrons and vacancies of the *elastic* scattering states are not observed in the quantum "atom + radiation" system. As a result, the quantum mechanics of many-particle effect is realized at a *virtual* level. We can detect the realizability of this dynamics in the scattering cross-section structure **experimentally** (see Fig. 2.19, 2.20). *Outside* the anomalous dispersive region of the elastic scattering the role of *many-particle effects* in cross-section determination is significantly reduced. For this reason, the results of the relevant experiment in the work [41] for the metallic molybdenum can be interpreted at approximation of the atomic core, unreconstructed in the deep 1s-vacancy field.

2.8 Anomalous Elastic X-Ray Photon Scattering by an Atomic Ion

The transition from the atom to its multicharged positive ion is accompanied by quantity reduction of symmetry-resolved radiative and Auger channels of the deep vacancy decay. This condition results in increasing the vacancy
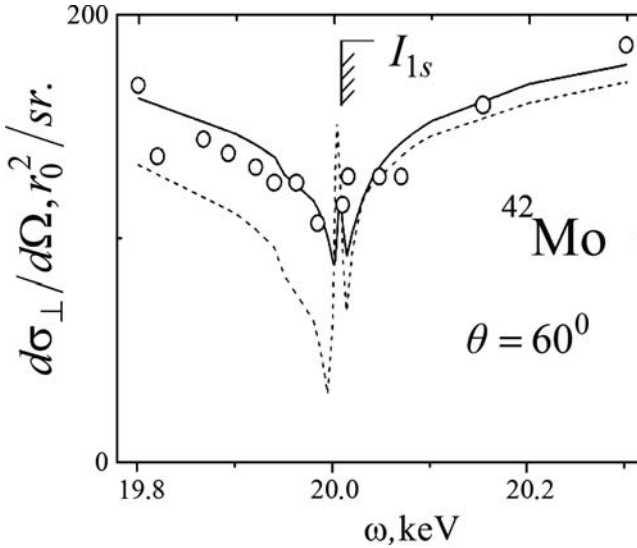
Fig. 2.19. Differential cross-section of the anomalous elastic linear polarized (at right angle to the scattering plane) X-ray photon scattering by molybdenum atom. The circles indicate the experiment for metallic molybdenum in the work [42]; the broken and continuous curves indicate Approximation 1 and Approximation 2. The calculated energy value for the $1s$-shell ionization threshold of molybdenum atom $I_{1s} = 20007,473$ eV. ω is the scattered photon energy, Ω is the solid angle, θ is the scattering angle

lifetime. We shall determine the many-particle effect of this sort as the *deep vacancy stabilization effect* [118] when transiting from atom to its positive ion. In this part of our treatise, we study in theory the resonance cross-section structure of the elastic X–ray photon scattering by an atom and its ion in the energy region of the $1s$–ionization threshold by the example of neon atom and its ion Ne^{6+}. Along with the radial relaxation effect of the electron shells in the $1s$–vacancy field we consider the deep vacancy stabilization effect in the scattering intermediate states.

The calculated width value of the $1s$-shell vacancy decay is $0,2660$ eV for the neon atom, and it corresponds well with the experimental result $0,27$ eV [129]. Let us remark here that the calculated width value $0,1508$ eV of the $1s$-vacancy Auger decay in the *partial* $1s$-$2p2p$ (^1D) channel corresponds well with the experimental value $0,160$ eV in the work [151]. The contribution of the radiative decay channels to the total $1s$-vacancy width of the neon atom does not exceed the value $0,0020$ eV [60].

The calculation for the ion Ne^{6+} is made in two versions (Table 2.5): without considering ($\Gamma_{1s} = 0,2660$ eV) and considering ($\Gamma_{1s} = 0,0486$ eV) the deep vacancy stabilization effect. The wave function of the photoelectron is obtained by solving the Hartree-Fock equation for the scattering
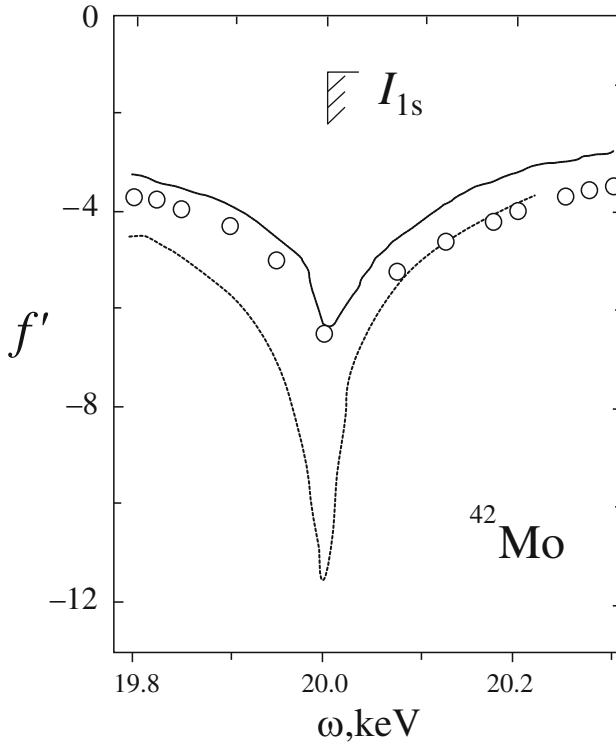
Fig. 2.20. Real component f' of the amplitude of the anomalous elastic nonpolarized X-ray photon scattering by molybdenum atom. The circles indicate the experiment for metallic molybdenum in the work [23]. Other symbols are the same as in **Fig. 2.19**

Table 2.5. Values of partial (Γ_{1s}^n, eV) and total $\left(\Gamma_{1s} = \sum\limits_n \Gamma_{1s}^n, \text{eV} \right)$ widths of the 1s-vacancy decay in the channels (n) of Auger-kind in neon atom and its ion Ne^{6+}

n	Γ_{1s}^n	
	^{10}Ne	Ne^{6+}
$1s - 2p2p \left(^1D\right)$	0,1508	
$\left(^1S\right)$	0,0130	
$1s - 2s2p \left(^3P\right)$	0,0254	
$\left(^1P\right)$	0,0520	
$1s - 2s2s \left(^1S\right)$	0,0248	0,0486
Γ_{1s}	0,2660	0,0486

state $1s^1 2s^2 (n, \varepsilon)\, p\, (^1P_1)$, $n \leq 8$. The difference of the scattering ampli-
tudes, calculated without considering and considering the radial relaxation
effect of the electron shells in the 1s-vacancy field, did not exceed 1%. This
can be explained as follows. The missing 2p-shell determines the stabilization
(*freezing*) of the valence 2s-shell midradius. The following destruction of the
$1s^2$-"screen" ($1s \rightarrow np$ transition) between core and 2s-shell does not lead to
decreasing its midradius.

The almost missing effect of the ion core shells relaxation in the deep
vacancy field determines the vanishing small intensity of the double excita-
tion/ionization processes (0,1% of contribution to the probability scattering
amplitude). By comparison we shall remark that for neon atom the radial
relaxation effect of the electron shells in the 1s-vacancy field results in
the strong suppression of the resonance intensity values, calculated without
considering this effect (Part 2.7.1).

For the width of the 2s-vacancy decay we accepted for neon atom the value
0,05 eV, judged by the experimental 2s-photoabsorption spectrum in the work
[127]. The information on the widths of the 2s-vacancy decay for neon atom
and of the 2s-vacancy for ion Ne^{6+} is not available in published works, and
we accepted them as equal to 10^{-9} eV.

The radiative 1s-assisted transitions amplitudes both for neon atom and
ion Ne^{6+} are calculated in the length form, since the RPAE correlations do
not change their values more than 1%.

The calculation results restricted by considering the 1s-np photoexcitation
states with $n \leq 8$ are represented in Tables 2.5, 2.6 ,and in Fig. 2.21 [118].
The calculation result for ion Ne^{6+} without considering the deep vacancy
stabilization effect is represented only as a part of the scattering full cross-
section.

It follows from the results in Fig. 2.21, that the transition from neon atom
to its ion is accompanied by reconstruction of the scattering cross-section – the
energy region of the scattering resonances is expanding, and the resonances
themselves take the form of elastic scattering giant resonances. The results of
considering (see Part 2.7.1) the set completeness of the 1s-np photoexcitation

Table 2.6. Spectral characteristics for the most intense resonances of the differential
cross-sections of the elastic linear polarized (at right angle to the scattering plane)
X-ray photon $90°$ angle scattering by neon atom and its ion Ne^{6+} in the energy
region of the 1s-shell ionization threshold

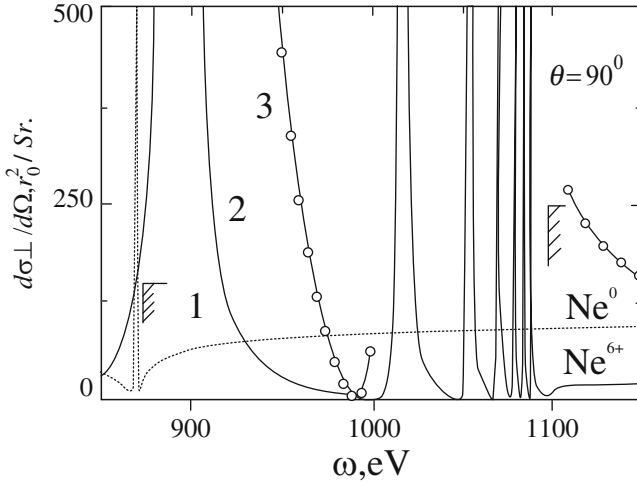| Element	Transition	ω, eV	$d\sigma_\perp/d\Omega$, $r_0^2/sr.$	Γ_{1s}, eV
^{10}Ne	$1s - 3p$	$869, 356$	$8,970 \cdot 10^2$	$0,2660$
Ne^{6+}	$1s - 2p$	$891, 520$	$1,448 \cdot 10^8$	$0,0486$
	$1s - 3p$	$1016, 979$	$5,977 \cdot 10^6$	
	$1s - 4p$	$1054, 286$	$8,674 \cdot 10^5$	

Fig. 2.21. Differential cross-section of the elastic linear polarized (at right angle to the scattering plane) X-ray photon scattering by neon atom and its ion Ne^{6+} in the energy region of the $1s$-shell ionization threshold: 1 – neon atom for $\Gamma_{1s} = 0,2660$ eV; 2 – ion Ne^{6+} for $\Gamma_{1s} = 0,0486$ eV; 3 – ion Ne^{6+} for $\Gamma_{1s} = 0,2660$ eV. θ is the scattering angle, Ω is the solid angle, ω is the scattered photon energy. The calculated energy values for the $1s$-shell ionization thresholds $I_{1s}\left(^{10}Ne\right) = 872,320$ eV and $I_{1s}\left(Ne^{6+}\right) = 1099,131$ eV are indicated

states, when calculating the cross-section (2.22), and the $f'-, f''-$ components of the amplitude of the elastic X-ray photon scattering by the ion Ne^{6+} are represented in Fig. 2.22, 2.23. We used the width value $0,0805$ eV for $1s$-vacancy decay, that was obtained by extrapolation of the theoretical results of the work [152]. For the width of the $2s$-vacancy decay we accepted the estimated value 10^{-9} eV. As expected (Fig. 2.22), considering the set completeness results in eliminating *un*physical minimum of the theoretical scattering cross-section in the energy region of the $1s$-shell ionization threshold.

The results for ion Ne^{6+} have a predictive character and can be particularly used in studying the ^4Be-like ions [153] that are important from the standpoint of plasma physics and astrophysics.

2.9 Many-Particle Effects in Formation of Scattering Indicatrixes

The scattering cross-section (2.22) determines the process characteristic – the *scattering indicatrix* that is important both for theory and application aspect. Many theoretical and experimental works (see for example [154]) are dedicated to studying this characteristic for scattered photon energies lying
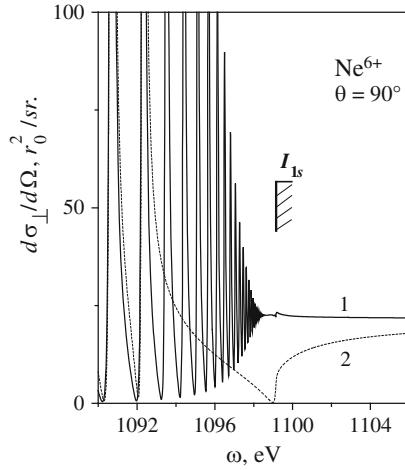
Fig. 2.22. Differential cross-section of the anomalous elastic linear polarized (at right angle to the scattering plane) X-ray photon scattering by ion Ne^{6+}: 1 – the $1s \rightarrow [2; \infty)p$ photoexcitations are considered; 2 – only $1s \rightarrow [2; 10]p$ photoexcitations are considered. θ is the scattering angle, Ω is the solid angle, ω is the scattered photon energy. The calculated energy location of the $1s$-shell ionization threshold $I_{1s} = 1099, 131$ eV is indicated

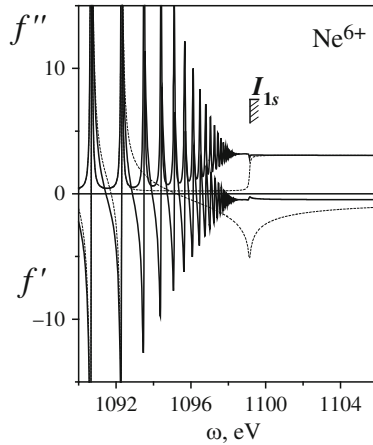**Fig. 2.23.** f'- and f''- components of the elastic scattering amplitude for ion Ne^{6+}. The symbols are the same as in **Fig. 2.22**

outside the energy regions of the atomic deep shells ionization thresholds. But there are no research papers on scattering indicatrixes in immediate proximity ($\pm 1 \div 100$ eV) to energy of the atomic deep shells ionization thresholds in published literature.

Taking into account the results of Part 2.7 we can naturally suggest the following fact. The smoothness breakings of the scattering cross-section that are determined by *many-particle effects* should lead to the relevant changes of the scattering indicatrix forms. The aim of this part of our treatise is to examine this suggestion in theory. As subjects of inquiry the atoms of neon and argon are taken.

Analysis method and calculation results. We shall define the scattering indicatrix as the energy function of scattered photon and scattering angle in the following manner:

$$\rho(\theta, \omega) = D(\theta, \omega) / D(\pi/2, \omega^*).$$

The values ρ and θ here mean the *polar* radius and angle correspondingly, ω^* is the fixed energy value of the scattered photon, and the cross-section (2.22) is indicated as $D(\theta, \omega)$. We accepted $\omega^* = I_{1s} + 5\,(\text{eV})$, where I_{1s} is the energy value of the atomic 1s-shell ionization threshold: $870, 10\,\text{eV}\,(^{10}\text{Ne})$ [129], $3206, 26\,\text{eV}\,(^{18}\text{Ar})$ [84]. For the widths of the 1s-vacancy decay we accepted the values $0, 50\,\text{eV}\,(^{10}\text{Ne})$ [74] and $0, 69\,\text{eV}\,(^{18}\text{Ar})$ [132].

The scattering amplitudes for 1s-shell are obtained at two approximations.

Approximation 1: the radial relaxation effect of the electron shells in the 1s-vacancy field is not considered.

Approximation 2: the radial relaxation effect of the electron shells in the 1s-vacancy field and the double excitation/ionization of the atomic ground state are considered.

The calculation results are represented in Fig. 2.24 and in Table 2.7.

Main conclusions. Analyzing the obtained results we can come to the following conclusions [115].

1. The radial relaxation effect and the double excitation/ionization processes reduce the 90° angle scattering intensity calculated at Approximation 1. In this connection, the reduction degree of the back scattering intensity $\alpha = \rho_1(\pi, \omega) / \rho_2(\pi, \omega)$, exceeds the reduction degree of the forward scattering intensity, $\beta = \rho_1(0, \omega) / \rho_2(0, \omega)$, where the indexes correspond with Approximations 1, 2. As a result, when transiting from Approximation 1 to Approximation 2, the asymmetry degree of the scattering indicatrix, $\gamma = \rho(0, \omega) / \rho(\pi, \omega)$, increases and the monotone character of its dependence on the photon energy disappears (Table 2.7). The monotone disappearance is determined by the double excitation/ionization processes. The increasing of the value γ can be interpreted physically as follows. The *many-particle effects* intensify the primary character of the photon penetrating process to material medium in comparison with its reflection by this medium.

2. If the nuclear charge of an atom increases, the role of the *many-particle effects* play a large role in reducing the reflecting power(back scattering)
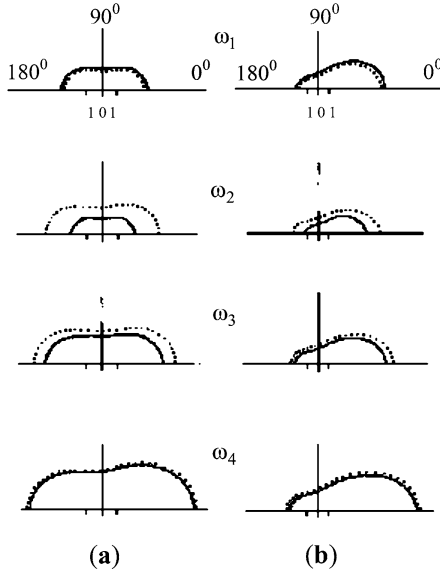
Fig. 2.24. Indicatrixes of the anomalous elastic nonpolarized X-ray photon scattering by atoms of ^{10}Ne (**a**) and ^{18}Ar (**b**). The *dots* indicate Approximation 1; the continuous *curves* indicate Approximation 2. The scattered photon energies (eV) are $\omega_{1,2,3,4} = I_{1s} + [-100, 5, 50, 1000]$. I_{1s} is the energy of the atomic $1s$-shell ionization threshold: 870,10 eV $\left(^{10}\text{Ne}\right)$, 3206,26 eV $\left(^{18}\text{Ar}\right)$

Table 2.7. Calculated dependence of the α, β, γ values for atoms of neon and argon on the X-ray photon energy in the energy region of the $1s$-shell ionization threshold

Atom	ω, keV	γ		α	β	α/β
		1	2			
^{10}Ne	0,875	1,055	1,078	1,885	1,844	1,022
	0,920	1,075	1,076	1,216	1,215	1,001
	1,870	1,324	1,329	1,028	1,025	1,003
^{18}Ar	3,211	2,694	3,937	1,926	1,318	1,461
	3,256	2,841	3,102	1,217	1,115	1,091
	4,206	3,493	3,574	1,056	1,032	1,023

of an atom. According to Table 2.7, the ratio α/β for argon atom exceeds the same for neon atom.

If the photon energies lie outside the anomalous dispersive scattering regions, the results of Approximation 2 repeat the ones of Approximation 1. As a consequence, the changes of the forms of the scattering indicatrixes specified above *disappear*.

Main Results of Chapter 2

1. The *many-particle* quantum theory and the analysis methods for the differential cross-section of the elastic X-ray photon scattering by an atom and atomic ion in the energy region of their deep shells ionization thresholds are developed.
2. The *analytical* structure of the form factor for an *open*-shell atom in the ground state is determined.
3. How the electron correlations in the ground state (^{10}Ne) and the atom nonsphericity effects (^{17}Cl, ^{21}Sc, ^{23}V, ^{35}Br, ^{39}Y, ^{73}Ta) influence the theoretical values and forms of their form factors in the X-ray region of elastic scattering is studied.
4. The differential cross-sections of the anomalous elastic X-ray photon scattering by the closed-shell atoms (ionization K-threshold of ^{10}Ne, ^{36}Kr; ionization K-, L_1-thresholds of ^{18}Ar; ionization K-, $L_{2,3}$-thresholds of ^{54}Xe), by the open-shell atoms (ionization K-threshold of ^{11}Na, ^{42}Mo) in the ground state and by the atomic ion (ionization K-threshold of Ne^{6+}) as well are calculated.
5. The method for considering the *completeness set* of the single photoexcitation states is developed and realized by the example of ^{10}Ne atom and Ne^{6+} ion, when describing the differential cross-section of the elastic scattering in theory.

3

Effect of the Deep Vacancy Auger-Decay When Anomalous Elastic X-Ray Photon Scattering by an Atom

In Chap. 2, we did not consider the effect of the post-collision interaction as we were developing the quantum theory and the calculation methods for the differential cross-section of the elastic X-ray photon scattering by an atom. The reason for this could be attributed to the fact that the effect of the post-collision interaction practically does not change the values and forms calculated for the cross-section of the X-ray absorption by the atomic deep shell in one-configurational Hartree–Fock approximation.

The aim of the present chapter of our treatise is to substantiate in theory this supposition. In Sect. 3.1, the extension of the Hartree–Fock equation for the photoelectron wave function is represented, with provision for the deep vacancy Auger-decay; also represented is the photoelectron-Auger-electron interaction. In Sect. 3.2, the calculation results are presented for the cross-sections of the photon absorption by the 1s-shell of beryllium, neon, and argon atoms with provision for the radial relaxation effect of the photoelectron wave function due to the deep vacancy Auger-decay. In Sect. 3.3, the analytical solution of the Schrödinger equation is determined for the wave function of the interacting photo- and Auger-electrons of the continuous spectrum. The chapter concludes by formulating the results obtained.

3.1 Effect of the Deep Vacancy Auger-Decay in Excitation/Ionization of an Atom: Theory

The aim of this section is to extend the Hartree–Fock equation for the photoelectron wave function, in accordance with the concept of configuration mixing of the atomic deep shell excitation/ionization and the deep vacancy Auger-decay [155].

3.1.1 Atom Photoexcitation

Let us consider the wave function of the final photoexcitation state as the wave function of the superposition of states $|E_0\rangle = \left|n_0 l_0^{-1} nl\right\rangle$ with a deep

$n_0 l_0-$ vacancy and the Auger-decay state of vacancy $|E_1\rangle = \left| n_2 l_2^{-1} n_3 l_3^{-1} \varepsilon_1 l_1 nl \right\rangle$
(where nl is the photoelectron of the discrete spectrum, $\varepsilon_1 l_1$ is the Auger-electron, and $n_{2,3} \leq f$ is the Fermi level):

$$|E\rangle = \alpha_E \left(|E_o\rangle + \int\limits_0^\infty d\varepsilon_1 \, \beta_{E1} \, |E_1\rangle \right); \tag{3.1}$$

$$\langle E| \, E'\rangle = \delta(E - E'); \quad \langle E_1| \, E_2\rangle = \delta(\varepsilon_1 - \varepsilon_2);$$
$$\langle E_o| \, E_o\rangle = 1; \, \langle E_o| \, E_1\rangle = 0.$$

For the wave function (3.1) to be the eigen function of the atom Hamiltonian:

$$\hat{H} |E\rangle = E |E\rangle. \tag{3.2}$$

According to the study of the matrix of intrachannel mixing, (3.2) takes the form:

$$\langle E_1| \, \hat{H} \, |E_2\rangle = E_{nl} \delta(\varepsilon_1 - \varepsilon_2) + \langle \varepsilon_1 l_1| \, \hat{h} \, |\varepsilon_2 l_1\rangle + A_{12}^{nl}; \tag{3.3}$$

where E_{nl} is the energy of the state $|E_{nl}\rangle = \left| n_2 l_2^{-1} n_3 l_3^{-1} nl \right\rangle$ without Auger-electron, $A_{12}^{nl} = (a_{12} + a_{12}^{nl})$ is the term describing the Auger-electron interaction with atomic core shells (a_{12}), and nl is the photoelectron (a_{12}^{nl}); $\hat{h} = -(1/2) d^2/dr^2 + l(l+1)/2r^2 - Z/r$.

It is possible to represent the matrix element (3.3) in the diagonal form as

$$\langle E_1| \, H \, |E_2\rangle \to E_1 \delta(\varepsilon_1 - \varepsilon_2), \tag{3.4}$$

assuming that the wave function of the Auger-electron satisfies the equation:

$$\langle \varepsilon_1 l_1| \, \hat{h} \, |\varepsilon_2 l_1\rangle + A_{12}^{nl} = \varepsilon_1 \delta(\varepsilon_1 - \varepsilon_2); \tag{3.5}$$
$$\varepsilon_1 = E_1 - E_{nl}.$$

Solving (3.5), we assume that the set of one-electron wave functions of the state $|E_{nl}\rangle$ is *already known*. It is specifically assumed that the wave function of the nl-photoelectron is obtained in the atomic core field, being changed due to the Auger-decay.

The problem of deducing such a wave function of the nl-photoelectron is the subject of our further study. Without solving this problem we cannot clarify the influence of the radial and angular correlations in the photo- and Auger-electron motion on the cross-section of the elastic X-ray photon scattering by an atom.

The authors [155] recommend solving the problem of deducing the wave function of the nl-photoelectron in two stages.

In the *first* stage, (3.5) is solved on the wave function of the "start-up" nl^*-photoelectron, the state in the Hartree–Fock field of the $\left| n_2 l_2^{-1} n_3 l_3^{-1} \right\rangle$

- core. Then, the expression (3.3) takes the form:

$$\langle E_1 | H | E_2 \rangle = E_1 \delta(\varepsilon_1 - \varepsilon_2) + \varphi_{12}; \tag{3.6}$$
$$\varphi_{12} = a_{12}^{nl} - a_{12}^{nl*}.$$

Thereafter, the value φ_{12} will represent the small parameter of the theory.

In the *second* stage, the analog of the multi-configuration Hartree–Fock–Jucys equation for the wave function of the nl-photoelectron is set up on the variation principle – the condition of the energy E extremeness wherein the value of $|\alpha_E|^2$ is high.

Calculating the matrix elements of the atom Hamiltonian and considering (3.6), we deduce the *integral equations* for the coefficient of configuration mixing

$$\beta_{E1} = \mu_1 \left(V_1 + \int_0^\infty d\varepsilon_2 \, \beta_{E2} \, \varphi_{12} \right); \quad V_1 = \langle E_0 | \hat{H} | E_1 \rangle; \tag{3.7}$$

and the energy of the state (3.1)

$$E = E_0 + \int_0^\infty d\varepsilon_1 \, V_1 \, \beta_{E1}; \quad E_0 = \langle E_0 | \hat{H} | E_0 \rangle. \tag{3.8}$$

In (3.7), the generalized function of the form is determined as

$$\mu_1 = P(E - E_1)^{-1} + z_E \delta(E - E_1),$$

where P is the symbol of the Cauchy integral principle value and the real function z_E will be determined later.

Using (3.7) and the operator equality for the product of singular functions [156, 157]

$$\frac{P}{(E' - E_1)} \cdot \frac{P}{(E - E_1)} = \frac{P}{(E' - E)} \left(\frac{P}{E - E_1} - \frac{P}{E' - E_1} \right) + \hat{B},$$
$$\hat{B} = \pi^2 \delta(E_1 - E') \delta(E_1 - E),$$

we can reduce the expression (3.8) to the form:

$$E = E_0 + F_E + z_E \, |V_E|^2 + \sum_{n=2}^\infty \int_0^\infty \Phi_n \prod_{i=1}^n \mu_i d\varepsilon_i; \tag{3.9}$$

$$\Phi_n = V_1 V_n \prod_{i=1}^{n-1} \varphi_{i,i+1}; \quad V_E = V_1 \, |_{E_1 = E} ;$$

$$F_E = P \int_0^\infty d\varepsilon_1 \, |V_1|^2 \, (E - E_1)^{-1}.$$

The second and the last terms in (3.9) describe the shift of the observed value for the resonance energy of the photoexcitation cross-section, relative to the theoretical value E_0. Owing to the smallness of the values $\varphi_{i,i+1}$ and under the supplementary condition for the z-function

$$|z_E \varphi_{i,i+1}| \ll 1 \tag{3.10}$$

we can transform expression (3.9) to:

$$E = E_0 + F_E + \Delta_E + z_E \left(|V_E|^2 + C_E \right); \tag{3.11}$$

$$\Delta_E = \sum_{n=2}^{\infty} \mathrm{P} \int_0^{\infty} \Phi_n \prod_{i=1}^{n} (E - E_i)^{-1} d\varepsilon_i;$$

$$C_E = 2\,\mathrm{P} \int_0^{\infty} d\varepsilon_1\, V_1 V_E\, \varphi_{1E}\, (E - E_1)^{-1}.$$

The relation (3.11) is used for the *definition* of the z-function. Now, the E-energy function in (3.11) cannot be the "object" of variation, because it determines the z-function. Thus, for this reason we *posit* the second stage, described above for solving the problem of determining the wave function of the photoelectron.

We can deduce the normalization factor in (3.1) from the condition:

$$\langle E|\, E' \rangle = \delta(E - E') = \alpha_E \alpha_{E'} \left(1 + \int_0^{\infty} d\varepsilon_1\, \beta_{E1}\, \beta_{E'1} \right). \tag{3.12}$$

On substitution of (3.7) in (3.12), we get on condition (3.10):

$$|\alpha_E|^2\, (\pi^2 + z_E^2) \left(|V_E|^2 + C_E \right) = 1. \tag{3.13}$$

Considering (3.11), we obtain from (3.13) the spectral density of the final states:

$$|\alpha_E|^2 = (\gamma_E/\pi)\, [(E - E_0 - F_E - \Delta_E)^2 + \gamma_E^2]^{-1}; \tag{3.14}$$
$$\gamma_E = \Gamma_E/2 = \pi\, (|V_E| + C_E).$$

Now, we shall state the analog of the multi-configuration Hartree–Fock–Jucys equation for the wave function of the nl-photoelectron.

According to (3.14), the *observed* value for the resonance energy E of the photoexcitation cross-section can be determined under the condition of the minimum denominator, by solving the integral equation:

$$E - E_0 - F_E - \Delta_E = 0. \tag{3.15}$$

From (3.15), it follows that the E-functional contrary to (3.11) can be represented in the form containing no z-function. In this case, it allows the variation at the wave function of the nl-photoelectron.

We shall find the E-functional. To solve (3.15) approximately, we represent the third and the fourth terms as Taylor's series in value neighborhood

$$\bar{E} = E_{nl} + \bar{\varepsilon}, \quad E_{nl} = \langle E_{nl}| \hat{H} |E_{nl}\rangle;$$

where $\bar{\varepsilon}$ is the observed resonance energy of the Auger-electron. Considering that $\Delta_E < F_E$, we can get:

$$F_E \cong F_{\bar{E}} + (\frac{\partial}{\partial E}F_E)_{E=\bar{E}} \cdot (E - \bar{E}); \quad \Delta_E \cong \Delta_{\bar{E}}. \tag{3.16}$$

We shall determine the so-called spectroscopic factor [158] of the $|E_0\rangle -$ state in the complete wave function (3.1):

$$s = \left\{ 1 - \left[\frac{\partial}{\partial E}P \int_0^\infty d\varepsilon_1 \, |V_1|^2 \, (E - E_1)^{-1} \right]_{E=\bar{E}} \right\}^{-1}.$$

Then, from (3.15) and (3.16), we deduce the desired approximate solution of the integral equation (3.15):

$$E = s\,(E_0 + F_{\bar{E}} + \Delta_{\bar{E}}) + (1 - s)\bar{E}. \tag{3.17}$$

We shall find the variation of the functional (3.17) at the radial part of the wave function of the nl-photoelectron

$$\frac{\delta}{\delta P_{nl}} \left(E - \sum_{n'l} \lambda_{nl,n'l} \langle nl| \, n'l\rangle \right) = 0; \tag{3.18}$$

where $\lambda_{nl,n'l}$ are the Lagrange multipliers.

Finally, on substitution of (3.17) in (3.18), we get the desired analog of the multi-configuration Hartree–Fock–Jucys equation for the wave function of the nl-photoelectron:

$$\left\{ \hat{h} + \sum_{n'l'\leq f} \left(N_s^{n'l'} Y_{n'n'}^{(0)} + \sum_{k>0} a_s^k Y_{n'n'}^{(k)} \right) - \varepsilon_{nl} \right\} |nl\rangle + sD_r =$$

$$= \sum_{n'l'\leq f}\sum_{k>0} b_s^k Y_{nn'}^{(k)} |n'l'\rangle + \sum_{n'\neq n} \lambda_{nl,n'l} |n'l\rangle; \tag{3.19}$$

$$N_s^{n'l'} = s\,N_0^{n'l'} + (1 - s)N_1^{n'l'}; \tag{3.20}$$
$$a_s^k = s\,a_0^k + (1 - s)a_1^k;$$
$$b_s^k = s\,b_0^k + (1 - s)b_1^k.$$

The *effective occupation numbers* of the atomic core electron shells and the angular coefficients are determined here through the occupation numbers and the angular coefficients for $|E_0\rangle -$ and $|E_{nl}\rangle -$ configurations, respectively. In (3.19), we obtained the *correlation potential* for the nl-photo- and εl_1- Auger-electron interaction in the deep vacancy Auger-decay state through the Δ_E-functional variation:

$$D_r = \sum_{k \geq 0} P \int_0^\infty \int_0^\infty d\varepsilon_1 d\varepsilon_2 \frac{V_1 V_2}{E_{10} E_{20}} \left(a^k Y_{12}^{(k)} |nl\rangle - b^k Y_{1n}^{(k)} |\varepsilon_2 l_1\rangle \right). \qquad (3.21)$$

The energy denominators are written as an approximation of the Koopmans' theorem [10]:

$$E_{10} \cong \varepsilon_{n_2 l_2} + \varepsilon_{n_3 l_3} - \varepsilon_{n_0 l_0} - \varepsilon_1;$$

and the angular coefficients belong to the configuration of the Auger-decay in (3.1).

We shall study the asymptotic of the *effective* potential for the photo-electron in (3.19). This study is required for testing the agreement of the developing theory, if it maintains the Coulomb type of asymptotic. If $r >> r_0$ (r_0 is the atom radius), it follows from (3.21) that:

$$D_r \propto \frac{1}{r} d_r |nl\rangle ; \qquad (3.22)$$

$$d_r = P \int_0^\infty \int_0^\infty d\varepsilon_1 d\varepsilon_2 \frac{V_1 V_2}{E_{10} E_{20}} Q_{12}(r);$$

$$Q_{12}(r) = \int_0^r dr' P_{\varepsilon_1 l_1}(r') P_{\varepsilon_2 l_1}(r').$$

Considering the concept definition of the Cauchy integral principle value (x_0 is the pole of the first order of the function $\psi(x)$),

$$P \int_0^\infty \psi(x) \, dx = \lim_{\Delta \to 0} \left\{ \left(\int_0^{x_0 - \Delta} + \int_{x_0 + \Delta}^\infty \right) \psi(x) dx \right\};$$

the Leibniz differentiation formula

$$\frac{d}{dx} \left(\int_\alpha^\beta f(x, y) \, dy \right) = f(x, \beta) \frac{d\beta}{dx} - f(x, \alpha) \frac{d\alpha}{dx} + \int_\alpha^\beta \frac{df(x, y)}{dx} \, dy$$

and the integral representation of the Dirac delta function

$$\delta(x - y) = \int_{-\infty}^{+\infty} dz \, \delta(x - z) \, \delta(z - y).$$

Then, considering the expression for the spectroscopic factor, we get from (3.22):

$$\lim_{r \to \infty} (1 + d_r) = s^{-1}. \tag{3.23}$$

Finally, considering (3.23) and (3.20), it follows from (3.19) that the asymptotic of the effective electrostatic potential for the nl-photoelectron holds the Coulomb ($\sim r^{-1}$) form, when transiting from the one-configuration Hartree–Fock representation to the wave function (3.1).

In the context of the analytical structure of (3.19), the *effect of the post-collisional* interaction can be concretized as follows. According to (3.20) for the effective occupation numbers *and* (3.21) for the correlation D_r-potential, the deep vacancy Auger-decay leads to the redistribution of the $n_2 l_2-, n_3 l_3-$ shell electron density between the $n_0 l_0-$ shell and the Auger-electron. As a result, the photoelectron interaction with the parent vacancy slackens, *but* its interaction with $n_2 l_2-, n_3 l_3-$ vacancies and the Auger-electron appears.

Considering (3.1) for the photoexcitation cross-section of the atomic deep shell, we obtain:

$$\sigma_n(\omega) = \frac{4}{3}\pi^2 \alpha a_0^2 \omega_n \, |\alpha_\omega|^2 \left(M + \int_0^\infty d\varepsilon_1 \beta_{\omega 1} M_1 \right)^2 ; \tag{3.24}$$

$$\omega_n = E_0 - E(0); \ \omega = E - E(0);$$

$$M = \langle E_o | \widehat{D} | 0 \rangle ; \quad M_1 = \langle E_1 | \widehat{D} | 0 \rangle .$$

Where α is the fine structure constant, a_0 is the Bohr radius, $E(0)$ is the energy of the atom in the ground state, ω is the absorbed photon energy, and $\widehat{D}$ is the radiative transition operator.

The matrix elements in (3.24) are calculated using the non-orthogonal orbitals theory (Sect. 2.2.1). The radial part of the wave function of the nl-photoelectron can be found by solving (3.19). The wave function of the Auger-electron in (3.19) is obtained at the one-configuration Hartree–Fock approximation considering the "start-up" nl^*- photoelectron field.

3.1.2 Photoionization of an Atom

The wave function of the photoionization state of the atomic deep shell is constructed in a form that is identical to (3.1):

$$|E_n\rangle = \alpha_{En} \left(|E_{0n}\rangle + \int_0^\infty \int_0^\infty d\varepsilon_1 dn' \beta_{E1}^{n'} |E_{1n'}\rangle \right). \tag{3.25}$$

The following analysis and results are similar to the photoionization of the atomic deep shell.

The deep shell ionization goes to the interval $(\varepsilon_n, \varepsilon_n + d\varepsilon_n)$ of the photoelectron energies. As a result, the differential cross-section of the atom photoionized to the final state (3.25) takes the form:

$$\frac{d\sigma(\omega)}{d\varepsilon_n} = \frac{4}{3}\pi^2\alpha a_0^2 \left(\varepsilon_n + I\right)|\alpha_{\omega n}|^2 \left(M + \int_0^\infty \int_0^\infty d\varepsilon_1 dn' \beta_{\omega 1}^{n'} M_{1n'}\right)^2 ; \quad (3.26)$$

where I is the ionization threshold energy of the studied atom shell, and the structure of the normalization factor is similar to (3.14). Integrating expression (3.26) gives the photoionization cross-section for the fixed value of the absorbed photon:

$$\sigma(\omega) = \int_0^\infty \left(\frac{d\sigma(\omega)}{d\varepsilon_n}\right) d\varepsilon_n. \quad (3.27)$$

3.2 Effect of the Deep Vacancy Auger-Decay in Excitation/Ionization of an Atom: Calculating Results

In this section, we shall consider the quantum theory of the post-collisional interaction (PCI) developed in Sect. 3.1.

As subjects of inquiry, we have chosen the cross-section of the neon atom $1s$-$3p$ photoexcitation and the cross-section of the argon atom $1s$-εp photoionization. The choice is determined by the following. According to the results in Table 2.2, the dominant resonance of the differential cross-section of the elastic X-ray photon scattering by the neon atom is determined by the virtual $1s$-$3p$ photoexcitation. But the absolute value of its theoretical intensity is highly susceptible to the many-particle effect. Therefore, the study of the PCI effect is of interest mainly at this resonance. For the argon atom (Sect. 2.7.1), the study of the PCI effect is interesting because of the high sensitivity of the theoretical scattering cross-section to the many-particle effects in the region of the $1s$-shell ionization threshold.

3.2.1 $1s$-$3p$ Photoexcitation of Neon

When constructing the wave function (3.1) and (3.19) for the neon atom, we considered only the main Auger-channel of the $1s$-vacancy decay $2p^4\varepsilon d3p$, its contribution to the total Auger-width 0,2660 eV amounts to 62% (see Table 2.5).

The transition amplitudes in the photoexcitation cross-section (3.24) are calculated from the formulas (see, for example, [66]):

$$M = \left(\frac{N_0 l_{\max}}{4l_0 + 2}\right)^{1/2} R_{n_0 l_0 nl}; \quad l_{\max} = \max(l_0, l); \quad (3.28)$$

$$M_1 = \left\langle n_2 l_2^{4l_2} \left(L_0 S_0\right) \varepsilon l_1 \left(L_{01} S_{01}\right) n' l;^1 P_1 \middle| \hat{D} \middle| n_2 l_2^{4l_2+2};^1 S_0 \right\rangle =$$

$$= N \left(-1\right)^\varphi \delta \left(l, l_2\right) \sqrt{2[L_0, S_0, L_{01}]} \left\langle \varepsilon l_1 \middle| \hat{r} \middle| n_2 l_2 \right\rangle \left\langle n'l \middle| n_2 l_2 \right\rangle \cdot$$

$$\left(l_1 \middle\| C^{(1)} \middle\| l_2\right) \cdot \left\{ \begin{matrix} L_0 & l_1 & L_{01} \\ 1 & l_2 & l_2 \end{matrix} \right\}; \tag{3.29}$$

$$\varphi = 1 + L_{01} + L_0 + l_2; \quad [x] \equiv 2x + 1;$$

in the instant case of the *closed*-shell atom in the ground state. The expression for the radial part of the $1s$-$3p$ transition amplitude R_{1s3p} from (3.28) is given in Sect. 2.7.1, and it follows from (3.29):

$$M_1 = \frac{2}{\sqrt{3}} N \left\langle \varepsilon d \middle| \hat{r} \middle| 2 p_0 \right\rangle \left\langle 3p_+ \middle| 2 p_0 \right\rangle, \tag{3.30}$$

$$N = \left\langle 1s_0 \middle| 1s \right\rangle^2 \left\langle 2s_0 \middle| 2s \right\rangle^2 \left\langle 2p_0 \middle| 2p \right\rangle^4.$$

The radiative transition operator in (3.28) and (3.30) is taken in the *length form*, since considering the RPAE correlations does not lead to more than 0,5% (neon atom) and 1% (argon atom) changes of the deep $1s$-vacancy assisted M-amplitude. In (3.30), the $1s_0-$, $2s_0-$, $2p_0-$ wave functions are deduced by solving the Hartree–Fock equations (2.26) for the configuration of the neon atom ground state, the wave function of the Auger-electron is obtained in the $2p^4 3p^*$ configuration field with the "start-up" photoelectron, and the $3p_+ -$ wave function of the photoelectron is deduced by solving (3.19).

For calculating the s-spectroscopic factor of the $1s$-vacancy in the vicinity of the Auger-pole, we need an *analytical* approximation of the function under the integral sign. Thus, we have chosen the approximation by Lagrange polynomials of the second order (2.73) and obtained the formula:

$$s = \lim_{\Delta \to 0} \left\{ 1 + \left(\int_0^\alpha + \int_\beta^\infty \right) \psi\left(x\right) dx + D \right\}^{-1};$$

$$\psi\left(x\right) = f\left(x\right) \cdot \left(x_0 - x\right)^{-2}; \ f\left(x\right) = V^2\left(x\right);$$

$$D = \left(1/\Delta\right) \left[f\left(\alpha\right) + f\left(\beta\right) - 4f\left(x_0\right)\right];$$

$$\alpha = x_0 - \Delta; \ \beta = x_0 + \Delta;$$

where $V\left(x\right)$ is the probability amplitude of the $1s$ vacancy Auger-decay and if $\Delta \to 0$ the integral singularities are balanced out by the singularity of the D function.

When calculating the correlation D_r potential in the sum (3.21), we considered the harmonics $\kappa = 0$ for the direct integral and $\kappa = 1, 3$ for the exchange integral of the interaction between the np-photo- and d-Auger-electrons, and

Table 3.1. Cross-section of the $1\,s - 3\,p$ photoexcitation of the neon atom at one-configuration (**HF**) and double-configuration (**DHF**) Hartree–Fock approximations. The width for the 1s-vacancy decay 0,50 eV is taken from the experiment [74]. ω is the absorbed photon energy, s is the spectroscopic factor of the $1\,s$-vacancy

ω, eV	σ, Mb	
	HF	DHF
864,97	0,2200	0,2135
865,22	0,5436	0,5356
865,47	1,0956	1,0956
865,72	0,5436	0,5520
865,97	0,2200	0,2267
s	0,999982	

the angular coefficients $a^0 = 1$, $b^1 = 1/15$ and $b^3 = 3/70$ averaged over the terms of the $(pd;\ LS)$-configuration.

The calculation has shown that the smallness of the values $(1-s)$, D_r, *and* their interference in (3.19) practically did **not** change the wave function of the 3p-photoelectron of the one-configuration Hartree–Fock approximation. So, the PCI effect practically does **not** influence the theoretical intensity and form of the leading resonance of the differential cross-section for the elastic scattering of the one-electron approximation. In other words, the effect of the deep vacancy Auger-decay does not lead to changing the *Hartree–Fock* resonances of the differential cross-section of the elastic scattering and forms only the finite widths of their sections. At the same time, the insignificant asymmetry (Table 3.1) of the resonance section for the 1s-3p photoexcitation is determined by the appearance of the amplitude of the transition to the Auger-decay state M_1 from (3.29).

3.2.2 1s-εp Photoionization of Argon

The choice of channel of the 1s-vacancy Auger-decay and the expressions for the phototransition amplitudes in (3.26) are the same as for the neon atom. As for the neon atom, the smallness of the values $(1 - s)$, D_r, *and* their interference in (3.19) practically does *not* change the wave function of the p-photoelectron of the continuous spectrum at the one-configuration Hartree–Fock approximation. As a result, 0,2% difference of the absolute values for the HF- and DHF-cross-sections of the argon atom photoionization in the energy region of the 1s-shell ionization threshold (Table 3.2) is only determined by the appearance of the amplitude of the transition to the Auger-decay state M_1 from (3.26). Hence, follows the conclusion for the differential cross-section of the elastic scattering that is the same as for the neon atom.

Table 3.2. Cross-section of the $1s-\varepsilon p$ photoionization of the argon atom at the one-configuration (**HF**) and double-configuration (**DHF**) Hartree–Fock approximations. The width for the $1s$-vacancy decay is $0{,}69$ eV [60]. Other symbols are the same as in Table 3.1

ω, eV	$\sigma \cdot 10^2$, Mb	
	HF	DHF
3197,02	8,000	7,984
3197,70	7,980	7,964
3198,38	7,970	7,954
3209,27	7,500	7,485
s	0,999976	

3.2.3 Study of the K-Photoionization of ^{4}Be, ^{10}Ne, and ^{18}Ar Atoms using the Methods of Multi-channel Resonance Quantum Scattering Theory

Prior to conducting such a study, we shall define the analytical structure of the overlap integral for the wave functions of the *continuous* spectrum of one symmetry from the non-orthogontal basis sets.

Such integral appears in the theoretical models for describing the PCI effect, where the idea of two "static" states of the field for the photoelectron is represented – the parent deep vacancy state and the state of its Auger-decay [123, 159]. At the same time, it is important to note that the desired structure should be obtained only by considering the *set completeness* [119] of the states being investigated *without* referring to the analytical structure of their wave functions. This is determined by the fact that we have at our disposal, for example, the analytical structure of the Hartree–Fock equation, but we do not have its *analytical* solutions. Let us remark that there is no integral of such type in our developing of the PCI effect theory (Part 3.1).

Below, we shall study [160] the PCI effect using the methods of the multi-channel resonance quantum scattering theory without considering the electrostatic interaction between photo- and Auger-electrons in the state of the deep vacancy Auger-decay. In Sect. 3.3 of our treatise, we shall demonstrate that it is possible to ignore the mentioned interaction.

Analytical structure of the overlap integral. We shall take a closer look at the wave functions of the m- and n-electrons of one symmetry of continuous spectrum from the non-orthogonal basis sets. For the generalized function of the form

$$R^n_{mk} = \langle m_+ | \, n \rangle \, \langle n | \, k_+ \rangle$$

we shall find the expression, where the singularities are distinguished. From condition of the completeness of the $|n\rangle -$ states set

$$\sum_{n \leq f, > f} \int_0^\infty dn \, |n_r\rangle \, \langle n_{r'}| = \delta \left(r - r' \right)$$

we deduced the integral equation for the desired function

$$\int_0^\infty dn\, R_{mk}^n = \delta\,(m-k) - L_{mk}; \quad L_{mk} = \sum_{n\le f,>f} R_{mk}^n. \tag{3.31}$$

Where f is the Fermi level and the integral is defined as

$$\left(\int_0^\infty\right) = \lim_{A\to 0}\lim_{B\to\infty}\left(\int_A^B\right).$$

For any $x, y > 0$, the integral expressions are

$$\delta(x - y) = \int_0^\infty dz\, \delta(x - z)\, \delta(z - y),$$

$$1 = (1/2)\int_0^\infty dz\, [\delta(x - z) + \delta(z - y)],$$

we get the solution of (3.31)

$$R_{mk}^n = \delta(m - n)\delta(n - k) - \frac{1}{2}\,[\delta\,(m - n) + \delta\,(n - k)]\, L_{mk}. \tag{3.32}$$

We do not analyze the problem of determining the possible solutions of equation (3.31) as an inhomogeneous first kind Fredholm integral equation [161] in the class of generalized functions. We shall mention only the fact that the problem of finding solutions for integral equations of such type refers to the class of the improperly posed problems in mathematical physics [162].

It follows from (3.22) for a certain real function of appropriate behavior ψ_m [160]:

$$\int_0^\infty dm\psi_m\,\langle m_+|\,n\rangle = \pm\left(\psi_n^2 - \psi_n\int_0^\infty dm\psi_m L_{mn}\right)^{1/2}, \tag{3.33}$$

where the sign of the right hand side in expression (3.33) is determined by the sign of the ψ_n function.

If returning to the one basis of the single-electron (m, n)-states, we have

$$L_{mn} \to 0, \quad \langle m_+|\,n\rangle \to \delta(m - n),$$

and instead of (3.33), we obtain the common result

$$\int_0^\infty dm\psi_m\,\langle m_+|\,n\rangle \to \psi_n.$$

The expression (3.33) gives the desired *analytical* solution of the overlap integral as a singular kernel of the linear integral operator:

$$\int_0^\infty dx \, \langle x_+ | y \rangle \sum_n \psi_{xn} = \sum_n \int_0^\infty dx \, \langle x_+ | y \rangle \, \psi_{xn}.$$

Calculation results. We shall examine the application of the result (3.32). By the example of the neon atom, we shall construct the expression for the cross-section of photon absorbing by the atomic $1\,s$-shell:

$$\sigma = \bar{\sigma} + \mu \int_0^\infty \int_0^\infty dm \, dk \, A_m A_k [(\omega_m + i\gamma)(\omega_k - i\gamma)]^{-1} Q_{mk}; \quad (3.34)$$

$$\bar{\sigma} = \mu \sum_{m>f} (\gamma_m/\pi) \left(\omega_m^2 + \gamma^2 \right)^{-1} A_m^2;$$

$$\mu = \frac{4}{3} \pi^2 \alpha \, a_0^2 \, \omega;$$

$$\omega_m = \omega - I_{1s} - m; \quad 2\gamma = \Gamma_{1s};$$

$$\pi \, Q_{mk} = \left(\sum_{n>f} + \int_0^{\omega - I} dn \right) \gamma_n \, R_{mk}^n.$$

In (3.34), we restricted ourselves to considering the main $2p^4 \varepsilon d(n, \varepsilon') p(^1P_1)$ channel of the $1\,s$-vacancy Auger-decay and defined the following values: ω is the absorbed photon energy, ω_m is the energy, and A_m is the amplitude of transition from the atom ground state to the $1s^1_+ mp_+(^1P_1)$ state without considering the channel of the $1\,s$-vacancy Auger-decay; $2\gamma_n = \Gamma(\omega - I - n)$ is the width for the $1\,s$-vacancy Auger-decay in the fixed main quantum n-number state, Γ_{1s} is the total width of the $1\,s$-vacancy Auger-decay, I is the energy of the $2\,p$-shell double ionization threshold, I_{1s} is the energy of the $1\,s$-shell ionization threshold, α is the fine structure constant, and a_0 is the Bohr radius. The wave function of the photoelectron *before* the $1\,s$-vacancy Auger-decay is deduced by solving the Hartree–Fock equation (2.26) for the $1\,s^1_+ mp_+(^1P_1)$ configuration. The wave functions of the photo- and Auger-electrons in the state of the $1s$-vacancy Auger-decay are deduced by solving the Hartree–Fock equations for the $2\,p^4 \varepsilon d(n, \varepsilon') p(^1P_1)$ configuration. In the photon energy region $\omega > I_{1s}$, the contribution to the cross-section of the $1\,s$–mp excitation absorption is reduced by the energy denominator, and it enables us to use the approximation $\langle m_+ | n \rangle \to \delta_{mn}$ for their accounting.

Considering (3.32) from (3.34), we obtain:

$$(\sigma - \bar{\sigma})/\sigma_0 \cong 1 + \pi \sum_{n>f} (\gamma_n - \gamma_0) \, a_n \equiv \xi; \quad (3.35)$$

$$a_n = \langle n | (\omega - I_{1s})_+ \rangle^2;$$

$$\sigma_0 = \mu \, A_{\omega - I_{1s}}^2; \quad 2\gamma_0 = \Gamma(I_{1s} - I).$$

The value (3.35) is numerically studied for atoms of beryllium, neon, and argon. When energy $\omega = I_{1s} + 1,3606\,(\text{eV})$, we obtained: $\xi = 0,9999(^4Be)$; $0,9993(^{10}Ne); 0,9990(^{18}Ar)$.

The overlap integral $\langle n\,|(\omega - I_{1s})_+\rangle$ can be interpreted from the physical standpoint as the amplitude of transition between the *virtual* states of the photoelectron of the $(\omega - I_{1s})p_+$ continuous and np discrete spectra: the $(\omega - I_{1s})p_+ - np$ transition describes the quantum *condensation* process of the continuous spectrum state to the np-state; the np-$(\omega - I_{1s})p_+$ transition describes the quantum *evaporation* process of the np-state to the continuous spectrum state. Such an interpretation does not break the Fermi–Dirac statistics [6, 7] for electrons as *fermions*, since the amplitudes of the condensation and evaporation processes for different quantum numbers n *do not interfere* in (3.35). The difference of probabilities for these processes is described through the sum in (3.35) and turns out to be vanishingly small: the competitive processes of the quantum evaporation and condensation practically countervail each other.

This way, in the multi-channel resonance quantum scattering theory (3.34), as well as in the theory by the authors (Sect. 3.1), the radial relaxation effect of the wave function of the continuous spectrum $\varepsilon p-$ photoelectron practically does not change the photoabsorbtion cross-section calculated at the one-configuration Hartree–Fock approximation.

3.3 Quantum Theory of the Post-Collisional Interaction Effect

The attempts to describe in theory the post-collisional interaction effect, in the context of the perturbation theory [123, 159], have left *open* the *main question*: the question of the convergence of the perturbation theory series in the interaction operator for the photo- and Auger-electrons of the *continuous* spectrum. This question arises from the following condition. It can be shown (the result by the authors has not been published yet) that in the context of the first-order perturbation theory in the interaction operator for the photo- and Auger-electrons of the continuous spectrum, the logarithmic divergence (if $\varepsilon \to \varepsilon_0$) of the probability photoionization amplitude:

$$A\,(\omega, \varepsilon) \propto f\,(\omega, \varepsilon)\,\ln\left|\frac{1 + \sqrt{\eta}}{1 - \sqrt{\eta}}\right|; \quad \eta = \varepsilon_0/\varepsilon.$$

Here ε_0 is the resonance value of the Auger-electron energy, ω is the absorbed photon energy, and $f(\omega, \varepsilon)$ is the function of appropriate behavior.

No attempts have been made to study the stipulated problem outside the perturbation theory in the published literature. Actually, the currently available variants for the generalization of the *non-perturbative* quantum theory of Fano autoionization [156] are restricted to considering the one-electron

autoionization channel in the continuous spectrum [163–166] and does not consider the intrachannel mixing effects of the two-electrons (photo- and Auger-electrons) autoionization states of the continuous spectrum [167, 168].

The theory of the post-collisional interaction effect developed in Sect. 3.1 has the form of the small φ_{12} - parameter perturbation theory. In this part of our treatise we lift the mentioned restrictions and for the first time outside the perturbation theory we find the **_analytical_** solution of the Schrödinger equation for the wave function of the interacting continuous spectra system of the atomic states – the atomic deep shell photoionization state and the state of the Auger-decay of the deep vacancy with two electrons (photo- and Auger-electrons) of the continuous spectrum [169–171].

Before developing such a solution, we shall point out two circumstances. First, in the work [172] the analytical solution of the Schrödinger equation is obtained for the first time for the wave function of the two interacting electrons of the continuous spectrum that are moving in the external laser field and nuclear field with the central Coulomb potential. But this solution as well as the similar approach to describing the states of the interacting electrons of the continuous spectrum through the *Coulomb* functions [173, 174] cannot be accepted. Actually, the wave functions of the one-electron states in atoms are the solutions of the Hartree–Fock equations, not of the Schrödinger equation, and they do not belong to the Coulomb function class in the field of the spatial localization of the atomic *deep* shell. Secondly, we do not examine the *radiative* channels of the deep vacancy decay. It is completely possible to ignore such channels if we describe the K-photoionization cross-section of the atoms with the nuclear charge $Z \leq 20$. Actually, in this case, the Auger-component of the total width of the $1s$-vacancy decay is 2–3 order greater than the radiative component [60].

3.3.1 One-channel Variant of the Theory

We shall develop the non-perturbative quantum theory of the post-collisional interaction effect in two stages. In the first stage (this part of the treatise), we shall restrict ourselves to examining the one (main) channel of the deep vacancy Auger-decay. While in the second stage, we shall represent the scheme of the generalization theory in the case of two and more channels of the deep vacancy Auger-decay.

Wave function of the system. Let us examine the interacting *continua* system of the atomic deep shell photoionization $|x_+\rangle-$ and $|xy\rangle-$ states of the Auger-decay of the resulting deep vacancy with photo- and Auger-electrons of the *continuous* spectrum. As an example, we can take the following: $|x_+\rangle \rightarrow \left|1s^1xp_+\right\rangle$ and $|xy\rangle \rightarrow \left|2p^4ydxp\right\rangle$ at $1s$-shell photoionization of the neon atom. We obtained the wave function of the xp_+- photoelectron here in the field of one $1s$-vacancy, and the wave functions of the xp-photo- and yd-Auger-electrons in the field of two $2p$-vacancies.

The following development of the theory does not depend on the kind of approximation used in deducing the wave functions basis for one-electron states though we shall have in mind the Hartree–Fock approximation basis.

The wave function of the system determined above as the eigen function of the Hamiltonian of the atom

$$\hat{H} |\psi_\omega\rangle = E_\omega |\psi_\omega\rangle;$$ (3.36)

$$\langle \psi_\omega | \psi_{\omega'} \rangle = \delta(\omega - \omega');$$

we shall search in the form of the linear combination

$$|\psi_\omega\rangle = a_\omega (|\varphi\rangle + |\varphi_\omega\rangle);$$ (3.37)

of the wave functions for two integral packs

$$|\varphi\rangle = \iint_D dx dy \alpha(x,y) |xy\rangle; \quad |\phi_\omega\rangle = \int_0^\infty dx\, \beta(\omega,x) |x_+\rangle.$$

We shall require the following equalities to be realized:

$$\langle x_+| \hat{H} |y_+\rangle = E_x \delta(x-y); \quad \langle \varphi| \hat{H} |\varphi\rangle = E_\varphi;$$

$$\langle \varphi| \varphi \rangle = 1; \quad \langle xy| x'y'\rangle = \delta(x-x\prime)\delta(y-y');$$

$$\langle x_+| y_+\rangle = \delta(x-y); \quad \langle x_+| xy\rangle = 0.$$

We used here the atomic system of units and determined the following values $E_\omega = \omega + E(0)$, ω is the energy of the photon absorbed by an atom, $E(0)$ is the energy of the atomic ground state, E_x is the energy of the atomic single photoionization, E_φ is the energy of the localized integral pack $|\varphi\rangle$, and the two-dimensional region of integration $D : 0 \leq x, y \leq C$.

The system of non-linear integral equations for desired functions a_ω, $\beta(\omega, x)$, $\alpha(x, y)$, C follows from (3.36) and (3.37):

$$\iint_D dx dy\, |\alpha(x,y)|^2 = 1;$$ (3.38)

$$E_\varphi = E_0 + \iint_D dx dy\, |\alpha(x,y)|^2 (x+y) + J;$$ (3.39)

$$J = \iint_D dx dy\, \alpha(x,y) \iint_D dx' dy'\, \alpha(x',y') Q^{yy'}_{xx'};$$

$$E_\omega = E_\varphi + \int_0^\infty dx\, \beta(\omega,x) W_x;$$ (3.40)

$$W_x = \iint_D dy dz\, \alpha(y,z) \langle x_+| \hat{H} |yz\rangle;$$

$$E_{\omega x}\beta(\omega, x) = W_x; \quad E_{\omega x} = E_\omega - E_x; \tag{3.41}$$

$$a_\omega a_{\omega'} \left(1 + \int_0^\infty dx\, \beta(\omega, x)\, \beta(\omega', x)\right) = \delta(\omega - \omega'). \tag{3.42}$$

In (3.39), the following values are determined: E_0 is the energy of the deep vacancy Auger-decay state and J is the energy of the continuous spectrum photo- and Auger-electrons interaction in the Auger-decay state. The singular interaction integral $Q_{xx'}^{yy'}$ (the linear combination of the F^0-Coulomb and G^k-exchange integrals) of the photo- and Auger-electrons is determined as the non-diagonal part of the *intra*channel mixing matrix

$$\langle xy|\,\hat{H}\,|x'y'\rangle = (E_0 + x + y)\,\delta(x - x')\,\delta\,(y - y') + Q_{xx'}^{yy'}.$$

We shall determine the solution of the equation system (3.40), (3.41) and (3.42).

We shall keep in mind, that the solution of the equation $x\,f(x) = g(x)$ under the given regular function $g(x)$ is the *generalized* function $f(x) = P[g(x)/x] + c\,\delta(x)$. This function can be interpreted as the singular kernel of the linear integral $\hat{L}$-operator forced on certain function $\eta(x)$ by convention:

$$\hat{L}_f\,[\eta] = \int_{-\infty}^{+\infty} f(x)\,\eta(x)\,dx = P\int_{-\infty}^{+\infty} \frac{dx}{x}\,g(x)\,\eta(x) + c\,\eta(0);$$

where P is the symbol of the main Cauchy principle value and c is any given value [119].

Then, we obtain:

$$a_\omega = [\gamma_\omega\,(z_\omega^2 + \pi^2)]^{-1/2}; \tag{3.43}$$

$$\beta(\omega, x) = W_x[P\,(E_{\omega x}^{-1}) + z_\omega\delta\,(E_{\omega x})]; \tag{3.44}$$

$$z_\omega = (E_\omega - E_\varphi - F_\omega)\,/\gamma_\omega;$$

$$F_\omega = P\int_0^\infty dx\, \gamma_x\, E_{\omega x}^{-1}; \qquad \gamma_x = |W_x|^2.$$

It follows from (3.43) and (3.44) that the values a_ω, $\beta(\omega, x)$ are the functionals from the function $\alpha(x, y)$, that turns (3.38) into the identity. For its part, any real regular function of the following form is in accordance with (3.38):

$$|\alpha(x, y)|^2 = N f\,(x, y); \quad N^{-1} = \iint_D dx dy\, f\,(x, y).$$

As a condition that fixes the analytical structure of the function $\alpha(x, y)$, we require that the energy E_φ from (3.39) equals:

$$E_\phi \to E_0 + C + J. \tag{3.45}$$

The value C here is defined as the potential difference of the atomic deep shell ionization and formation of the deep vacancy Auger-decay state.

Then, calculating the double integral in (3.39) we find out that the condition (3.45) is satisfied in the class of functions:

$$f(x, y) = \eta \left[(C - x - y)^2 + (\pi \eta)^2 \right]^{-1}; \tag{3.46}$$
$$\eta = |V(C)|^2,$$

where the $V(C)$ is the amplitude of the deep vacancy Auger-decay. Thus, for the example initiated above for the $1s$-vacancy, Auger-decay of the neon atom $V(C) = \langle 1s^1 | \hat{H} | 2p^4 Cd \rangle$.

The parameter η in (3.46) remains arbitrary (the integrating result in (3.45) does not depend on η). As a consequence, we consider it fixed too, reasoning from the following additional requirement. The structure of the J−integral should correspond with the structure (and topology) of the Goldstone-Hubbard-Feynman diagrams describing the continuous spectrum photo- and Auger-electrons interaction. Such diagrams are determined and represented in the work by the authors [155] for the photoelectron of the discrete spectrum.

The expressions (3.37), (3.43), (3.44), and (3.46) give the analytical solution of the Schrödinger equation (3.36) that should be found *outside* the perturbation theory.

Photoionization cross-section. The obtained solution determines the analytical structure of the atomic deep shell photoionization cross-section:

$$\sigma_\omega = \frac{4}{3} \pi^2 \, \alpha \, a_0^2 \, \omega \, L_\omega \, |X_\omega + (\Delta E_\omega / W_\omega) Y_\omega|^2. \tag{3.47}$$

In (3.47), the amplitudes are defined as

$$X_\omega = \langle 0 | \hat{D} | \chi_\omega \rangle;$$
$$|\chi_\omega\rangle = |\varphi\rangle + P \int_0^\infty dx \, (\omega - I - x)^{-1} W_x \, |x_+\rangle;$$
$$Y_\omega = \langle 0 | \hat{D} | (\omega - I)_+ \rangle;$$

as well the spectral density of the final states

$$L_\omega = \gamma_\omega [(\Delta E_\omega)^2 + (\pi \gamma_\omega)^2]^{-1}; \tag{3.48}$$
$$\Delta E_\omega = \omega - (I + F_\omega + J).$$

Where I is the energy of the atomic deep shell ionization threshold and $\hat{D}$ is the radiative transition operator.

The absence of analytical solutions for Hartree–Fock equations makes possible to study the W- and J-integrals using only *numerical* techniques. This can be revealed as an independent problem and is the subject of future inquiry. Here we shall represent the result of the quantitative estimation for the J-integral at the plane wave approximation

$$P_k(r) \rightarrow (2/\pi k)^{1/2} \quad \sin(kr), \quad k^2 = 2x$$

for the wave functions of the continuous spectrum photo- and Auger-electrons.

We shall examine the main contribution to the J integral from (3.39) determined by the $F^0(xy; x'y')$ Coulomb integral. We consider the resonance (if $x + y \rightarrow C$) character of the function $\alpha(x, y)$ and, as a result, confine the integration domain through the D limits $C - 2\gamma \leq x, y \leq C$. Then, we obtain:

$$J = \int_0^\infty dr \left\{ \frac{1}{r} \int_0^r dr'\, R(r, r') + \int_r^\infty \frac{dr'}{r'} R(r, r') \right\};$$

$$R(r, r') = q\, \psi_\alpha(r)\, \psi_\beta(r)\, \psi_\alpha(r')\, \psi_\beta(r');$$

$$\psi_\alpha(r) = \frac{1}{r} \left[1 - \cos(\alpha r) \right];$$

$$\alpha = (8C)^{1/2}; \quad \beta = \gamma\, (2/C)^{1/2}; \quad q = \frac{1}{\gamma \pi^3}.$$

Finally, considering the $\psi-$functions localized state

$$\lim_{r \to 0, \infty} \psi_\alpha(r) = 0;$$

and satisfying the inequality $C \gg 2\gamma$, we have:

$$J = (\gamma\sqrt{2}/\pi)^2 (2C)^{-3/2} \left(1 + 4 \ln \frac{2C}{\gamma} \right);$$

$$\lim_{\gamma \to 0} J = 0;$$

where the values C and γ are in atomic units.

Then, by the example of neon atom having the $1s$-vacancy decay width $2\gamma_{1s} = 0,23$ eV [129] and the potential difference $C = 808,43$ eV, we find out that the J integral $\approx 10^{-5}$ eV. Agreeing with (3.48), the J integral describes the ionization threshold shift of the deep shell of the one-electron approximation atom to the short-wave ($J \geq 0$) region of the absorbed photon energies. The obtained value of the J integral is negligible for the neon atom in comparison with the experimental energy value of the $1s$-shell ionization threshold $I_{1s} = 870,23$ eV [125].

By this means, we can predict that the interaction effect of the *continuous* spectrum photo- and Auger-electrons for the atoms having nuclear charge

$Z \leq 20$ practically *does not* change the photoionization cross-section of the one-electron approximation deep shell. We have obtained this result outside the limits of the perturbation theory, and thus this result has a fundamental character for the atomic spectroscopy of the X-ray range.

To complete the creation of the one-channel variant of the non-perturbative quantum theory for the atomic deep shell photoionization, we shall point out two conditions.

The *first* condition: in the limit of neglect of the transition amplitude to the $|\varphi\rangle -$ pack state and $\gamma_\omega \rightarrow 0$ the known expression follows from (3.37) for the photoionization cross-section of the atomic deep shell at the one-configurational Hartree–Fock approximation [10, 158]:

$$\sigma_\omega \rightarrow \sigma_\omega^{\mathrm{HF}} = \frac{4}{3} \pi^2 \alpha a_0^2 \omega |Y_\omega|^2 .$$

The *second* condition: in published literature, the post-collisional interaction effect is traditionally connected with the energy shift and profile deformation effect of the Hartree–Fock resonances of photo- and Auger-electron spectra observed in the experiment [123, 175]. To study the *electron* spectra is not the aim of our treatise. Here we point once again to the result we have obtained. Both in absorption and differential cross-sections of the elastic X-ray photon scattering by an atom, the post-collisional interaction effect *is depleted* of "visible" manifestations [171].

3.3.2 Generalization of the Theory

If we have to consider two or more channels of the deep vacancy Auger-decay, it is possible to generalize the non-perturbative quantum theory outlined in this part of our treatise in the following manner [170].

In the aggregate of the N localized integral packs of the Auger-decay states with x-photo- and y-Auger-electrons of continuous spectrum

$$|\varphi_i\rangle = \iint_D dx\,dy\, \alpha_i(x, y)\, |xy, i\rangle; \quad \langle\varphi_i|\,\varphi_j\rangle = \delta_{ij};$$

$$\langle\varphi_i|\,\hat{H}\,|\varphi_j\rangle = H_{ij}; \quad H_{ii} = E_{\varphi_i};$$

$$D : 0 \leq x, y \leq C_i; \quad i = 1, 2, \ldots, N;$$

we determine the system of the wave functions

$$|\Phi_n\rangle = \sum_{i=1}^{N} a_{in} |\varphi_i\rangle; \quad \langle\Phi_n|\,\Phi_m\rangle = \delta_{nm}. \tag{3.49}$$

The weight coefficients are deduced using preliminary diagonalization of the energy matrix and the following is realized (E_n is the energy of the $|\Phi_n\rangle$ state)

$$\langle\Phi_n|\,\hat{H}\,|\Phi_m\rangle = E_n \delta_{nm}; \quad n, m = 1, 2, \ldots, N.$$

Finally, substituting in the wave function (3.37)

$$|\varphi\rangle \rightarrow \sum_{n=1}^{N} \rho_n |\Phi n\rangle;$$

$$W_x \rightarrow W_{nx} = \langle \Phi_n| \hat{H} |x_+\rangle ;$$

to determine the values $a_\omega, \rho_n, \alpha_i(x, y), C_i, \beta(\omega, x)$, we realize the mathematical methods of the works [156, 163, 167, 168].

Inclusion of the $|n_+\rangle$ states of the atomic deep shell photo*excitation* and the localized integral packs of the deep vacancy Auger-decay with the photoelectron of the discrete spectrum in the linear combination (3.49) of the wave functions

$$|\varphi_i^n\rangle = \int_D dy\, \alpha_i^n(y)\, |ny, i\rangle; \quad \langle\varphi_i^n| \varphi_j^m\rangle = \delta_{ij}\, \delta_{nm};$$
$$D : 0 \leq y \leq C_i^n;$$

lets us formulate the non-perturbative quantum theory of the atomic deep shell excitation/ionization by the X-ray photon.

3.4 Main Results of Chapter 3

1. The quantum theory of the post-collisional interaction effect is developed when the X-ray photon is absorbed in the region of the atomic deep shell ionization threshold. The analog of the multi-configurational Hartree–Fock–Jucys equation is deduced for the wave function of the photoelectron. The theory being developed predicts among other factors, the width of the deep vacancy Auger-decay to depend on the absorbed photon energy:

$$\Gamma_E \rightarrow \Gamma_\omega = 2\pi \left(|V_\omega|^2 + C_\omega \right);$$
$$V_E \rightarrow V \left(\varepsilon = \omega - I_{12} - \varepsilon_n \right) \equiv V_\omega.$$

I_{12} is the energy of the formation of the deep vacancy Auger-decay, ε is the Auger-electron energy, and ε_n is the photoelectron energy. To study this prediction numerically is not the aim of our treatise, but is of fundamental interest for the resonance absorption spectroscopy, elastic, and inelastic X-ray photon scattering by an atom.

2. The analytical structure is determined for the overlap integral of the wave function of one symmetry continuous spectrum from the non-orthogonal basis sets. The result is obtained without turning to one or another type of the wave functions analytical structure of the one-electron states. This way, it has a general character for *any* quantum states meeting the condition of completeness.

3. Using the methods of the developed theory, as well the multi-channel resonance quantum scattering theory, the cross-sections of the $1s$-$3p$ photoexcitation are calculated for the neon atom as well the cross-sections of the near-threshold K-photoionization for the atoms of beryllium, neon, and argon considering the post-collisional interaction effect. It is found that this effect practically does not change the cross-sections of the one-configuration Hartree–Fock approximation. As a consequence, the post-collisional interaction effect practically does not change the calculation results at one-configuration approximation of the differential cross-sections of the elastic X-ray photon scattering by an atom in the region of the deep shell ionization threshold.

4. *Outside* the limits of the perturbation theory, the analytical solution of the Schrödinger equation is determined for the wave function of the interacting atomic states system – the state of the atomic deep shell photoionization and the state of the deep vacancy Auger-decay with two (photo- and Auger-) electrons of continuous spectrum. The solution takes into account the radial relaxation effects of the photoelectron wave function and its interaction with the Auger-electron. The scheme for generalizing the obtained solution is recommended in the case of considering two and more channels of the deep vacancy Auger-decay, as well the atomic deep shell photoexcitation states.

4

Many-Particle and Orientation Effects When Anomalous Elastic X-Ray Photon Scattering by a Linear Molecule

When measuring the spectral characteristics of the many-electron systems that do not possess spherical symmetry and are preliminarily constructed with reference to the polarization vector of the incident photon, the strong *orientation effects* are expected to appear. This conclusion of the molecular spectra theory [176] is studied in the present chapter of our treatise by the example of developing the quantum theory and calculation methods for the differential cross-section of the elastic X-ray photon scattering by the *linear* molecule having hydrogenic (HF, HCl) and non-hydrogenic (CO) ligands. In Sect. 4.1, we present the developing of this theory and calculation methods for the differential cross-section of the process. We determine the *analytical* structure of the linear molecule form factor at the one-center approximation [177] of the wave functions of the molecular orbitals. In Sect. 4.2, we present the calculation results for differential cross-section of the elastic X-ray photon scattering in the energy region of the deep orbitals ionization thresholds for molecules HF, HCl, and CO.

4.1 Differential Cross-Section of the Process

The construction of the differential cross-section for the elastic X-ray photon scattering by a molecule is the same as for an atom. Not repeating the details of construction given in Chap. 2, we shall describe only the main structures and new elements of the theoretical scheme. We shall restrict ourselves to the case, when the polarization vectors of the incident and scattered photon are at right angle to the scattering plane. It will be remembered that the scattering plane is determined as a plane passing through the wave vectors of the incident and scattered photons.

We shall define the electron $\varphi_{n\gamma}$ wave function being transformed, in accordance with an indecomposable representation γ with the line μ in the shape of the one-center expansion in functions with the fixed value of the orbital

moment l:

$$|\varphi_{n\gamma}\rangle = |n\gamma\mu\chi\rangle = |n\gamma\mu\rangle |\chi\rangle, \qquad (4.1)$$

$$|n\gamma\mu\rangle = \sum_{l=0}^{\infty} a_l^{n\gamma} |n\gamma l\mu\rangle,$$

$$|n\gamma l\mu\rangle = \frac{1}{r} P_l^{n\gamma}(r) Y_l^{\gamma\mu}(\vartheta, \varphi),$$

where n is the main quantum number; χ is the spin part of the wave function; $a_l^{n\gamma}$ are weight coefficients; $P_l^{n\gamma}(r)$ is the radial part; and $Y_l^{\gamma\mu}(\vartheta, \varphi)$ is the angular part of the wave function of the l- symmetry having a fixed (for a linear molecule) value of the μ impulsive moment projection on the quantization axis OZ (linear molecule axis) and r, ϑ, φ spherical coordinates.

Thus, the expression for the differential cross-section of the elastic X-ray photon scattering by a linear molecule takes the form in the atomic system of units:

$$\mathrm{d}\sigma_\perp/\mathrm{d}\Omega = r_0^2 \left| F(\theta; \omega) + \sum_q \sum_{n\gamma \leq f} Q_{n\gamma}^q(\omega) \right|^2. \qquad (4.2)$$

q is the irreducible tensor operator for radiative transition, $F(\theta; \omega)$ is the form factor of the linear molecule, $Q_{n\gamma}^q(\omega)$ are the Kramers-Heisenberg-Waller terms for the $n\gamma$-molecular orbital, and f is the Fermi level.

Let us define concretely the analytical structures of the functions in (4.2).

4.1.1 Form Factor of the Linear Molecule

In the published literature, the analytical structure of the molecule form factor has been examined using two approximations: "atoms in molecules" approximation [178] and approximation of the form factor as an electron inventory in the molecule [59]. In our treatise, we remove the restrictions of the mentioned approximations. The result of our construction will be, among other factors, the fact that the form factor of the linear molecule is a function of its spatial orientation. This result, however, is missing in the approximation mentioned above.

Considering (4.1), the exponent expansion in spherical functions (2.20) and the Wigner–Eckart theorem (2.21) for the form factor of the *linear* molecule ($\mu_1 = \mu_2 = \mu$), we obtain the expression:

$$F(\theta; \omega) = \left\langle \phi \left| \sum_{j=1}^N \exp\left[i\left(\boldsymbol{k} \cdot \boldsymbol{r}_j\right)\right] \right| \varphi \right\rangle = \sum_{n\gamma \leq f} F_{n\gamma}(\theta; \omega); \qquad (4.3)$$

$$|\phi\rangle = (N!)^{-1/2} \det \|\varphi_{n\gamma}\|;$$

$$F_{n\gamma}(\theta; \omega) = N_{n\gamma} \sum_{l_1 l_2} \sum_{t=0}^{\infty} i^t (2t+1) \langle n\gamma l_1 | j_t | n\gamma l_2 \rangle C_{l_1 l_2}^{t\mu} P_t\left(\cos \Theta_{\boldsymbol{k}}\right);$$

$$\langle n\gamma l_1 | j_t | n\gamma l_2 \rangle = a_{l_1}^{n\gamma} a_{l_2}^{n\gamma} \int_0^\infty P_{l_1}^{n\gamma}(r) P_{l_2}^{n\gamma}(r)\, j_t(kr)\, dr;$$

$$k = |\boldsymbol{k}| = |\boldsymbol{k}_1 - \boldsymbol{k}_2| = \frac{2\omega}{c} \sin\left(\frac{\theta}{2}\right);$$

$$C_{l_1 l_2}^{t\mu} = (-1)^\beta \left(l_1 \left\| C^{(t)} \right\| l_2\right) \begin{pmatrix} l_1 & t & l_2 \\ -\mu & 0 & \mu \end{pmatrix};$$

$$\beta = l_1 - \mu; \quad |l_1 - l_2| \le t \le l_1 + l_2 .$$

Here $|\varphi\rangle$ is the wave function of the molecule ground state, $N_{n\gamma}$ is the occupation number of the $n\gamma-$molecular orbital, $\Theta_{\boldsymbol{k}}$ is the angle between the scattering vector and the molecular axis OZ, j_t is the t-order Bessel spherical function of the first kind, P_t is the t-degree Legendre polynomial of the first kind. The value of μ impulsive moment projection is fixed by the term structure of the molecule ground state (for example, $\mu = 0$ for the term $^1\Sigma$ of the molecules studied in the treatise).

When calculating the special functions in (4.3), the following mathematical facts [179] are realized. We calculated the Legendre polynomials using the recurrence relation:

$$(n+1)P_{n+1}(x) + nP_{n-1}(x) = (2n+1)x\, P_n(x); \quad n \ge 1;$$
$$P_0(x) = 1; \; P_1(x) = x.$$

The Bessel functions were calculated using the integral approximation (*Poisson integral*):

$$j_n(x) = x^n \left(2^n n!\right)^{-1} \int_0^1 (1 - \eta^2)^n \cos(x\eta) d\eta. \tag{4.4}$$

The numerical experiments were carried out as shown in the following. For $x \to 0$, if $n >> 1$ using the recurrence relation:

$$j_{n+1}(x) + j_{n-1}(x) = \frac{1}{x}(2n+1)j_n(x); \quad n \ge 1;$$
$$j_0(x) = \frac{1}{x}\sin x; \quad j_1(x) = \frac{1}{x}(j_0(x) - \cos x);$$

turns out to be an ineffective algorithm. On the other hand, the representation (4.4) requires for its realization relative dense decomposition of the interval of integration $\eta \in [0; 1]$.

4.1.2 Anomalous Dispersing Kramers-Heisenberg-Waller Terms

At *dipole* approximation for N-electron, the irreducible tensor operator of the photon-linear molecule interaction (length form) is given as [66]:

$$\hat{D}_q = \sum_{i=1}^{N} \hat{r}_i C_{qi}^{(1)}; \quad q = 0, \pm 1;$$

the Kramers–Heisenberg–Waller terms considered in accordance with (1.5) takes the form:

$$Q_{n\gamma}^q(\omega) = \xi \underset{\varepsilon > f}{S} \frac{\bar{\omega}_\varepsilon \omega_\varepsilon^2}{\omega^2 - \bar{\omega}_\varepsilon^2} \left| \left(\phi_{n\gamma,\varepsilon} \left| \hat{D}_q \right| \phi \right) \right|^2 ; \tag{4.5}$$

$$\bar{\omega}_\varepsilon = \omega_\varepsilon - i\Gamma_{n\gamma}/2,$$

where $\{\xi = 2/3, \ q = 0; \ \xi = 1/3, \ q = \pm 1\}$; ε is the set of quantum numbers of the photoelectron; ω_ε is the transition energy from the ground state to the excited molecular state; $\Gamma_{n\gamma}$ is the total width of the vacancy decay of the excited state.

We shall examine the calculation algorithms for the structural constituents (4.5).

Matrix elements calculation of the dipole transition operator. According to Chap. 2, the main many-particle effect, when absorbing the X-ray photon with the energy close to the atomic deep shell ionization threshold (atom in molecule), is the electron shell relaxation in the deep vacancy field. And what is more, in molecules, the relaxation effect can lead to changing the composition and the degree of the atomic l-components participation in the wave function of the molecular orbital [180].

In order to consider the relaxation effect, the method of the non-orthogonal orbitals theory is realized [181], it is given in Sect. 2.2.1. According to this method, the wave functions $|\varepsilon\gamma_1\mu_1\chi\rangle$ of the excited one-electron states are determined with provision for the vacancy field, and are non-orthogonal to the wave functions of the one-electron state of the original molecular configuration.

Then, the matrix element of the transition operator in (4.5) takes the form:

$$(\phi_{n\gamma,\varepsilon} |\hat{D}_q| \phi) = N \langle \Phi_\varepsilon^{\gamma_1\mu_1} | \hat{d}_q | n\gamma\mu \rangle ; \tag{4.6}$$

$$|\Phi_\varepsilon^{\gamma_1\mu_1}\rangle = |\varepsilon\gamma_1\mu_1\rangle - \sum_{k\gamma\mu \leq f} \frac{\langle k\gamma\mu| \ \varepsilon\gamma_1\mu_1\rangle}{\langle k\gamma\mu| \ k\gamma\mu\rangle} |k\gamma\mu\rangle ;$$

$$\langle \varepsilon\gamma_1\mu_1| \hat{d}_q | n\gamma\mu\rangle = \sum_{ll_1} \langle \varepsilon\gamma_1 l_1| \hat{r} | n\gamma l \rangle \, C_{qll_1}^{1\mu_1\mu};$$

$$C_{qll_1}^{1\mu_1\mu} = (-1)^\beta \left(l_1 \left\| C^{(1)} \right\| l \right) \begin{pmatrix} l_1 & 1 & l \\ -\mu_1 & q & \mu \end{pmatrix};$$

$$\beta = l_1 - \mu_1; \quad q - \mu_1 + \mu = 0;$$

where N is the product of the overlap integral of the wave functions of electrons not participating in the transition.

The structure of the transition amplitude in (4.5), when considering the *double* excitation/ionization effect of the molecule ground state, will be represented in Sect. 4.2 (see (4.20)).

Wave function calculation of the excited states. The construction of the wave function of the photoelectron for a linear molecule, with ligands being heavier as hydrogen, deals with the problem of the slow convergence of series (4.1). In our treatise we shall follow the method described in [181, 182] that virtually enables to circumvent this difficulty.

According to this method, the wave function of the photoelectron is constructed as:

$$|n\gamma\mu\rangle = \sum_{l \leq l_0} \left|\psi_{n\gamma}^{l\mu}\right\rangle + \sum_{i \leq f} \alpha_i^n \sum_{l > l_0} \left|\psi_{i\gamma}^{l\mu}\right\rangle, \tag{4.7}$$

where the functions $\left|\psi_{n\gamma}^{l\mu}\right\rangle$ with $l \leq l_0$ are determined through the expansion in basis set

$$\left|\psi_{n\gamma}^{l\mu}\right\rangle = \underset{k>f}{S} \, b_{kl}^{n\gamma} |kl\gamma\mu\rangle + \sum_{i \leq f} \alpha_i^n \sum_{l \leq l_0} \left|\psi_{i\gamma}^{l\mu}\right\rangle. \tag{4.8}$$

The wave functions $|kl\gamma\mu\rangle$ here are found by solving the Hartree–Fock equations:

$$\left(\hat{\Phi} - \varepsilon_{kl\gamma\mu}\right) |kl\gamma\mu\rangle = 0; \tag{4.9}$$

where $\hat{\Phi}$ is the Fock integral operator [69].

Considering the states of the continuous spectrum in (4.8), we substitute the integration domain $D : \varepsilon \in [0; \infty)$ for the domain $\varepsilon \in [0; \varepsilon_{\max}]$ and form the *quasidiscrete* spectrum:

$$\int_D b_{\varepsilon l}^{n\gamma} |\varepsilon l\gamma\mu\rangle \, d\varepsilon \rightarrow \sum_m b_{ml}^{n\gamma} |ml\gamma\mu\rangle;$$

$$b_{ml}^{n\gamma} = b_{\varepsilon_0 l}^{n\gamma} \sqrt{\Delta\varepsilon_m}; \quad |ml\gamma\mu\rangle = |\varepsilon_0 l\gamma\mu\rangle \, \sqrt{\Delta\varepsilon_m};$$

where the value ε_0 is selected in the middle of the partial interval $\Delta\varepsilon_m$. The value $\varepsilon_{\max}$ is selected under condition of the saturation of the system formulated below – if $\varepsilon > \varepsilon_{\max}$ the computational solution of the system practically does not change.

After substitution of (4.8) for (4.7) and considering (4.9), we arrive at the system of algebraic equations:

$$\sum_m \sum_{l \leq l_0} b_{ml}^{n\gamma} \left(\langle m'l'\gamma\mu| \, \hat{\Phi} \, |ml\gamma\mu\rangle - \varepsilon_{n\gamma}\delta_{mm'}\delta_{ll'}\right) +$$

$$+ \sum_{i \leq f} \alpha_i^n \sum_l \langle m'l'\gamma\mu| \, \psi_{i\gamma}^{l\mu}\rangle (\varepsilon_i - \varepsilon_{n\gamma}) = 0; \tag{4.10}$$

$$\sum_m \sum_{l \leq l_0} b_{ml}^{n\gamma} \left\langle \psi_{i'\gamma}^{l'\mu}\right| ml\gamma\mu\rangle (\varepsilon_{i'} - \varepsilon_{n\gamma}) \delta_{ll'} +$$

$$+ \sum_{i \leq f} \alpha_i^n \left(\sum_{ll'} \left\langle \psi_{i\gamma}^{l\mu}\right| \hat{\Phi} \left|\psi_{i'\gamma}^{l'\mu}\right\rangle - \varepsilon_{n\gamma}\delta_{ii'}\right) = 0; \tag{4.11}$$
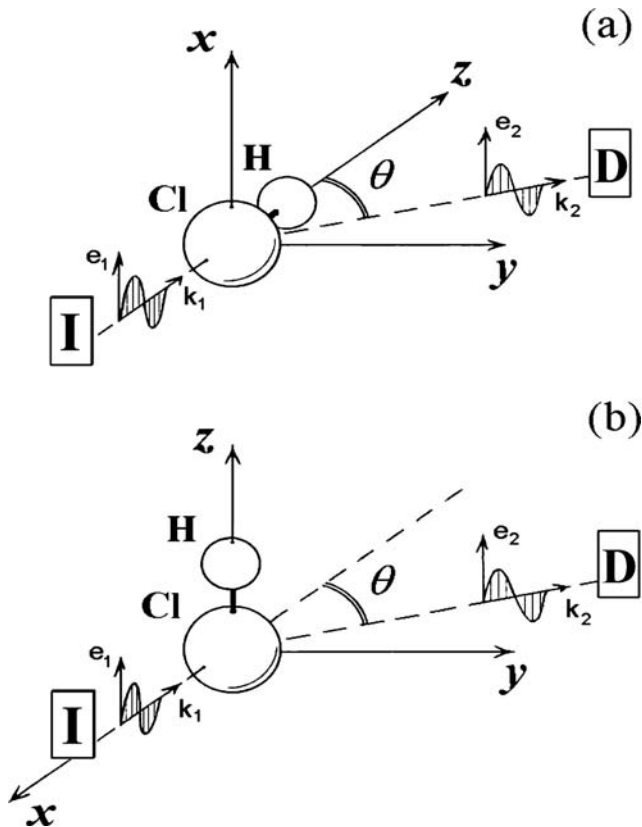
Fig. 4.1. Orientation of the linear molecule (for example, **HCl** molecule) with regard to polarization vectors of the incident (e_1) and scattered (e_2) X-ray photons in the schemes of intended anomalous elastic scattering experiment. It is indicated that k_1-, k_2- are the wave vectors of the incident and scattered photons; θ is the scattering angle; OZ is the quantization axis (linear molecule axis); **I** is the photon source; and **D** is the scattered photon detector. The scattering plane goes through the wave vectors of photons

that determine the desired weight $\alpha-$, $b-$ coefficients in expansion of the wave function of the photoelectron.

Spatial orientation of molecule. The spatial orientation types of linear molecule that are examined in our treatise (schemes for *intended* experiment) are represented in Fig. 4.1 by an example of the HCl molecule. ***Scheme (a):*** the molecular axis and the quantization axis OZ are co-directional, the molecular axis is at right angle to the photon polarization vectors and parallel to the wave vector of the incident photon. *Scheme (b)*: the molecular axis and the quantization axis OZ are co-directional, the molecular axis is parallel to the photon polarization vectors and at right angle to the scattering plane.

We shall find the analytical expressions for the probability of the transition to (4.5) and for arguments of the Legendre polynomials in the schemes represented in Fig. 4.1. To be concrete, we shall examine the photon absorption by $1\sigma^2$ -molecular orbital.

Scheme (a): in this case $e_{1,2} = (1; 0; 0) \Rightarrow (e_1 \cdot D) = \hat{D}_x$ and the square of the matrix element of the transition operator in (4.5) takes the form:

$$\frac{1}{2} \left\{ \left| \left(1\sigma \left| \hat{D}_{-1} \right| \varepsilon\pi \right) \right|^2 + \left| \left(1\sigma \left| \hat{D}_{+1} \right| \varepsilon\pi \right) \right|^2 \right\} ;, \qquad (4.12)$$

where we have considered the connection of the Cartesian and spherical coordinates of the transition operator $\hat{D}_x = \frac{1}{\sqrt{2}} \left(\hat{D}_{-1} - \hat{D}_{+1} \right)$.

In (4.12), the π-symmetry of the photoelectron is held fixed. The photoelectron escapes along the axis *OX,* having the projections of the impulsive moment on the axis *OZ* that are equal ± 1. The projections of the impulsive moments of the incident photon and the $1\sigma-$ molecular orbital on the axis *OZ* were zero.

After photon absorption and photoelectron formation, the "zero" survives: $(+1) + (-1) = 0$. In addition, if the term of the molecule ground state equals $^1\Sigma$, as a result of the transition $1\sigma \to \varepsilon\pi$ the term $^1\Pi :^2 \Sigma \oplus^2 \Pi \to^1 \Pi$ appears, where the terms of the molecular core and photoelectron are "summarized". The resulting $^3\Pi$ term of the transition is not realized at the approximation of the *LS*-bonding because of the rule of spin selection $\Delta S = 0$.

In *Scheme (a)*, the angle $\Theta_{\boldsymbol{k}} = \frac{1}{2}(\pi - \theta)$, the Legendre polynomials in (4.3) takes the form:

$$P_t \left(\cos \Theta_{\boldsymbol{k}} \right) \to P_t \left(\sin \frac{\theta}{2} \right) ; \qquad (4.13)$$

and this modifies the scattering angle dependence of the linear molecule form factor that is determined by Bessel functions.

Scheme (b): in this case $e_{1,2} = (0; 0; 1) \Rightarrow (e_1 \cdot D) = \hat{D}_z$ and the square of the matrix element of the transition operator in (4.5) takes the form:

$$\left| \left(1\sigma \left| \hat{D}_0 \right| \varepsilon\sigma \right) \right|^2 ; \; \hat{D}_z = \hat{D}_0. \qquad (4.14)$$

In (4.14), the σ-symmetry of the photoelectron is held fixed. Essentially, the photoelectron being incident along the axis *OZ* must keep the "zero" value of the projections of impulsive moments on this axis of the incident photon and 1σ-molecular orbital. In addition, if the term of the molecule ground state equals $^1\Sigma$, as a result of the transition $1\sigma \to \varepsilon\sigma$ the term does not change: $^2\Sigma \oplus^2 \Sigma \to^1 \Sigma$, where the terms of the molecule core and the photoelectron are "summarized". The resulting $^3\Sigma$ term of the transition with $\Delta S = 1$ is not realized at the approximation of the *LS*-bonding.

In *Scheme (b)*, the angle $\Theta_{\boldsymbol{k}} = \pi/2$, the Legendre polynomial in (4.3) takes the form:

$$P_t \left(\cos \Theta_{\boldsymbol{k}} \right) \to P_t(0); \tag{4.15}$$

and does not depend on the scattering angle, compared to (4.13).

Thus, the range sum in (4.2) in *Scheme (a)* consists of two terms ($q = \pm 1$), while in *Scheme (b)* it has only one term ($q = 0$). In addition, according to (4.13) and (4.15), the form factor of the linear molecule turns out to be the function of its spatial orientation types.

4.2 Differential Cross-Sections of the Anomalous Elastic X-Ray Photon Scattering by a Two-Atom Molecule

As a subject of our inquiry, we have chosen two-atoms of molecules HF, HCl, and CO in the *gas phase*. We shall represent the calculation results for the scattering differential cross-sections in the context of the quantum theory developed in Sect. 4.1.

4.2.1 Scattering by the Molecules HF and HCl in the Energy Region of the $1\sigma-$ Shell Ionization Threshold

We calculated the one-electron wave functions of the molecules HF and HCl by solving the system of (4.10) and (4.11). At the same time, we did not substitute the items with $l > l_0$ for the items of functions of occupied states. In this case, we obtained the equations for one-electron functions from the mentioned system, keeping only the first item of the first equation:

$$\sum_m \sum_{l \leq l_0} b_{ml}^{n\gamma} \left(\langle m'l'\gamma\mu | \hat{\Phi} | ml\gamma\mu \rangle - \varepsilon_{n\gamma} \delta_{mm'} \delta_{ll'} \right) = 0. \tag{4.16}$$

This calculation method is used [183] for studying the role of many-particle and vibronic effects in making the structure and form of the $1\sigma-$ photoabsorption spectra of the molecules HF and HCl, this corresponds well with the experiment [184].

If calculating the wave functions in (4.1), (4.16) and the values (4.2), (4.5), (4.6), the one-center expansion is restricted by the value of the orbital moment $l_0 = 6$.

The calculation results are shown in Figs. 4.2 and 4.3.

Let us remark here that in the case of molecules HF and CO (see Sect. 4.2.2), the form and absolute values of the differential cross-sections of the elastic scattering practically does not depend on the scattering angle. The criterion of this independence satisfies the inequality [59]:

$$R < \eta = \lambda \cdot \left(4\pi \left| \sin \left(\frac{\theta}{2} \right) \right| \right)^{-1}; \tag{4.17}$$

where R is the internuclear distance, θ is the scattering angle, and λ is the wave length of the scattered photon. In the region of the deep shell ionization
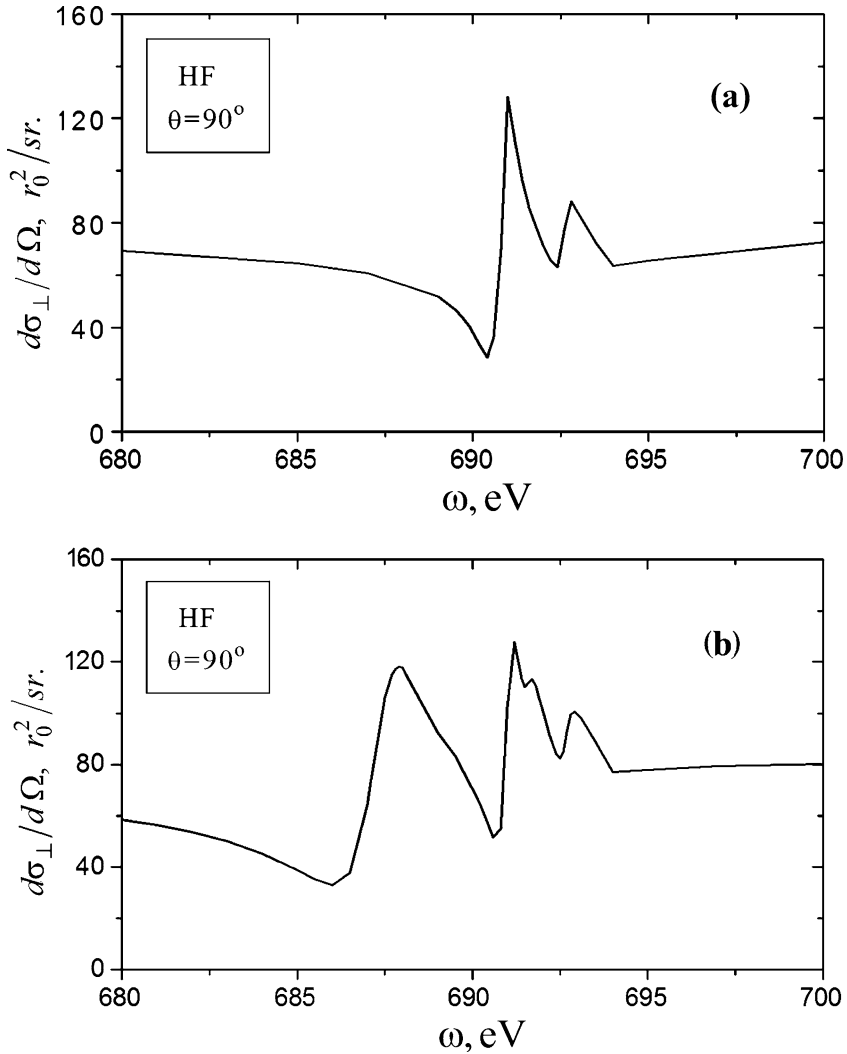
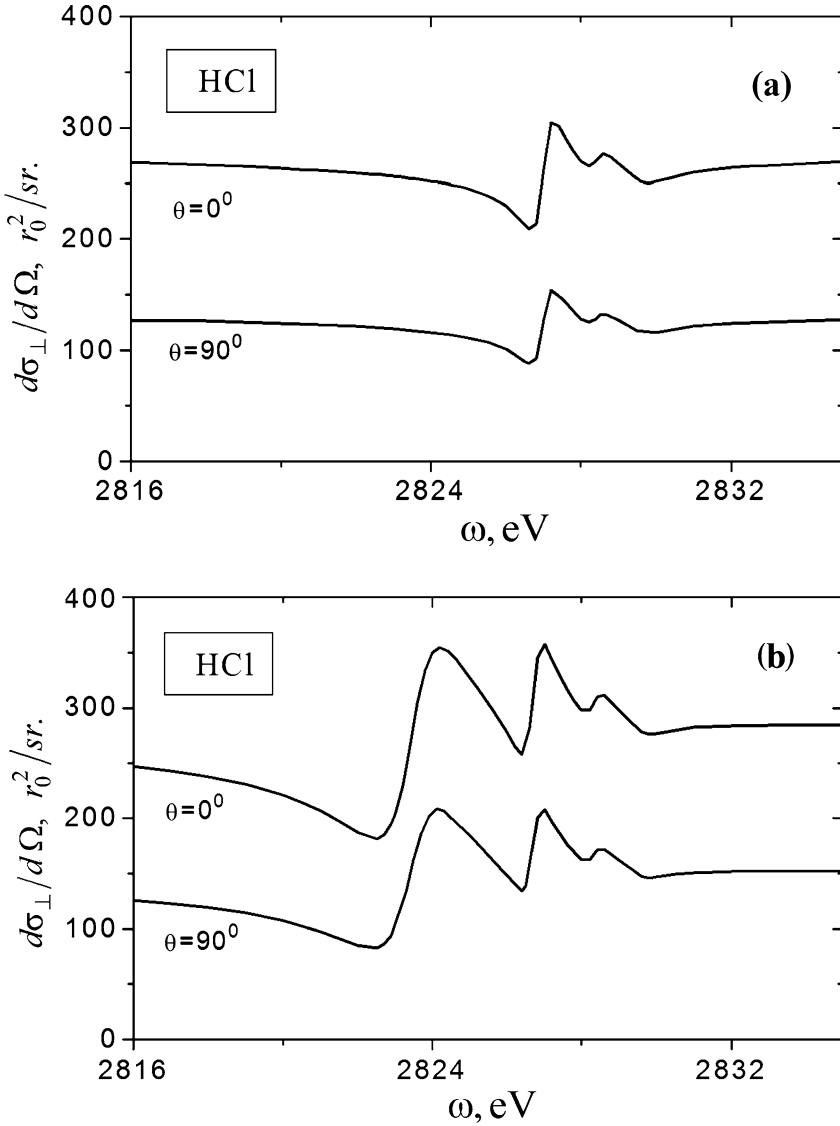**Fig. 4.2.** Differential cross-section of the anomalous elastic linear polarized (at right angle to the scattering plane) X-ray photon by the HF molecule for the schemes of the intended experiment (Fig. 4.1a, b, respectively). ω is the scattered photon energy and θ is the scattering angle. The experimental energy value of the 1σ shell ionization threshold is 694,10 eV [184]

thresholds, the inequality (4.17) is fulfilled for molecules HF and CO and is not fulfilled for molecule HCl as we have wide scattering angles (see Table 4.1). Thus, for the molecule HCl we represent the calculation results for the scattering angles 0° and 90°, and for molecules HF and CO, only the scattering angle 90°.

Fig. 4.3. Differential cross-section of the anomalous elastic linear polarized (at right angle to the scattering plane) X-ray photon scattering by the HCl molecule for schemes of the intended experiment (Fig. 4.1a, b, respectively). ω is the scattered photon energy and θ is the scattering angle. The theoretical energy value of the 1σ shell ionization threshold is 2829,50 eV [183]

Table 4.1. Values R and η from (4.17) in the region of the deep shell ionization thresholds for molecules $HF(1\sigma), HCl(1\sigma), CO(2\sigma)$

Molecule	R, Å	ω, eV	λ, Å	η, Å		
				$\theta = 0°$	$\theta = 90°$	$\theta = 180°$
CO	1,128	300	41,36	∞	4,66	3,29
HF	0,920	695	17,85	∞	2,01	1,42
HCl	1,274	2830	4,38	∞	0,50	0,35

The data for the internuclear distances are taken from the works [178, 185]

The resonances of the scattering cross-sections represented in Fig. 4.2, 4.3 are determined by the transitions from the ground state of the molecules HF (the configuration of the ground state $1\sigma^2\,2\sigma^23\,\sigma^2\,1\pi^4\,[^1\Sigma]$) and HCl (the configuration of the ground state $1\sigma^2\,2\sigma^2\,3\sigma^21\pi^4\,4\sigma^2\,5\sigma^2\,2\pi^4\,[^1\Sigma]$) to the states of the single photoexcitation $1\sigma^{-1}n\pi\,[^1\Pi]$ (Scheme Fig. 4.1a) and $1\sigma^{-1}n\sigma\,[^1\Sigma]$ (Scheme Fig. 4.1b). The broad ($\Gamma = 1,90\,\mathrm{eV}$) and intensive (oscillator strength $f = 0,0149$) resonance for the molecule HF ($n = 4$) opens a series of the $1\sigma \to n\sigma$ photoexcitation states if the scattered photon energy $\omega = 687,30\,\mathrm{eV}$, as well as the similar ($\Gamma = 1,80\,\mathrm{eV}$; $f = 0,0036$) resonance for the molecule HCl ($n = 6$) if $\omega = 2823,50\,\mathrm{eV}$. In addition, the first resonance of the $1\sigma \to n\pi$ photoexcitation appears only if $\omega = 690,80\,\mathrm{eV}$ for the molecule HF ($n = 2$) and $\omega = 2827,00\,\mathrm{eV}$ for the molecule HCl ($n = 3$).

It follows from Figs. 4.2 and 4.3 that the transition from **scheme (a)** to **scheme (b)** is accompanied by a profound *orientation effect*. Actually, the states of $1\sigma \to 4\sigma$ photoexcitation of the molecule HF and $1\sigma \to 6\sigma$ photoexcitation of the molecule HCl become apparent in the differential cross-section in the form of additional broad resonance of the elastic scattering [186–188].

4.2.2 Scattering by the Molecule CO in the Energy Region of the $2\sigma-$ Shell Ionization Threshold

In the experimental research of the X-ray [135, 189–194] and electron [195, 196] spectra of the molecule CO (configuration of the ground state $1\sigma^22\sigma^23\sigma^24\sigma^21\pi^45\sigma^2\,[^1\Sigma]$) in the region of the deep 2σ-shell ionization threshold, we can discover their complicated fine structure. The sub-threshold region of the photoabsorption spectrum contains a very intense first line connected with the $2\sigma - 2\pi$ transition, as well as a series of less intense lines of the $2\sigma \to n(\sigma, \pi)$ photoexcitation. The post-threshold region of the spectrum, with an extension $\sim 25\,\mathrm{eV}$ is mainly formed by the processes of the single $2\sigma \to \varepsilon(\pi, \sigma)$ photoionization, as well by transitions to the states of multiple excitation/ionization [193].

Measurements [197, 198] and calculation [199] make it possible to evaluate the integral contribution of the *multiple* excitations/ionization processes to

the total intensity of photoabsorption of 25–30% magnitude. At the same time the calculations [182, 200, 201] show that the thresholds of the onset of multiple excitation/ionization main channels are situated in close proximity to the $2\sigma-$ shell ionization threshold $\omega_{2\sigma} = 296,05$ eV.

By this means, the theory and the experiment show that *multiple* excitation/ionization effect of the ground state of the CO molecule plays a significant role in making the structure and form of its photoabsorption spectrum in the region of the deep $2\sigma-$ shell ionization threshold. We can suggest that this statement remains for the elastic scattering spectra too.

The present part of our treatise is devoted to studying this suggestion.

We calculated the matrix element of the transition operator (4.6) in two stages. In the first stage, we obtained the one-electron wave functions of the initial and final states of the transition by solving the multi-centre problem using the basis set 6–31 GE of the Gaussian functions. The wave functions of the final states are calculated to the approximation $\ll Z + 1 \gg$ for the Fock operator $\left(\hat{\Phi}_{Z+1}\right)$, and are subsequently transformed to the one-centre form (4.1). In the second stage, we determined the one-electron wave functions of the final states of transition in the form (4.1), where the weight coefficients are deduced by solving the secular (4.16) with operator $\hat{\Phi} \to \hat{\Phi} - \hat{\Phi}_{Z+1}$.

To study the influence of the multiple excitation/ionization effect on the theoretical differential cross-section of the elastic scattering, we considered the main [182, 201] channels of double excitation/ionization:

$$1\pi^{-1}2\pi^1 \left(^{1,3}\Sigma^+;^{1,3}\Sigma;^{1,3}\Delta\right) 2\sigma^{-1}\varepsilon\gamma;$$
$$2\sigma^{-1}n\sigma^{-1} \left(^3\Sigma\right) 2\pi^1 \left(^2\Pi\right)\varepsilon\sigma; \quad n = 4,5;$$
$$2\sigma^{-1}5\sigma^{-1} \left(^{1,3}\Sigma\right) n\sigma\varepsilon\gamma; \quad n = 6,7. \tag{4.18}$$

The wave functions of the configurations (4.18) with the segregated $\varepsilon\left(\gamma,\sigma\right)-$ photoelectron for the fixed term are obtained in the form:

$$|k; \Gamma S M_\Gamma M_S\rangle = \sum_i \alpha_{ki}\left(\Gamma S\right) \left|2\sigma^{-1}n\gamma^{-1}n_1\gamma_1\left(\xi_i M_\Gamma M_S\right)\right\rangle; \tag{4.19}$$

where the basis functions appear as single-determinant wave functions with uncombined one-electron moments, M_Γ, M_S correspond with the line of the indecomposable representation and projection of the total spin momentum, index i numbers the sets of the quantum numbers of the electron configuration (ξ_i), index k numbers the configuration terms, $\alpha_{ki}(\Gamma S)$ are the coefficients of the multiplet mixing.

Having solved the secular equation, we determined the wave functions of the final states of the photoabsorption by *adding* the corresponding functions of the photoelectrons $|\varepsilon\gamma\mu\chi\rangle$ to the functions (4.19):

$$|\Phi_k\left(\Gamma_0 S_0 = 0\right)\rangle = \frac{1}{\sqrt{2}}\left(\left|\Phi_{+-}^k\right\rangle - \left|\Phi_{-+}^k\right\rangle\right);$$

$$\left|\Phi_{+-}^k\right\rangle = \left|k; \Gamma S M_\Gamma M_S = +\frac{1}{2}\right\rangle \cdot \left|\varepsilon\gamma\mu\chi = -\frac{1}{2}\right\rangle;$$

where the values Γ_0 and S_0 correspond with the indecomposable representation and the spin of the configuration term of the final states.

Then, the matrix element of the transition operator to the double excitation/ionization states takes the form:

$$\left(\Phi_k \left(\Gamma_0 S_0 = 0 \right) \left| \hat{D}_q \right| \phi \right) = \sum_i \alpha_{ki} \left(a_i A_q + \beta_i B_q \right); \qquad (4.20)$$

$$A_q = N \left(\langle n_1 \gamma_1 \mu_1 | \, \hat{d}_q \, | 2\sigma \rangle - \sum_{\bar{k} \leq f} \langle n_1 \gamma_1 \mu_1 | \, \bar{k} \rangle \right) \langle \varepsilon \gamma \mu | \, \bar{n} \rangle;$$

$$B_q = N \left(\langle \varepsilon \gamma \mu | \, \hat{d}_q \, | 2\sigma \rangle - \sum_{\bar{k} \leq f} \langle \varepsilon \gamma \mu | \, \bar{k} \rangle \right) \langle n_1 \gamma_1 \mu_1 | \, \bar{n} \rangle;$$

$$\left| \bar{k} \right\rangle \equiv \left| k \gamma_2 \mu_2 \right\rangle \langle k \gamma_2 \mu_2 | \, \hat{d}_q \, | 2\sigma \rangle \, \langle k \gamma_2 \mu_2 | \, k \gamma_2 \mu_2 \rangle^{-1};$$

$$\left| \bar{n} \right\rangle \equiv \left| n \gamma \mu \right\rangle \langle n \gamma \mu | \, n \gamma \mu \rangle^{-1}.$$

The following values are determined: a_i, β_i are the angular coefficients and N is the product of the overlap integrals of the electron wave functions, not participating in the transition. Summing over the terms (index k) is made for the squares of the transition amplitudes (4.20) in the Kramers-Heisenberg-Waller terms (4.5).

The calculation results are represented in Fig. 4.4. It follows from Fig. 4.4 that the transition from *scheme (b)* (series of the $2\sigma^{-1}n\sigma$ photoexcitation states) to *scheme (a)* (series of the $2\sigma^{-1}n\pi$ photoexcitation states) leads to a profound *orientation effect*. Actually, in the differential cross-section the additional giant resonance of scattering appears *through* the resonance of the $2\sigma \rightarrow 2\pi$ photoexcitation having a width 0,16 eV, oscillator strength 0,118, and energy 287,40 eV. At the same time, if we consider the double excitation/ionization effect for the ground state of the molecule CO, it can make the resonance structure of the differential cross-section of the elastic scattering more precise.

Since there is no experiment referring to the elastic X-ray scattering by the linear molecule CO oriented in space, the results of our calculation (including the calculation for the molecules HF and HCl) have a predictive character. At the same time the results of our calculations in Fig. 4.5 are compared with the theoretical results of the work [59] that are only known from the published literature. We can see that the scattering resonances agree well in the energetic position and form. The reasons for disagreement in resonance intensity values can be mainly connected with two factors. The first factor is as follows: the authors of the work [59] accepted the value 0,097 eV for the width of the $2\sigma-$ vacancy decay, it is 1,65 time less than the value 0,16 eV being accepted by us. The second factor lies in the fact that the authors of the work [59] did not consider the double excitation/ionization processes of the ground state of the molecule CO.
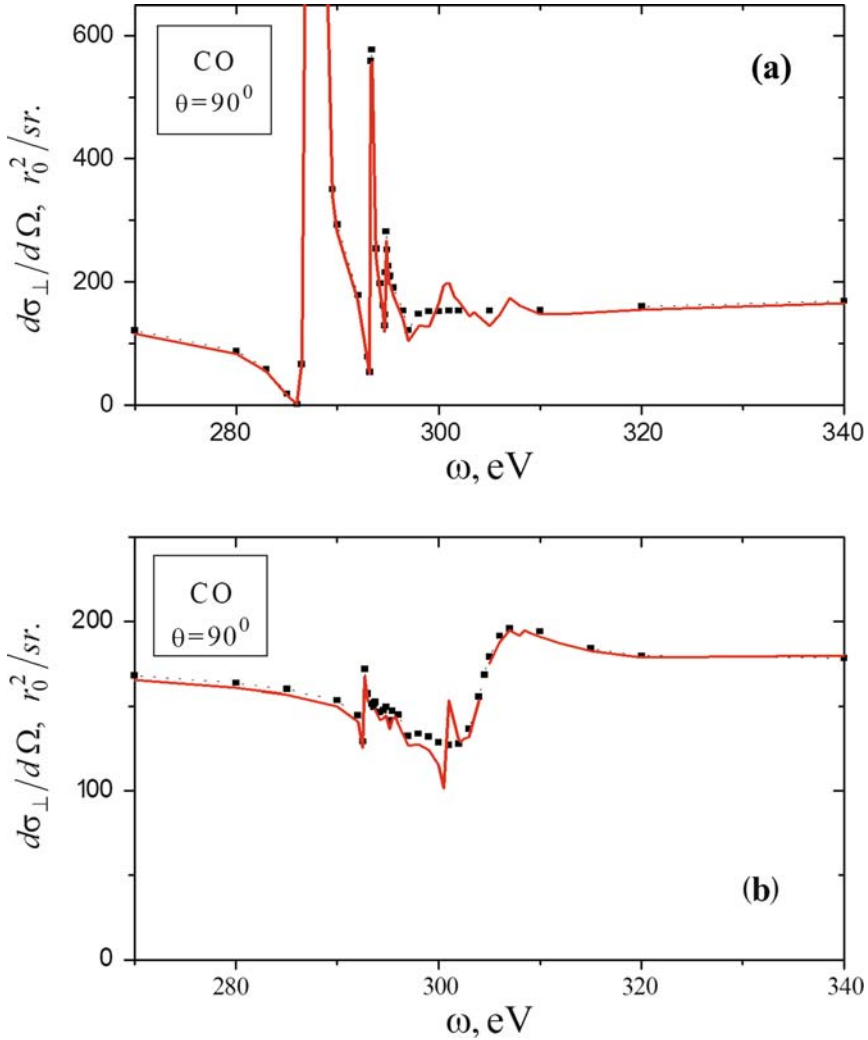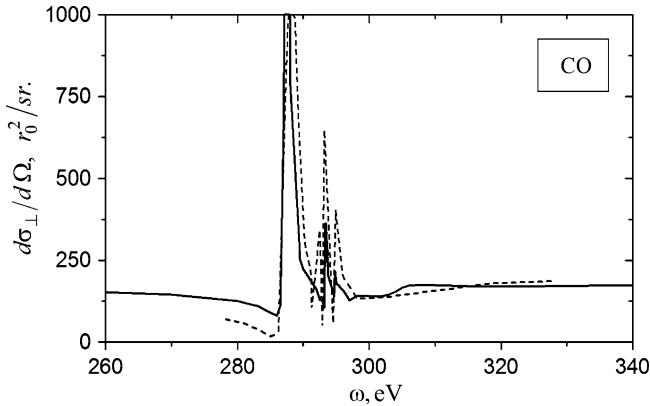
Fig. 4.4. Differential cross-section of the anomalous elastic linear polarized (at right angle to the scattering plane) X-ray photon scattering by CO molecule for schemes of intended experiment (Fig. 4.1a, b, respectively): squares designate the calculation if only the single excitation/ionization states are considered; the continuous curve designates the calculation if the double excitation/ionization states are additionally considered. ω is the scattered photon energy, θ is the scattering angle. The experimental energy value for the 2σ-shell ionization threshold amount to 296,05 eV [202]

Fig. 4.5. Differential cross-section of the anomalous elastic linear polarized (at right angle to the scattering plane) X-ray photon scattering by CO molecule, ***not*** oriented in space. The continuous curve designates the calculation of the present work, where the single and double excitation/ionization processes ($\Gamma_{2\sigma} = 0{,}16\,eV$) are considered; the broken curve designates the calculation of the work [59] ($\Gamma_{2\sigma} = 0{,}097\,eV$). The scattering angle $\theta = 90°$, ω is the scattered photon energy

4.3 Main Results of Chapter 4

1. The quantum theory and the calculation methods are developed for the differential cross-section of the elastic X-ray photon scattering in the region of the deep shell ionization thresholds of the linear molecule.
2. The analytical structure of the form factor for the linear molecule is determined in the one-center representation of the wave functions of molecular orbitals. The appearance of Legendre polynomials in the form factor structure determines its dependence on the molecular orientation in space.
3. The influence of the relaxation effects, orientation effects, vibronic effects (scattering in the region of the ionization $1\sigma-$ sthreshold for molecules HF and HCl), and the processes of additional excitation/ionization of outer shells (scattering in the region of the ionization $2\sigma-$ threshold for molecule CO) on the differential cross-section of the elastic scattering is studied.

Conclusions

We shall formulate the main results of our study, devoted to the problem of theoretically describing the spectral characteristics of the anomalous elastic X-ray photon scattering by an atom, atomic ion, and linear molecule, with provision for many-particle effects.

1. In the second-order non-relativistic quantum mechanical perturbation theory (approximation of the Kramers–Heisenberg–Waller formula), we have developed the many-particle quantum theory and the calculation methods for the differential cross-section of the elastic X-ray photon scattering by an atom and atomic ion in the energy region of their deep shell ionization thresholds. The quantum interference of the many-particle effects is considered by the structure of the probability amplitude of the scattering, both to the one- and multi-configuration Hartree–Fock approximation using the methods of the irreducible tensor operator theory, non-orthogonal orbital theory, the generalized function theory, and the non-relativistic quantum theory of many bodies.

2. For the components of the elastic scattering amplitude in the region of the atomic deep shell ionization threshold, we have stated the following:

   (a) The form and absolute values of the real component f' are mainly determined by the following many-particle effects:

   - In the near sub-resonance and post-threshold regions of scattering by the single and double ionization processes, the radial relaxation effects, and the intershell correlation effects
   - In the resonance region of the scattering by the single excitation process, the radial relaxation effects, the Auger- and radiative deep vacancy decay processes, the intershell correlations, and the multiplet splitting.

   The calculation error amounts to a significant value of 40%, without considering the amplitudes of the photon *exchange* processes in the real component. We shall remark here that such processes are attributed to the missing quantum effect in the presentations of classical physics [203].

(b) The form and absolute values of the imaginary component f'' are mainly determined by the following many-particle effects:
- In the resonance region of the scattering by the single excitation process, the radial relaxation effects, the Auger- and radiative deep vacancy decay processes, the intershell correlations, and the multiplet splitting
- In the near post-threshold region of the scattering by the single and double ionization processes and the radial relaxation effects. In the sub-resonance region of the scattering, the imaginary component is negligibly small.

The calculation error does not exceed 1%, neglecting the amplitudes of the photon *exchange* virtual processes in the imaginary component.

3. We have determined the analytical structure of the form factor of the atom with an arbitrary $^{2S+1}L_J$ term of the ground state. It is illustrated that the form factor of the atom is spherically symmetric for the values of the total moment $J = 0$, $1/2$, while for $J \geq 3/2$ and the total orbital moment $L \geq 1$, the spherically non-symmetrical contribution appears.

By the example of the atoms ^{17}Cl, ^{21}Sc, ^{23}V, ^{35}Br, ^{39}Y, and ^{73}Ta having one open shell and the total moment $J = 3/2$ of the ground state, we have studied the influence of the atom non-sphericity effect on the absolute values and the form of its form factor in the X-ray region of the elastic scattering. We have determined that this effect leads to the -2 to $+3\%$ change of the form factor values of the spherically symmetric approximation. At the same time, the departures from the spherically symmetric approximation have an *oscillating* character and when the nuclear charge of the atom increases, they localize in the region of the scattering angles $[0°, 45°]$.

4. Using the example of the neon atom, we have demonstrated that the electron correlations modify the Hartree–Fock function of the space charge distribution of the atomic ground state. This is a reason for changing the absolute values of the atom form factor of the one-electron approximation. The correlation effects in the case of forward scattering do not change the Hartree–Fock values of the form factor of neon atom. For any non-zero values of the scattering angle, the changes are enclosed in the limits from $-0,15\%$ to $+0,15\%$.

5. The theoretical study of the differential cross-sections for the anomalous elastic X-ray photon scattering by atoms with closed (^{10}Ne, ^{18}Ar, ^{36}Kr, ^{54}Xe) and open (^{11}Na, ^{42}Mo, ^{25}Mn [204], ^{29}Cu [205]) shells in the ground state has made us ascertain the following:
(a) The radial relaxation effect leads to a significant suppression of the intensity values and a shift in the short-wave region of the resonance energies, having been calculated without provision for it
(b) In the region of the near-threshold scattering, the radial relaxation effect leads to the redistribution of the scattering intensity between the short- and long-wave regions of the scattering cross-section

(c) When considering the double excitation/ionization processes of the atomic ground state, it fundamentally determines the value and direction of the redistribution of the resonance theoretical intensity

(d) Many-particle effects intensify the original character of the X-ray photon penetration (forward scattering) to the material medium, comparing with its reflection (backward scattering) by this medium

(e) The more the scattering angle, the more is the influence of the radial relaxation effects and double excitation/ionization processes of the atomic ground state on the theoretical values and the form of the scattering cross-section

(f) According to the increase of the nuclear charge of the atom:
- The influence of the spatial domain of the many-particle effects on the value and the form of the scattering cross-section corresponds with the larger scattering angles
- The role of the many-particle effect in its reflecting power decrease (backward scattering) is strengthened.

We have obtained a good agreement of the calculation results with the results of the synchrotron experiment for atoms ^{36}Kr and ^{54}Xe. The calculation results in the region of the $1\,s$-shell ionization threshold have a predictive character.

The availability of the experimental measurement results for absolute values and forms of the functions $d\sigma/d\Omega$ and f' in the region of the $1\,s$-shell ionization threshold of the metal molybdenum has allowed us to test the theory being developed in this treatise. We have obtained a good agreement of the theory with the experiment. Thus, the quantum dynamics of the many-particle effects being realized in the form and structure of the scattering cross-section on *virtual level* can be experimentally discovered. As a result of the existing dispersion Kramers–Kronig relation, this conclusion of the treatise also holds for the imaginary component f'' measured in the work [206] (see also the measurements of the f'' component in the region of the $1\,s$-shell ionization threshold for atoms ^{29}Cu [207] and ^{50}Sn [208]).

6. The theoretical study of the differential cross-section of the elastic X-ray photon scattering by an atomic ion in the region of the $1\,s$-shell ionization threshold by the example of the Ne^{6+} ion (see also Si^{4+}, Ar^{8+} [209]) has allowed us to ascertain the following. The transition from atom to its ion with loss of outer shells is followed by the rearrangement of the differential cross-section – the energy region of the scattering resonances become wider, and the resonances themselves take the form of the giant scattering resonances. At the same time, the effect of the deep vacancy stabilization becomes dominant compared to the radial relaxation effects and the multiple excitation/ionization of the ground state of an ion.

The calculation results of the differential cross-section of the anomalous elastic X-ray photon scattering by the Ne^{6+} ion have a predictive character.

7. We have developed the method for considering the set completeness of the single photoexcitation states when describing in theory the amplitude of the elastic X-ray photon scattering by an atom (ion). This method has been realized [210] in the calculation of the scattering cross-sections for the atom ^{10}Ne and its ion Ne^{6+} in the region of the $1s$-shell ionization threshold. The method allows the generalization for the single- and multi-photon [211–213] absorption processes and the inelastic [214–220] X-ray photon scattering by an atom (ion).

8. The theoretical study of the post-collisional interaction effect has allowed us to ascertain the following. In the anomalous dispersing regions of the elastic X-ray photon scattering by an atom, this effect practically *does not change* the scattering cross-sections calculated to the one-electron approximation. This fact has been interpreted from the physical standpoint in the presentation of the competitive processes of *quantum evaporation* and *quantum condensation* as transitions between virtual states of the photoelectron of discrete and continuous spectra.

9. Outside the limits of the quantum mechanical perturbation theory, we have determined the *analytical solution* of the Schrödinger equation for the wave function of the system of interacting continuous spectra – the state of the atomic deep shell photoionization and the state of the Auger-decay of the deep vacancy having two (photo- and Auger-) electrons of continuous spectrum. The generalization scheme of obtained solution is formulated for considering two and more channels of the deep vacancy Auger-decay, as well the states of photoexcitation of the atomic deep shell. In presentation of the plane waves for the wave functions of the photo- and Auger-electrons of the continuous spectrum, we have given the analytical estimation to the energy values of their electrostatic interaction in the deep vacancy Auger-decay.

10. In the second-order non-relativistic quantum mechanical perturbation theory (approximation of the Kramers–Heisenberg–Waller formula), we have formulated the many-particle quantum theory and the calculation methods for the differential cross-section of the anomalous elastic X-ray photon scattering by two-atom molecule oriented in space.

11. We have determined the analytical structure of the form factor of the linear molecule and discovered its dependence on the orientation of a molecule in space.

12. The theoretical study of the differential cross-sections of the elastic X-ray photon scattering by the molecules HF, HCl, and CO oriented in space in the region of the deep molecular orbital ionization thresholds has allowed us to determine:

    (a) The appearance of the *orientation effect* when changing the schemes of suggested experiment dealing with elastic scattering

    (b) The significant role of the radial relaxation effects and double excitation/ionization processes of the molecule ground state in defining the structure and form of the scattering cross-section.

References

1. H.A. Kramers, W. Heisenberg, Zs. Phys. **31** 681 (1925)
2. I. Waller, Zs. Phys. **51** 213 (1928)
3. I. Waller, Zs. Phys. **58** 75 (1929)
4. B. Ravel, C.E. Bouldin, H. Renevier, J.L. Hodeau, J.F. Berar, J. Synchrotron Radiat. **6** 338 (1999)
5. H. Daido, Rep. Prog. Phys. **65** 1513 (2002)
6. P.A.M. Dirac, *The Principle of Quantum Mechanics.* (Clarendon Press, Oxford, 1958)
7. A.I. Akhiezer, V.B. Berestetsky, *Quantum Electrodynamics.* (Interscience Publication, New York, 1965)
8. P.P. Kane, L. Kissel, R.H. Pratt, S.C. Roy, Phys. Rep. **140** 75 (1986)
9. L. Kissel, B. Zhou, S.C. Roy, S.K. Sen Gupta, R.H. Pratt, Acta Crystallogr. A. **51** 271 (1995)
10. R. Karazija, *Introduction to the Theory of X-Ray and Electronic Spectra of Free Atoms.* (Plenum Press, New York, 1992)
11. T.Y. Wu, T. Ohmura, *Quantum Theory of Scattering.* (Prentice-Hall, New York, 1962)
12. J.D. Bjorken, S.D. Drell, *Relativistic Quantum Fields.* (McGraw-Hill, New York, 1965)
13. R. Loudon, *The Quantum Theory of Light.* (Clarendon Press, Oxford, 1973)
14. P.M. Bergstrom Jr., L. Kissel, R.H. Pratt, A. Costescu, Acta Crystallogr. A **53**(1) 7 (1997)
15. T. Fukamachi, S. Hosoya, Acta Crystallogr. A **31** 215 (1975)
16. U. Bonse, G. Materlik, Z. Phys. B **24** 189 (1976)
17. T. Fukamachi, S. Hosoya, T. Kawamura, S. Hunter, Y. Nakano, Jpn, J Appl Phys **17**(Sup. 17–2) 326 (1978)
18. U. Bonse, P. Spieker, J.T. Hein, G. Materlik, Nucl. Instrum Methods **172** 223 (1980)
19. L.K. Templeton, D.H. Templeton, J. Am. Chem. Soc. **102**(3) 1185 (1980)
20. D.H. Templeton, L.K. Templeton, J.C. Phillips, K.O. Hodgson, Acta Crystallogr. A **36**(3) 436 (1980)
21. L.K. Templeton, D.H. Templeton, R.P. Phizackerley, K.O. Hodgson, Acta Crystallogr. A **38** 74 (1982)
22. D.T. Cromer, D. Liberman, J. Chem. Phys. **53**(5) 1891 (1970)

23. M. Hart, Nucl. Instrum Methods **172** 209 (1980)
24. M. Hart, D.P. Siddons, Proc. R. Soc. Lond. A **376** 465 (1981)
25. B.L. Henke, P. Lee, T.J. Tanaka, R.L. Shimabukuro, B.K. Fujikawa, At. Data Nucl Data Tables **27**(1) 1 (1982)
26. B.L. Henke, E.M. Gullikson, J.C. Davis, At. Data Nucl. Data Tables **54**(2) 181 (1993)
27. D.L. Windt, Appl Opt **30**(1) 15 (1991)
28. L. Kissel, R.H. Pratt, Acta Crystallogr. A **46** 170 (1990)
29. G. Basavaraju, L. Kissel, J.C. Parker, R.H. Pratt, S.C. Roy, S.K. Sen Gupta, Phys. Rev. A **34**(3) 1905 (1986)
30. B. Zhou, R.H. Pratt, S.C. Roy, L. Kissel, Phys. Scr. **41** 495 (1990)
31. B. Zhou, L. Kissel, R.H. Pratt, Nucl. Instrum Methods Phys. Res. B **66** 307 (1992)
32. J.H. Barkyoumb, T.I. Morrison, D.Y. Smith, Phys. Lett. A **143**(9) 462 (1990)
33. J.H. Barkyoumb, D.Y. Smith, Phys. Rev. A **41**(9) 4863 (1990)
34. F. Stanglmeier, B. Lengeler, W. Weber, H. Göbel, M. Schuster, Acta Crystallogr. A **48** 626 (1992)
35. R.V. Vedrinskii, V.L. Kraizman, A.A. Novakovich, V.S.h. Machavariani, J. Phys. Condens. Matter **4**(28) 6155 (1992)
36. A.I. Frenkel, J.O. Cross, D.M. Fanning, I.K. Robinson, J. Synchrotron Radiat **6** 332 (1999)
37. L. Kissel, R.H. Pratt, S.C. Roy, Phys. Rev. A **22**(5) 1970 (1980)
38. L. Kissel, Radiat. Phys. Chem. **59**(2) 185 (2000)
39. J.C. Slater, *The Self-Consistent Field for Molecules and Solids.* (McGraw-Hill, New York, 1974)
40. A.I. Milstein, M. Schumacher, Phys. Rep. **243**(4) 183 (1994)
41. M. Schumacher, Z. Phys. A **283** 15 (1977)
42. M. Hribar, A. Kodre, B. Ajlec, International Conference on X-Ray and Inner-Shell Processes in Atoms, Molecules and Solids. 20–24 August, Leipzig (GDR), Post-Deadline, Abstracts, pp. 23–24 (1984)
43. F. Smend, D. Schaupp, H. Czerwinski, M. Schumacher, A.H. Millhouse, L. Kissel, Phys. Rev. A **36**(11) 5189 (1987)
44. P.P. Kane, G. Basavaraju, S.M. Lad, K.M. Varier, L. Kissel, R.H. Pratt, Phys. Rev. A **36**(12) 5626 (1987)
45. G. Basavaraju, P.P. Kane, S.M. Lad, L. Kissel, R.H. Pratt, Phys. Rev. A **51**(3) 2608 (1995)
46. N. Bhattacharyya, S.K. Ghose, N. Choudhuri, Can. J. Phys. **66** 987 (1988)
47. E. Casnati, C. Baraldi, A. Tartari, Phys. Rev. A **42**(5) 2627 (1990)
48. J.S. Shahi, S. Puri, D. Mehta, M.L. Garg, N. Singh, P.N. Trehan, Phys. Rev. A **57**(6) 4327 (1998)
49. I.S. Elyaseery, A. Shukri, C.S. Chong, A.A. Tajuddin, D.A. Bradley, Phys. Rev. A **57**(5) 3469 (1998)
50. D.V. Rao, R. Cesareo, G.E. Gigante, Eur. Phys. J. D At. Mol. Opt. Phys. **7**(1) 45 (1999)
51. A. Kumar, J.S. Shahi, M.L. Garg, S. Puri, D. Mehta, N. Singh, Nucl. Instrum Methods Phys. Res. B **183**(3–4) 178 (2001)
52. A.C. Mandal, D. Mitra, M. Sarkar, D. Bhattacharya, Phys. Rev. A **66** 042705 (2002)

53. M. Jung, R.W. Dunford, D.S. Gemmell, E.P. Kanter, B. Krässig, T.W. LeBrun, S.H. Southworth, L. Young, J.P.J. Carney, L. LaJohn, R.H. Pratt, P.M. Bergstrom Jr., Phys. Rev. Lett. **81**(8) 1596 (1998)
54. Y.K. Kim, M. Inokuti, Phys. Rev. **165**(1) 39 (1968)
55. R.T. Brown, Phys. Rev. A **1**(5) 1342 (1970)
56. R.T. Brown, Phys. Rev. A **2**(3) 614 (1970)
57. R.T. Brown, Phys. Rev. A **5**(5) 2141 (1972)
58. R.T. Brown, Phys. Rev. A **10**(1) 438 (1974)
59. F. Gel'mukhanov, H. Ågren, Phys. Rev. A **56**(4) 2676 (1997)
60. O. Keski-Rahkonen, M.O. Krause, At. Data Nucl. Data Tables **14**(2) 139 (1974)
61. T. Papp, J.L. Campbell, D. Varga, X-Ray Natural Widths, Level Widths and Coster-Kronig Transition Probabilities. 17th International Conference on X-Ray and Inner-Shell Processes. AIP Conference Proceedings, New York (USA), No. 389, pp. 431–445 (1997)
62. H. Feshbach, Ann. Phys. **5**(4) 357 (1958)
63. B.W. Shore, Rev. Mod. Phys. **39**(2) 439 (1967)
64. J.R. Taylor, *Scattering Theory. The Quantum Theory on Nonrelativistic Collisions.* (Wiley, New York, 1972)
65. I.I. Sobel'man, *An Introduction to the Theory of Atomic Spectra.* (Pergamon Press, Oxford, 1972)
66. A.P. Jucys, A.J. Savukynas, *Mathematical Foundations of the Atomic Theory.* (Mintis, Vilnius, 1973), in Russian
67. M.Ya. Amusia, N.A. Cherepkov, Case Stud. Atom. Phys. **5**(2) 47 (1975)
68. A.P. Jucys, Adv. Chem. Phys. **14** 131 (1969)
69. L. von Zülicke, *Quantenchemie. Band 1. Grundlagen und Allgemeine Methoden.* (VEB Deutscher Verlag der Wissenschaften, Berlin, 1973)
70. M. Reed, B. Simon, *Methods of Modern Mathematical Physics. V.1. Functional Analysis.* (Academic, New York, 1972)
71. P.O. Löwdin, Phys. Rev. **97**(6) 1474 (1955)
72. A.P. Jucys, V.I. Tutlis, Lithuanian J. Phys. **11**(6) 913 (1971)
73. A.P. Jucys, V.I. Tutlis, Lithuanian J. Phys. **11**(6) 927 (1971)
74. J.M. Esteva, B. Gauthe, P. Dhez, R.C. Karnatak, J. Phys. B At. Mol. Phys. **16**(9) L263 (1983)
75. R.E. La Villa, Phys. Rev. A **19**(5) 1999 (1979)
76. M.H. Tuilier, D. Laporte, J.M. Esteva, Phys. Rev. A **26**(1) 372 (1982)
77. R.D. Deslattes, R.E. La Villa, P.L. Cowan, A. Henins, Phys. Rev. A **27**(2) 923 (1983)
78. M. Deutsch, M. Hart, Phys. Rev. A **34**(6) 5168 (1986)
79. E. Bernieri, E. Burattini, Phys. Rev. A **35**(8) 3322 (1987)
80. V.L. Sukhorukov, A.N. Hopersky, I.D. Petrov, V.A. Yavna, V.Ph. Demekhin, J. Phys. (Paris). **48**(9) 45 (1987)
81. V.A. Yavna, A.N. Hopersky, L.A. Demekhina, V.L. Sukhorukov, Opt. Spektroskopiya. **61**(2) 435, (1986) in Russian
82. V.L. Sukhorukov, A.N. Hopersky, I.D. Petrov, J. Phys. II (France) **1**(5) 501 (1991)
83. A. Kodre, I. Arcon, J. Padeznik Gomilsek, R. Preseren, R. Frahm, J. Phys. B At. Mol. Opt. Phys. **35**(18) 3497 (2002)
84. M. Deutsch, N. Maskil, W. Drube, Phys. Rev. A **46**(7) 3963 (1992)
85. H. Smid, J.E. Hansen, J. Phys. B At. Mol. Phys. **16**(18) 3339 (1983)

86. V.Ph. Demekhin, V.L. Sukhorukov, T.V. Shelkovich, V.A. Yavna, S.A. Yavna, Y.I. Bairachny, Zh. Strukt. Khim. **20**(1) 38–48, (1979) in Russian

87. V.A. Yavna, I.D. Petrov, L.A. Demekhina, A.N. Hopersky, V.L. Sukhorukov, Opt. Spektroskopiya. **61**(4) 880 (1986) in Russian

88. B.R. Judd, *Second Quantization and Atomic Spectroscopy.* (John Hopkins Press, Baltimore, 1967)

89. T. Åberg, G. Howat, *Handbuch der Physik. Encyclopedia of Physics*, 31, ed. by S . Flugge, W. Mehlhorn. (Springer, Berlin, 1982), pp. 469–619

90. M.H. Chen, 15th International Conference on X-Ray and Inner-Shell Processes. 1990. AIP Conference Proceedings, New York (USA), No. 215, pp. 391–407

91. S.V. Lavrent'ev, V.L. Sukhorukov, A.N. Hopersky, I.D. Petrov, Opt. Spektroskopiya. **62**(2) 466 (1987) in Russian

92. A.N. Hopersky, V.A. Yavna, Opt. Spectrosc. **82**(1) 1 (1997)

93. N.H. March, W.H. Young, S. Sampanthar, *The Many-Body Problem in Quantum Mechanics.* (Cambridge University Press, Cambridge, 1967)

94. A.N. Hopersky, V.A. Yavna, Opt. Spektroskopiya. **74**(3) 438 (1993) in Russian

95. A.N. Hopersky, V.A. Yavna, V.Ph. Demekhin, Opt. Spektroskopiya. **77**(6) 880 (1994) in Russian

96. A.N. Hopersky, V.A. Yavna, Sov. Phys. JETP. **80**(2) 174 (1995)

97. A.N. Hopersky, V.A. Yavna, Sov. Phys. JETP. **82**(2) 196 (1996)

98. A.N. Hopersky, V.A. Yavna, V.A. Popov, J. Phys. B At. Mol. Opt. Phys. **29**(3) 461 (1996)

99. A.N. Hopersky, V.A. Yavna, V.A. Popov, J. Phys. B At. Mol. Opt. Phys. **30**(22) 5131 (1997)

100. A.N. Hopersky, V.A. Yavna, Sov. Phys. JETP. **81**(4) 671 (1995)

101. M. Born, E. Wolf, *Principles of Optics.* (Pergamon Press, Oxford, 1964)

102. W. Heitler, *The Quantum Theory of Radiation.* (Clarendon Press, Oxford, 1954)

103. P. Carruthers, M. Nieto, Rev. Mod. Phys. **40**(2) 411 (1968)

104. R. Lynch, Phys. Rep. **256**(6) 367 (1995)

105. M.B. Mensky, *Quantum Measurements and Decoherence: Models and Phenomenology.* (Kluwer, Dordrecht, 2000)

106. P.A.M. Dirac, Proc. R. Soc. (London) A **114** 243 (1927)

107. L. De Broglie, *Les Incertitudes d'Heisenberg et l'Interpretation Probabiliste de la Mecanique Ondulatoire.* (Bordas, Paris, 1982)

108. M.Ya. Amusia, N.B. Avdonina, E.G. Drukarev, S.T. Manson, R.H. Pratt, Phys. Rev. Lett. **85**(22) 4703 (2000)

109. J.J. Yeh, I. Lindau, At. Data. Nucl. Data Tables. **32**(1) 1 (1985)

110. C.T. Chantler, J. Phys. Chem. Ref. Data **29**(5) 597 (2000)

111. V.Ph. Demekhin, Ph.V. Demekhin, A.G. Kochur, N.V. Demekhina, Zh. Strukt. Khim. **39**(6) 1001 (1998) in Russian

112. A.N. Hopersky, V.Ph. Demekhin, S.A. Novikov, V.V. Timoshevskaya, Opt. Spectrosc. **89**(1) 6 (2000)

113. A.N. Hopersky, V.A. Yavna, S.A. Novikov, V.V. Chuvenkov, J. Phys. B At. Mol. Opt. Phys. **33**(12) L439 (2000)

114. A.N. Hopersky, V.A. Yavna, Opt. Spectrosc. **85**(6) 826 (1998)

115. A.N. Hopersky, V.A. Yavna, Opt. Spectrosc. **87**(2) 301 (1999)

116. A.N. Hopersky, V.A. Yavna, A.M. Nadolinsky, Opt. Spectrosc. **88**(6) 803 (2000)

117. A.N. Hopersky, V.A. Yavna, S.A. Novikov, V.V. Chuvenkov, J. Phys. B At. Mol. Opt. Phys. **33**(12) L433 (2000)

118. A.N. Hopersky, S.A. Novikov, V.V. Chuvenkov, Radiat. Phys. Chem. **64**(1) 102 (2001)

119. A. Messiah, *Quantum Mechanics.* (Dover Publication, New York, 1999)

120. H.P. Kelly, Comp. Phys. Commun. **17**(1–2) 99 (1979)

121. S. Garpman, I. Lindgren, J. Lindgren, J. Morrison, Phys. Rev. A **11**(3) 758 (1975)

122. J.P.J. Carney, R.H. Pratt, N.L. Manakov, A.V. Meremianin, Phys. Rev. A **61** 042704 (2000)

123. J. Tulkki, G.B. Armen, T. Åberg, B. Crasemann, M.H. Chen, Z. Phys. D At. Mol. Clasters. **5** 241 (1987)

124. H.A. Bethe, E.E. Salpeter, *Quantum Mechanics of One- and Two- Electron Atoms.* (Academic, New York, 1978)

125. R.D. Deslattes, E.G. Kessler Jr., P. Indelicato, L. de Billy, E. Lindroth, J. Anton, Rev. Mod. Phys. **75**(1) 35 (2003)

126. J.L. Campbell, T. Papp, At. Data Nucl. Data Tables **77**(1) 1 (2001)

127. O. Wilhelmi, G. Mentzel, B. Zimmermann, K.H. Schartner, H. Schmoranzer, F. Vollweiler, S. Lauer, H. Liebel, J. Electron Spectrosc. Relat. Phenom. **101** 155 (1999)

128. M. Zinner, P. Spoden, T. Kraemer, G. Birkl, W. Ertmer, Phys. Rev. A **67** 010501 (2003)

129. M. Coreno, L. Avaldi, R. Camilloni, K.C. Prince, M. de Simone, J. Karvonen, R. Colle, S. Simonucci, Phys. Rev. A **59**(3) 2494 (1999)

130. I.H. Suzuki, N. Saito, J. Electron Spectrosc. Relat. Phenom. **129**(1) 71 (2003)

131. J.W. Cooper, Phys. Rev. A **38**(7) 3417 (1988)

132. K. Ueda, E. Shigemasa, Y. Sato, A. Yagishita, M. Ukai, H. Maezawa, T. Hayaishi, T. Sasaki, J. Phys. B At. Mol. Opt. Phys. **24**(3) 605 (1991)

133. V.L. Sukhorukov, V.Ph. Demekhin, V.A. Yavna, A.I. Dudenko, V.V. Timoshevskaya, Opt. Spectrosc. **55**(2) pp. 135–137 (1983)

134. J. Tulkki, T. Åberg, J. Phys. B At. Mol. Phys. **18**(15) L489 (1985)

135. B.S. Itchkawitz, B. Kempgens, H.M. Köppe, J. Feldhaus, A.M. Bradshaw, W.B. Peatman, Rev. Sci. Instrum. **66**(2) 1531 (1995)

136. P. Glans, R.E. La Villa, M. Ohno, S. Svensson, G. Bray, N. Wassdahl, J. Nordgren, Phys. Rev. A **47**(2) 1539 (1993)

137. A.N. Hopersky, V.A. Yavna, Opt. Spectrosc. **81**(4) 505 (1996)

138. K.C. Prince, M. Vondracek, J. Karvonen, M. Coreno, R. Camilloni, L. Avaldi, M. de Simone, J. Electron Spectrosc. Relat. Phenom. **101** 141 (1999)

139. S.J. Schaphorst, A.F. Kodre, J. Ruscheinski, B. Crasemann, T. Åberg, J. Tulkki, M.H. Chen, Y. Azuma, G.S. Brown, Phys. Rev. A **47**(3) 1953 (1993)

140. M. Deutsch, P. Kizler, Phys. Rev. A **45**(3) 2112 (1992)

141. M.H. Chen, B. Crasemann, H. Mark, Phys. Rev. A **21**(2) 436 (1980)

142. J. Tulkki, Phys. Rev. A **32**(5) 3153 (1985)

143. A. Mantukentta, B. Crasemann, S.L. Sorensen, M.H. Chen, 15th International Conference on X-Ray and Inner-Shell Processes. 9–13 July, 1990. Knoxville (USA), Abstracts, P. GO 3

144. E.J. McGuire, Phys. Rev. A **5**(3) 1043 (1972)

145. J.E. Hansen, W. Persson, J. Phys. B At. Mol. Phys. **12**(12) L331 (1979)

146. K.N. Huang, M. Aoyagi, M.H. Chen, B. Crasemann, H. Mark, At. Data Nucl. Data Tables **18**(3) 243 (1976)

147. I. Arcon, A. Kodre, M. Stuhec, D. Glavic-Cindro, Phys. Rev. A **51**(1) 147 (1995)
148. A.N. Hopersky, V.A. Yavna, Opt. Spectrosc. **83**(1) 12 (1997)
149. M. Deutsch, G. Brill, P. Kizler, Phys. Rev. A **43**(5) 2591 (1991)
150. D. Lutzenkirchen-Hecht, R. Frahm, J.Synchrotron Radiat. **6** 591 (1999)
151. H. Yoshida, J. Sasaki, Y. Senba, Y. Suto, Y. Shimizu, A. de Fanis, H. Tanaka, K. Ueda, 19th International Conference on X-Ray and Inner-Shell Processes June 24–28, Rome (Italy), Abstracts, p. 129 (2002)
152. M.H. Chen, B. Crasemann, R. Karim Kh, H. Mark, Phys. Rev. A **24**(4) 1845 (1981)
153. J.B. West, J. Phys. B At. Mol. Opt. Phys. **34** (20) R45 (2001)
154. P. Beckmann, *The Scattering of Electromagnetic Waves from Rough Surface. Part 1.* (Pergamon Press, Oxford, 1963)
155. A.N. Hopersky, V.A. Yavna, J. Phys. II (France) **3**(9) 1319 (1993)
156. U. Fano, Phys. Rev. **124**(6) 1866 (1961)
157. N.I. Muskhelishvili, *Singular Integral Equations.* (Noordhoff LTD, Groningen, 1953)
158. M.Ya. Amusia, *Atomic Photoeffect.* (Plenum Press, New York, 1990)
159. A.N. Hopersky, Opt. Spectrosc. **85**(3) 346 (1998)
160. T. Åberg, Phys. Scr. **21** 495 (1980)
161. A.B. Vasil'eva, N.A. Tikhonov, *Integral Equations.* (Moscow University Press, Moscow, 1989), in Russian
162. A.N. Tikhonov, V.Ya. Arsenin, *Methods of Solution of the Non-Correct Tasks.* (Nauka, Moscow, 1979), in Russian
163. A.F. Starace, *Handbuch der Physik. Encyclopedia of Physics*, **31**, ed. by S. Flugge, W. Mehlhorn. (Springer, Berlin, 1982), pp. 1–121
164. L. Armstrong Jr., C.E. Theodosiou, M.J. Wall, Phys. Rev. A **18**(6) 2538 (1978)
165. Ph. Durand, I. Paidarova, F.X. Gadea, J. Phys. B At. Mol. Opt. Phys. **34**(12) 1953 (2001)
166. Ph. Durand, I. Paidarova, J. Phys. B At. Mol. Opt. Phys. **35**(3) 469 (2002)
167. F.H. Mies, Phys. Rev. **175**(1) 164 (1968)
168. F. Combet Farnoux, Phys. Rev. A **25**(1) 287 (1982)
169. A.N. Hopersky, V.Ph. Demekhin, Opt. Spectrosc. **90**(5) 646 (2001)
170. A.N. Hopersky, Radiat. Phys. Chem. **64**(3) 89 (2001)
171. A.N. Hopersky, V.V. Chuvenkov, J. Phys. B At. Mol. Opt. Phys. **36**(14) 2987 (2003)
172. F.H.M. Faisal, Phys. Lett. A **187**(2) 180 (1994)
173. J.S. Briggs, V. Schmidt, J. Phys. B At. Mol. Opt. Phys. **33**(18) R1 (2000)
174. J. Berakdar, A. Lahman-Bennani, C. Dal Cappello, Phys. Rep. **374**(2) 91 (2003)
175. B. Rouvellou, S. Rioual, L. Avaldi, R. Camilloni, G. Stefani, G. Turri, Phys. Rev. A **67** 012706 (2003)
176. R. Zare, *Angular Momentum.* (Wiley, New York, 1988)
177. S. Wilson, *Electron Correlation in Molecules.* (Clarendon Press, Oxford, 1984)
178. W.H. Flygare, *Molecular Structure and Dynamics.* (Prentice-Hall, Englewood Cliffs, NJ, 1978)
179. M. Abramowitz, I.A. Stegun (eds.) *Handbook of Mathematical Function with Formulas, Graphs, and Mathematical Tables.* (Dover Publication, New York, 1965)

180. V.I. Nefedov, V.I. Vovna, *Electronic Structure of Chemical Compounds.* (Nauka, Moscow, 1987), in Russian
181. V.A. Yavna, A.M. Nadolinsky, V.Ph. Demekhin, J. Electron Spectrosc. Relat. Phenom. **68** 267 (1994)
182. V.A. Yavna, A.M. Nadolinsky, A.N. Hopersky, J. Electron Spectrosc. Relat. Phenom. **94**(1–2) 49 (1998)
183. V.A. Yavna, V.A. Popov, S.A. Yavna, Opt. Spectrosc. **75**(1) 23 (1993)
184. A.P. Hitchock, C.E. Brion, J. Phys. B At. Mol. Phys. **14**(22) 4399 (1981)
185. K.P. Huber, G. Herzberg, *Molecular Spectra and Molecular Structure. V.4. Constants of Diatomic Molecules.* (Van Nostrand Reinhold Company, New York-London-Toronto, 1979)
186. A.N. Hopersky, V.A. Yavna, A.M. Nadolinsky, V.V. Timoshevskaya, Opt. Spectrosc. **88**(3) 365 (2000)
187. V.A. Yavna, A.N. Hopersky, A.M. Nadolinsky, S.A. Yavna, J. Phys. B At. Mol. Opt. Phys. **33**(12) 3249 (2000)
188. V.A. Yavna, A.N. Hopersky, A.M. Nadolinsky, S.A. Yavna, J.Synchrotron Radiat. **8** 240 (2000)
189. R.B. Kay, Ph.E. van der Leew, M.J. van der Wiel, J. Phys. B At. Mol. Phys. **10**(12) 2513 (1977)
190. D.M. Barrus, R.L. Blake, A.J. Burek, K.C. Chambers, A.L. Pregenzer, Phys. Rev. A **20**(3) 1045 (1979)
191. M. Domke, C. Xue, A. Puschmann, T. Mandel, E. Hudson, D.A. Shirley, G. Kaindl, Chem. Phys. Lett. **173**(1) 122 (1990)
192. Y. Ma, C.T. Chen, G. Meigs, K. Randall, F. Sette, Phys. Rev. A **44**(3) 1848 (1991)
193. E. Shigemasa, T. Hayaishi, T. Sasaki, A. Yagishita, Phys. Rev. A **47**(3) 1824 (1993)
194. M. Schmidbauer, A.L.D. Kilcoyne, H.M. Köppe, J. Feldhaus, A.M. Bradshaw, Chem. Phys. Lett. **199**(1–2) 119 (1992)
195. O. Hemmers, F. Heiser, J. Eiben, R. Wehlitz, U. Becker, Phys. Rev. Lett. **71**(7) 987 (1993)
196. K.J. Randall, A.L.D. Kilcoyne, H.M. Köppe, J. Feldhaus, A.M. Bradshaw, Phys. Rev. Lett. **71**(8) 1156 (1993)
197. J. Schirmer, G. Angonoa, S. Svensson, D. Nordfors, U. Gelius, J. Phys. (France) Coll. C9 **1** 711 (1987)
198. H.M. Köppe, A.L.D. Kilcoyne, J. Feldhaus, A.M. Bradshaw, J.Electron Spectrosc. Relat. Phenom. **75** 97 (1995)
199. J. Schirmer, M. Braunstein, V. McKoy, Phys. Rev. A **41**(1) 283 (1990)
200. G. Bandarage, R.R. Lucchese, Phys. Rev. A **47**(3) 1989 (1993)
201. V.A. Yavna, A.M. Nadolinsky, A.N. Hopersky, Opt. Spectrosc. **88**(6) 844 (2000)
202. D.A. Show, G.C. King, D. Cvejanovic, F.H. Read, J. Phys. B At. Mol. Phys. **17**(10) 2091 (1984)
203. R.P. Feynman, *The Theory of Fundamental Processes.* (W.A. Benjamin, New York, 1961)
204. A.N. Hopersky, A.M. Nadolinsky, V.A. Yavna, R.V. Koneev, Opt. Spectrosc **98**(2) 161 (2005)
205. A.N. Hopersky, I.D. Petrov, A.M. Nadolinsky, V.A. Yavna, R.V. Koneev, J. Phys. B At. Mol. Opt. Phys. **37**(16) 3313 (2004)

206. M.D. De Jonge, Ch.Q. Tran, C.T. Chantler, Z. Barnea, B.B. Dhal, D.J. Cookson, W.K. Lee, A. Mashayekhi, Phys. Rev. A **71** 032702 (2005)
207. C.T. Chantler, Ch.Q. Tran, Z. Barnea, D. Paterson, D.J. Cookson, D.X. Balaic, Phys. Rev. A **64** 062506 (2001)
208. M.D. De Jonge, Ch.Q. Tran, C.T. Chantler, Z. Barnea, B.B. Dhal, D. Paterson, E.P. Kanter, S.H. Southworth, L. Young, M.A. Beno, J.A. Linton, G. Jennings, Phys. Rev. A **75** 032702 (2007)
209. A.N. Hopersky, A.M. Nadolinsky, D.V. Dzuba, V.A. Yavna, J. Phys. B At. Mol. Opt. Phys. **38**(10) 1507 (2005)
210. A.N. Hopersky, V.A. Yavna, A.M. Nadolinsky, D.V. Dzuba, J. Phys. B At. Mol. Opt. Phys. **37**(12) 2511 (2004)
211. S.A. Novikov, A.N. Hopersky, J. Phys. B At. Mol. Opt. Phys. **33**(12) 2287 (2000)
212. S.A. Novikov, A.N. Hopersky, J. Phys. B At. Mol. Opt. Phys. **34**(23) 4857 (2001)
213. S.A. Novikov, A.N. Hopersky, J. Phys. B At. Mol. Opt. Phys. **35**(15) L339 (2002)
214. T. Åberg, J. Tulkki, *Atomic Inner-Shell Physics*, ed. by B. Crasemann (Plenum Press, New York, 1985). Chapter **10**, pp. 419–463
215. P.P. Kane, Phys. Rep. **218**(2) 67 (1992)
216. F. Gel'mukhanov, H. Ågren, Phys. Rep. **312**(3–6) 87 (1999)
217. A.N. Hopersky, A.M. Nadolinsky, V.A. Yavna, Sov. Phys. JETP. **101**(4) 597 (2005)
218. A.N. Hopersky, A.M. Nadolinsky, V.A. Yavna, Phys. Rev. A **75** 012719 (2007)
219. A.N. Hopersky, A.M. Nadolinsky, Sov. Phys. JETP. **105**(3) 549 (2007)
220. A.N. Hopersky, A.M. Nadolinsky, Phys. Rev. A **77** 022712 (2008)

Index

Springer Series on
ATOMIC, OPTICAL, AND PLASMA PHYSICS